Hollow Hydrogel Cocoons for the Encapsulation of Therapeutic Cells Using a Microfluidic Platform

Nicholas Soucy

A thesis submitted to the University of Ottawa
in partial fulfillment of the requirements for the degree of

Master of Applied Science

in

Biomedical Engineering

Ottawa Carleton Institute for Biomedical Engineering

University of Ottawa

Ottawa, Ontario

Abstract

Microencapsulation of stem cells in hydrogel for use in therapeutic applications has been shown to improve cell retention at the site of injuries due to their mechanical and immunoprotective properties. These microscale droplets (cocoons) can be produced at high throughputs within microfluidic channels. Currently, the ability for cells to egress hydrogel cocoons is under investigation. This egress can correlate with therapeutic efficacy, and so promoting or inhibiting the egress of cells can be a vital component of viable treatments. Previously, a second hydrogel layer was shown to reduce egress, but issues involving cell proliferation were unchanged. We propose a microfluidic process to encapsulate cells in two layers of thermoresponsive hydrogels, in which the inner core melts at physiological temperatures to form hollow cocoons that allow cells free motion inside the immunoprotective shell. We hypothesize that the open volume would increase cell viability and proliferation, without increasing cell egress due to the uninterrupted hydrogel shell.

In this project the encapsulation of NIH 3T3 cells in hollow agarose cocoons was achieved. 3T3 cells were first encapsulated in thermoreversible gelatin which were then re-encapsulated in agarose through the use of a flow-focusing microfluidic channel with on-chip mixing of two inlet flows to produce hollow cocoons. The production of these cocoons showed the potential of high throughput, monodisperse samples with future investment. Preliminary investigation in the behavior of the encapsulated cells showed that the cells maintain high viability over the course of 48 hours. There are early indications that the hollow nature of correctly formed cocoons can limit cell egress, and may allow for proliferation in the cocoon.

Statement of Originality:

The content contained in this thesis is to the best of the author's knowledge original and the product of work done under the supervision of Dr. Michel Godin at the University of Ottawa, Ottawa Ontario.

As partial fulfillment of the requirements for Master of Applied Science in Biomedical Engineering at the University of Ottawa, an early version of this work was presented at the Ottawa Carleton Institute for Biomedical Engineering Seminar Series on February 28, 2019 as "Hollow Hydrogel Cocoons for Therapeutic Stem Cell Therapy"

Additionally, aspects of this work were presented on posters at:

SCORR Seminar 2019

CREATE-BEST Research Poster Day 2019

Statement of Contribution

All text present in this document is original and written solely by the author. Figures and tables are created by the author unless otherwise noted, with proper credit provided.

The original work on single encapsulation devices was done in the lab of Professor Godin, adapted by Ainara Benavente-Babace, PhD from the original design by Nicolas Cataford, MASc. Original double encapsulation devices were designed by Rushi Panchal, MASc. “Co-Inlet” devices for producing hollow cocoons designed by the author were adapted using aspects of designs originally made by Ainara Benacente-Babace, PhD for on-chip mixing of photo-initiators.

Programs in Labview used in pressure and temperature control were developed by Professor Godin, PhD.

All subsequent designs were done by the author, as well as data acquisition and analysis, microfabrication and cell culture.

Acknowledgements

Firstly, I would like to provide great thanks to my supervisor Dr. Michel Godin. He has managed to create an amazing lab, both in the resources available to bring together projects spanning disciplines and the members to make the most of them. He was a constant presence of support and knowledge throughout this project and I am grateful for all he has done to get me to this point. I look forwards to continuing this research going forwards into my PhD in his group.

Dr. James Harden was very helpful in the understanding of the physics and behavior of hydrogel solutions. His PHYS8191 course on the physics of soft matter, and his advice on working with Poloxamer materials helped form the basis of the strategies of HLB interactions found in this thesis.

Thank you to the other current members of the Godin Lab, Kaitlyn Kean and Megan Dutcher. Working together in the lab and bouncing ideas off each other has been nothing but helpful and enjoyable and I'm happy it will continue moving forwards.

For all their help during their time at the Godin Lab, I would like to thank Dr. Ainara Benavente-Babace, Dr. Ali Najafu Sohi, Dr. Eric Beamish, Rushi Panchal and Karan Dhingra. Their advice and assistance when starting in this Master's program, both in training in the multitude of skills needed for such an interdisciplinary topic and providing insights into issues and challenges, contributed greatly to my successes in this project and reaching this point.

I would also like to give special thanks to my mother, Susan Ryder-Soucy, my father Roger Soucy and my sister Jane Soucy.

Figures

Tables

Equations

Abbreviations

HLB	Hydrophile Lipophile Balance
O/W	Oil in Water Emulsion
W/O	Water in Oil Emulsion
PDMS	Poly(dimethylsiloxane)
MSC	Mesenchymal Stem Cells
ECM	Extra-Cellular Matrix
PEO	Poly(ethylene oxide)
PPO	Poly(propylene oxide)
PEEK	Polyether Ether Ketone
CMC	Critical Micelle Concentration
CMT	Critical Micelle Temperature
ATPS	Aqueous Two-Phase Solution
PBS	Phosphate Buffered Saline
DMEM	Dulbecco's Modified Eagle Medium
FBS	Fetal Bovine Serum

Symbols

ρ	Density
u	Velocity
t	Time
P	Pressure
μ	Viscosity
γ	Interfacial Tension
B	"Body" Force
L	Characteristic Length Scale
$-^*$	Non-Dimensionalized signifier
D	Diffusivity
k_B	Boltzman Constant
T	Temperature
d	Particle Diameter
Q	Flow Rate
w	Channel Width Fraction
λ	Mean Number of Events in a Time Frame
x	Number of Events Occurred
θ	Contact Angle
C	Concentration of Cocoons
V	Volume of a Cocoon
Re	Reynolds Number
We	Weber Number
Ca	Capillary Number
Oh	Ohnesorge Number
Pe	Peclet Number

Table of Contents

1 Introduction

Stem cells are undifferentiated therapeutic cells that are notable due to their ability to renew themselves by generating identical daughter cells, as well as differentiating into somatic cell types to replenish populations in tissue. There are numerous types, ranging from pluripotent cells found in the embryo that give rise to the germ layers, to the progenitor cells found in adults that are limited to differentiating into a limited number of cell types. [1] These cells are currently used in regenerative medicine, by taking cells from allogenic or autologous sources and placing them at the site of chronic injuries. [1], [2] These are often paired with hydrogel "scaffolds" that encapsulate the cells to provide an immunoprotective barrier while allowing for the diffusion of oxygen and nutrients, and can promote the migration of cells into the site of the implant. [3]–[5] When injecting therapeutic cells into the heart in particular, injected cells require a scaffold as suspended cells show almost no long-term persistence after injection. When cells are inserted through use of a hydrogel scaffold, retention shows notable improvement even after several weeks. [6]–[9]

A downside of these scaffolds is that due to gradients in the diffusion of oxygen and nutrients, these scaffolds cannot typically be densely populated with cells so as to avoid the death of cells located in the center of the scaffold due to lack of resources and build up of waste. [3] By encapsulating cells in microencapsulations, the cells are spread throughout numerous smaller scaffolds. This increases the overall surface area, reducing the diffusion distance in each scaffold allowing for a denser cell population per unit volume. [3] This can be done through processes like electrospraying where small droplets are produced by electrostatic forces, or through vortex mixing where the creation of a vortex forcibly creates an emulsion of liquid hydrogel and an oil phase to produce droplets. but the polydispersity of cocoon diameter produced through these methods tends to be high. [9], [10] More recently, microencapsulations have been created through microfluidic channels. By flowing immiscible fluids through micrometer scale nozzles monodisperse emulsions can be created to encapsulate cells, often at throughputs reaching hundreds to thousands of hertz. [11]–[13]

There remain issues with these encapsulations. Encapsulated therapeutic cells show a tendency for a portion of the population to escape the cocoons within a few hours of encapsulation, while remaining cells suffer a large loss of viability over subsequent days. [14] Previous work in this lab has shown that egress can be mitigated by coating the encapsulated cells in a second layer of hydrogel. It was found that cells do not typically actively dig through the bulk hydrogel, but cells located near the surface of cocoons appear to be able to break through a thin surface layer, so adding additional layers of hydrogel removes this avenue of egress. [15] The purpose of this project is to extend upon the concept of doubly encapsulated cells and produce hollow cored cocoons. The aim is to create an encapsulation process that not only maintains the immunoprotective properties and the reduced egress of former methods, but also provides an open volume where therapeutic cell types can spread and adhere to the inside surface and each other to ideally improve long term encapsulation viability.

1.1 Microfluidics

Microfluidics consists of the manipulation of fluid flows where the characteristic length of the system is on the order of micrometers. Due to the small volumes, often picolitre, and the effects of scaling there are many important differences in manipulating features of the flows when compared to macroscale flows. One that is most apparent is the disappearance of turbulence making microfluidic devices operate primarily in the laminar flow regime. At a macro scale, if one were to follow a path line through a flow there would be numerous instabilities leading to the flow changing directions in vortices and eddies. Repeating the flow would then lead to a completely different path due to small differences in boundary conditions creating variation in inertial forces. This turbulence acts under a range of length and time scales making it difficult to account for, and the fact that it is chaotic and non-replicable makes precise control over macroscale flows infeasible. [16] At lower length scales and velocities, the inertial forces that lead to these instabilities drop off allowing for laminar flows. The path lines for these flows exists as individual “sheets” of flows that do not cross or mix, leading to the iconic and replicable

flow profiles such as Couette and Poiseuille. [17] A visual example of laminar compared to turbulent flow lines can be seen in Figure 1.

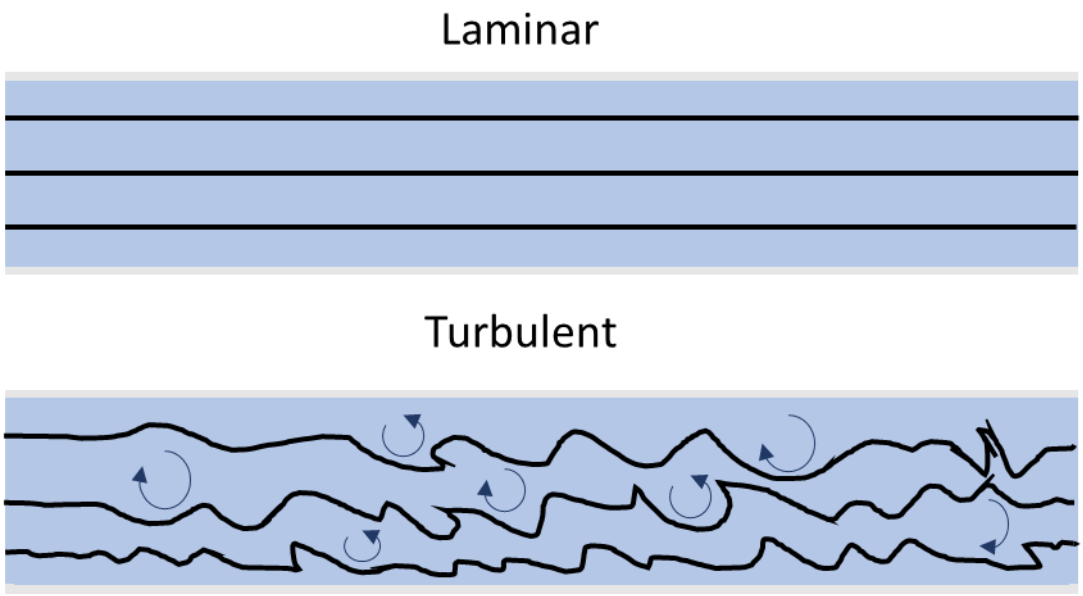

Figure 1: Laminar and Turbulent Flow. Laminar flow acts as individual sheets that flow next to each other without mixing. Turbulent flow is seemingly random, with the disruptions it causes being practically unpredictable and nonrepeatable. These perturbations include eddies that lead to mixing.

The decreased length scale also affects other forces due to the differences in scaling laws. The increase of the ratio of surface area to volume leads to the domination of pressure, shear forces and surface tension, creating new considerations and opportunities to create specific flows.[18] As well, strategies such as mixing through diffusion can become viable due to the reduced diffusion length required, and the lack of turbulence induced mixing due to laminar flow. At the same time, forces that scale with length at the third power, such as gravity, become negligible as the size of the sample continues to decrease. [19]

1.1.1 Navier Stokes

The Navier Stokes equations are a series of equations, or tensors, that describe the motion of fluids in three dimensions. They were originally derived from Newton's Second law, the continuity equation for fluid flow and the Cauchy stress tensor and are presented in terms of the

velocity of the fluid. There are many forms but for an incompressible fluid such as water under regular conditions the Navier-Stokes equation is:

$$\rho \frac{\delta u}{\delta t} + \rho u \cdot \nabla u = -\nabla P + \mu \nabla^2 u + \rho B$$

Equation 1: Navier-Stokes Equation for an Incompressible Fluid

Where ρ is density, u is the velocity tensor, P is pressure, μ is viscosity, t is time and B is a body force. The first term is the change of momentum over time, the second is the "convective" term which relates the change of velocity at a point, the third is an external pressure acting on the fluid and the forth is the viscous force from the fluid being sheared. The fifth is a general force term that can include gravitational force, forces caused by external electric fields or other external factors but is often negligible unless a specific application is in use. [16], [20]

Typically, the Navier-Stokes equation cannot be solved analytically due to the complexities of turbulence, especially applied to an entire flow. For engineering purposes there are simplifications that can be made, especially within the range of flows occurring in microfluidic channels.

1.1.2 Reynolds

The Reynolds number is one of several useful dimensionless numbers that compares forces in fluid dynamics. It relates the inertial force to the viscous force where L is the characteristic length of the fluid channel. For a microchannel, the characteristic length is its hydraulic diameter.

$$Re = \frac{\rho u L}{\mu}$$

Equation 2: Reynolds Number

By finding the magnitude of the Reynolds number, one can determine whether the flow is in the laminar or turbulent flow regime. A high Reynolds number means that there is a high inertial force or a small viscous force acting on the fluid, meaning there is enough inertial effects to generate turbulent flows. Typically, a Reynolds number less than 2000 is considered to be the

laminar flow regime, and microchannels can often have a Reynolds number below 1 due to the low flow velocities and characteristic lengths of the channel. [17], [21]

1.1.3 Stokes

Stokes flow, or creeping flow, is a linearization of the Navier-Stokes equation that occurs at low Reynolds numbers. It is a simplification that arises through non-dimensionalization of the equation, substituting the variables with a non-dimensionalized variable multiplied by a reference value such as the characteristic length of the channel. The substitutions can be found in Table 1, and the revised equation can be seen here.

$$\frac{\rho u L}{\mu}\frac{l}{U t_{ref}}\frac{\delta u^*}{\delta t^*} + \frac{\rho u L}{\mu} u^* \cdot \nabla^* u^* = -\nabla^* P^* + \nabla^{*^2} u^*$$

Equation 3: Non-Dimensionalized Navier-Stokes

The important thing to note is the $\frac{\rho u L}{\mu}$ coefficient found on the acceleration and convective term. This is again the Reynolds number. The $\frac{l}{U t_{ref}}$ coefficient also on the acceleration term is the Strouhal number which is 1 if the boundary condition is not changing, as t_{ref} would simply be $\frac{l}{U}$ and is thus the Strouhal number not important in the cases found in this thesis. When the Reynolds number is very small, as in the case of microfluidic flows, the two terms cease to have an effect on the overall flow profile. One can then re-dimensionalize the remaining terms, leading to the Stoke's Flow equation.

$$\nabla P = \mu \nabla^2 u$$

Equation 4: Stoke's Flow

*Table 1: Non-dimensionalized variable substitutions. A * denotes a non-dimensionalized variable. l, U and t_{ref} are the characteristic length, velocity and time scales.*

Non-Dimensionalized	Equivalent	Substitution
x^*, y^*, z^*	$\frac{x}{l}, \frac{y}{l}, \frac{z}{l}$	$lx^*, ly^* l, z^*$
∇^*	$l\nabla$	∇^*/l
u^*	$\frac{u}{U}$	$u^* U$
t^*	t/t_{ref}	$t^* t_{ref}$
P^*	$P/\frac{\mu U}{l}$	$P^* \frac{\mu U}{l}$

1.1.4 Pressure Driven Flow

The microfluidic devices used in this thesis all operate under pressure driven flow. That is, a pressure gradient is produced that drives the fluid from the inlet to the outlet. Fluid flows in channels operate under a "no-slip condition" where the fluid flow at the surface of the wall of the channel has the velocity of the wall of the channel, in this case at rest. As flows are continuous this creates an increasing gradient of flow velocity as you leave the wall of the channel. Starting from the Stokes flow equation and using the no-slip condition as the boundary conditions, one can solve for the velocity profile.

For pressure flow between two plates that are longer and wider than they are distant from each other, the stokes flow simplifies to $\frac{d^2P}{dy^2} = \mu\frac{d^2u}{dx^2}$ where y is the coordinate perpendicular to the plates and x is the direction of flow. Solving for the velocity profile shows that it is a parabola, as can be seen in Figure 2.

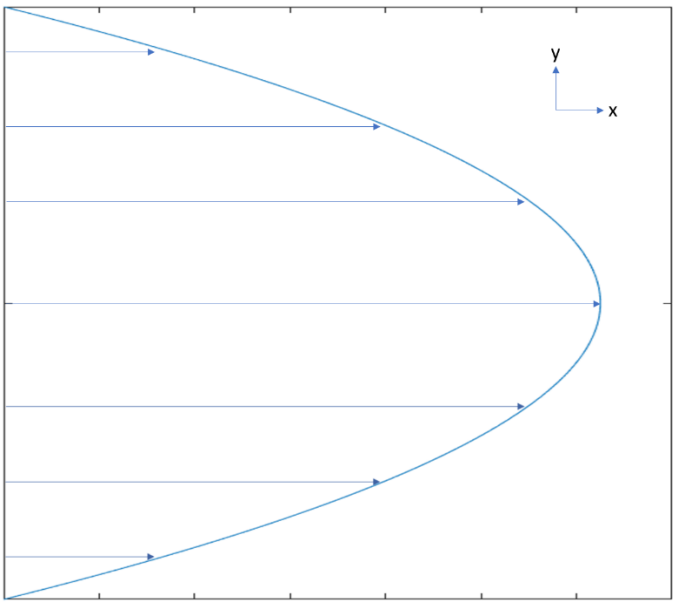

Figure 2: Poiseuille Flow Profile between two infinite plates. The highest velocity is found in the center of the channel away from the walls, while flow at the walls is held still due to the no-slip conditions in the channel.

For channel geometries that are fully rectangular the profile gains dependence along z as well, making the exact profile much more difficult to determine. However, as the paraboloid nature of the Poiseuille flow persists no matter the aspect ratio the exact profile is unlikely to be a cause for concern for most applications. [20], [22]

1.1.5 Diffusion and Multiphase Flow

When two flows meet in a laminar flow regime, they will not immediately mix due to the lack of turbulence. In these conditions, the length it takes for the phases to diffuse into each other is represented by the dimensionless Peclet Number, where D is the diffusion coefficient of the solute, u is velocity and L is again the characteristic length of the channel. [21], [23]

$$Pe = \frac{uL}{D}$$

Equation 5: Peclet Number

The higher the Peclet number, the longer it takes for diffusion to mix the two phases, due to either a wider characteristic length of the channel, or a smaller diffusion constant, which is

generally defined by the Stokes-Einstein relation, where k_B is the Boltzmann constant, T is temperature and d is the diameter of a particle. [17]

$$D = \frac{k_B T}{3\pi\mu d}$$

Equation 6: Stokes-Einstein Relation

A general rule of thumb is the length of a channel needed to mix the two phases is the characteristic length of the channel, multiplied by the Peclet number. [17] In general the diffusion follows the one dimensional case of Fick's second law, starting as an asymptotic boundary then becoming a sigmoidal function of decreasing slope as it progresses along the channel, a representation of which for an infinite channel can be seen in Figure 3. [20], [24]

For high Peclet numbers, or more typically with immiscible fluid phases, each phase maintains a portion of the channel to flow in. The width of a flow w, depends on the viscosity of the fluids μ, their flow rate Q, and the diameter of the channel d. [23] This is under the assumption of a significantly wide channel.

$$\frac{\mu_1 Q_1}{w_1} = \frac{\mu_2 Q_2}{w_2}$$

Equation 7: Relationship of Channel Fraction based on Viscosity and Flow Rate

When viscosities are similar, the equation can be rearranged to give the width as the fraction of the flow compared to the combined flow rate of every phase. This can be adjusted by modifying the hydrophobicity of the surface of a channel. High interfacial energy between a phase and the channel wall promotes the other phase to wet it in its place, leading to the detachment of a phase from the walls of the channel creating instead jets or drops instead of a defined flat interface. [25]

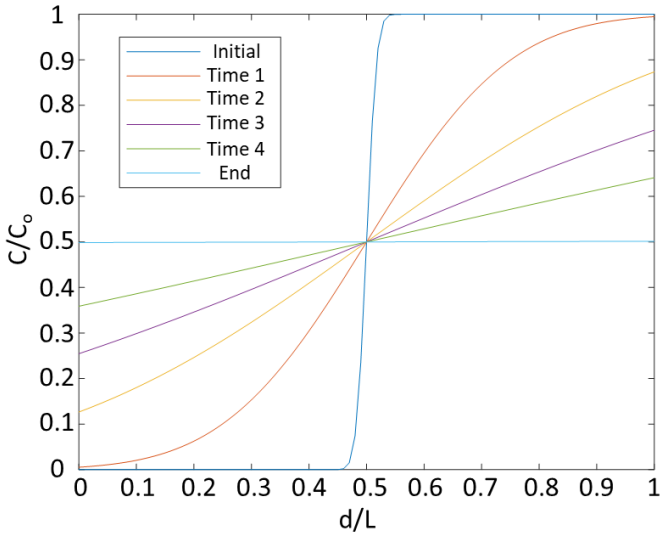

Figure 3: Diffusion in an infinite microchannel. When two flow meet, there is a slow diffusion down the microchannel until the concentration equalizes. C is the current concentration of the phase at a given point in the cross section of the channel, C_o concentration of the phase in the inlet before diffusion, d is the position of the point in the cross section of the channel and L is the characteristic length of the channel.

1.1.6 Microfluidic Emulsions Droplet, Flow-focusing

By manipulating immiscible flows using special geometries, microfluidic channels can passively generate emulsions with far greater control over the droplet properties than in bulk methods. These systems use a continuous phase as a carrier and as a cleaving agent which impinges on the flow of the second dispersed phase leading to the creation of droplets due to the interfacial tension between the phases. [11], [21], [26]

The most common passive pressure driven geometry types are crossflowing, co-flowing and flow-focusing. These are differentiated by the intersection of the two phases, and how that influences droplet formation. Diagrams of these three geometries can be seen in Figure 4.

Crossflowing devices, also known as “T-Junctions” operate by creating an orthogonal channel for the dispersed phase that meets into the continuous phase channel. As the dispersed phase flows into the main channel, it begins to block the continuous phase causing a pressure build up that eventually forces the extrusion to break off from the flow into a droplet. The droplets

produced by these geometries are controlled by the size of the channels and the flow rates and typically boast the greatest monodispersity, but without parallelization produce droplets at the lowest frequency as high flow rates eventually lead to the two phases co-flowing down the main channel without droplet formation. [11], [26]

Co-Flowing geometries are often either three parallel channels that combine into a single channel, with the dispersed phase sandwiched between two continuous phase flows, or a coaxial geometry with a capillary centered in a larger channel. As the streams meet, the disperse phase begins to have applied shear stress from the surrounding continuous phase which breaks off into droplets as it overcomes the interfacial tension. [11], [26], [27]

Flow-focusing geometries are similar to co-flow, but the continuous phase flows meet to pinch the dispersed phase in a smaller jet. Typical flow-focusing geometries consist of the dispersed phase meeting two perpendicular continuous phase flows followed by a "focusing nozzle" which is often simply a smaller section of channel that limits the cross-sectional flow. The dispersed phase is deformed into a thin stream by the continuous phase and the effects of the shrinking area, which then breaks into droplets. The size of the nozzle constrains the dispersed phase stream, allowing for improved stability of droplet formation at higher flow rates compared to the other geometries and can be produced with simpler microfabrication processes than the insertion of glass capillaries found in co-flow. [11], [13], [21], [26] When using water as the dispersed phase, these channels can produce droplets at 10s of kHz, at only a few microns in diameter with monodispersity less than 5% variation. [11] This geometry was the one used in this thesis, as flow-focusing geometries typically allow for higher throughputs than crossflow, and for smaller cocoon sizes than co-flow devices. [11]

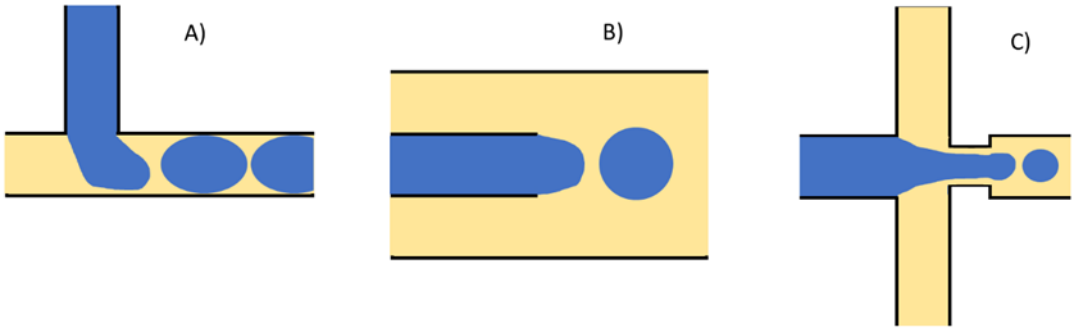

Figure 4: Common Passive Microfluidic Droplet Generating Geometries: A) Crossflow B) Co-Flow C) Flow-Focusing

1.1.7 Reyleigh-Plateau Instability and Dimensionless Numbers

Droplet formation in flow-focusing geometries can occur under various regimes based on the flow rate of the two phases and is driven by the Rayleigh-Plateau Instability where thin streams will break up to equilibrate surface tension. The two main regimes are the "Dripping" regime where the instability breaks off the droplet close to the nozzle, and the "Jetting" regime where the disperse phase maintains a thin jet until after the nozzle which breaks into droplets along its length.[28], [29] An example of the dripping and jetting regimes can be seen in Figure 5.

Two dimensionless numbers mark the transitions between the regimes, based on the ratio of viscous, inertial and surface tension forces acting at the nozzle. The first is the Capillary number, which is the ratio of viscous and interfacial forces. μ is the viscosity of the continuous phase, u_c is the velocity and $\gamma$is the interfacial tension between the two phases. [29]

$$Ca = \frac{\mu u_c}{\gamma}$$

Equation 8: Capillary Number

The other is the Weber number which is a ratio between the inertial and interfacial forces where u_d is the velocity of the dispersed phase, ρ is the density of the dispersed phase and L is the characteristic length of the channel. [29]

$$We = \frac{\rho u_d^2 L}{\gamma}$$

Equation 9: Weber Number

When both numbers are small, much lower than 1, surface tension forces dominate allowing the instability to form monodisperse droplets in the dripping regime. When the Weber number increases, the flow rate of the dispersed phase outstrips the timescale of droplet formation causing a jet to form. When the Capillary number instead increases the viscous force prevents the "wave" formation that begins early in the instability, again forming a long jet rather than monodisperse particles. [29] As both of these numbers depend on surface tension, it is possible to moderate them through the concentration and HLB value of the surfactant used. Increasing surface tension of the two phases helps increase the range of the dripping regime, but as mentioned earlier high surface tension leads to the created droplets being unstable and recoalescing. [30] The formation of a stable emulsion is thus a balancing act of keeping the generated droplets from collapsing and forming monodispersed droplets higher flow rates.

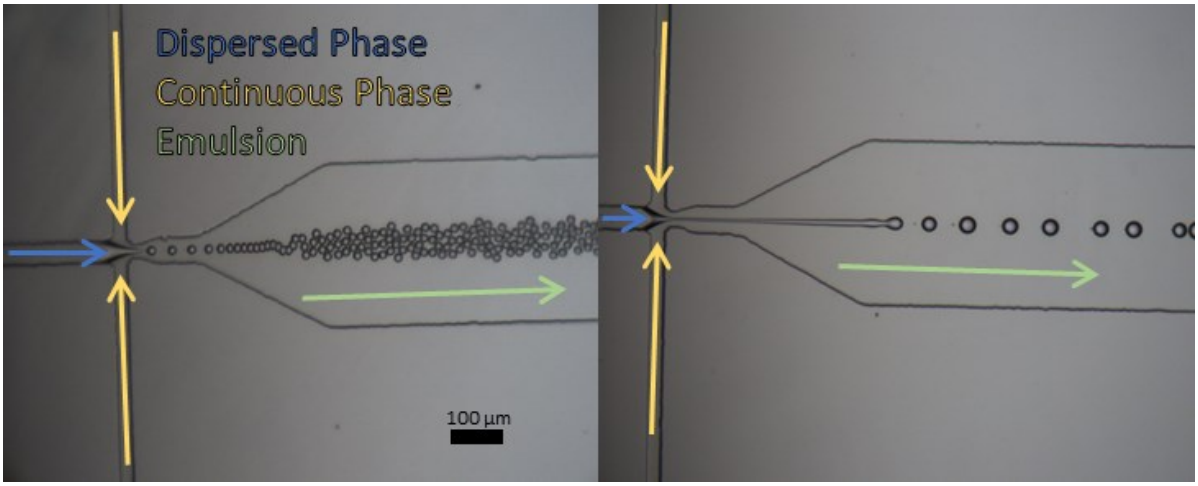

Figure 5: Dripping (Left) and Jetting (Right) in a Flow-focusing Nozzle. At low Ca and We, the dispersed phase quickly breaks into monodisperse droplets. When either number increases, the dispersed phase instead extends into a long jet before beading.

A third dimensionless number, the Ohnesorge number, also acts on the formation of jetting behaviour and relates the viscosity of the dispersed phase to the inertial forces. It is a relation between the Reynolds and Weber numbers. [17], [31]

$$Oh = \frac{\sqrt{We}}{Re} = \frac{\mu}{\sqrt{\rho\gamma L}}$$

Equation 10: Ohnesorge Number

As the Ohnesorge number increases, either through an increasing Weber number or increasing viscosity of the dispersed phase, the instability in the flow cylinder becomes depressed leading to the formation of a jet. [32] Thus not only is the surface tension between the two phases important to optimize, but the viscosity of the dispersed phase also needs to be as minimal as possible for the formation of monodisperse droplets.

1.2 Emulsions

As mentioned, microfluidic devices are capable of creating emulsions out of two immiscible phases. These are typically oil-in-water (O/W) or water-in-oil (W/O) where an aqueous phase and an organic phase are broken up through the addition of energy by agitation creating a suspension of droplets. These suspensions are inherently thermodynamically unstable as the high surface energy of the interface drives the droplets to recombine into a single phase to reduce the energy of the system. [33]

1.2.1 Surfactants

To stabilize emulsions, surfactants are used. These are compounds that lower the surface energy by gathering at the interface and creating a steric barrier between droplets. Surfactants are typically designed with hydrophilic heads, and hydrophobic tails which are typically fatty chains. Depending on the head group, surfactants can be anionic, cationic or non-ionic with varying use cases. [30], [33], [34]

When creating an emulsion, the choice of surfactant needs to account for the conditions of the emulsion, the phases being used and the type of emulsion being made. For instance, anionic surfactants need alkaline pH to be effective, while cationic surfactants cannot be used in biological applications as they interact poorly with negatively charged cell membranes. Nonionic surfactants can be used in a broad pH range where they exist with no predominant charge, but may be too viscous for certain applications. [34]

Many nonionic surfactants are made with alcohols, ethers or esters as a hydrophilic head group, bonded to long fatty carbon chains or silicon based chains like polydimethylsiloxane. One particular group, sold as “Spans”, are esters of sorbitol connected to a fatty acid and are extremely widespread in pharmaceuticals and foods as they are low-toxicity even at high concentrations. [34], [35] Another group known as “Tweens” are Spans that have had a 20 mole chain of ethylene oxide bonded to the head group, known as polysorbates. While Spans are mainly hydrophobic and are used in W/O emulsions, the hydrophilic ethylene oxide group makes Tweens more suitable for O/W emulsion. [34] Additionally, the similar chemical structure of Spans and Tweens means that they can stack along the oil-water interface making a denser surfactant layer at the surface. [35]

Increasing the concentration of a dissolved surfactant results in a decrease in interfacial tension between two phases, up to the “critical micelle concentration” where the interface is saturated and any further dissolved surfactant forms micelles in the solvent to limit the exposure of the headgroup. [34], [36] This decrease is tied to an increase in the Capillary and Weber numbers, and so stabilizing the two phases has a negative impact on the formation of monodisperse droplets but a positive impact on keeping the resulting droplets from coalescing in the microchannel.

1.2.2 HLB

W/O and O/W emulsions require different surfactants to properly stabilize as the surfactant needs to orient to provide the steric barrier between pockets of the dispersed phase. Nonionic surfactants fall on a “Hydrophile Lipophile Balance” (HLB) scale which predicts how they interact

with the organic phase by comparing the molecular weights of the hydrophilic and hydrophobic sections of the surfactant. A higher HLB "appears" more hydrophilic and helps stabilize O/W emulsions, while a lower value stabilizes W/O. [28], [30], [34], [35] These values can be determined through the "Davies Method", a proprietary titration method to determine Hydroxyl content from an American Oil Chemists' Society publication AOCS Cd 13-60, or from finding existing values in literature tables. [35] Sorbitol based surfactants HLB values change based on the length of the fatty tail, with more carbons lowering the HLB. A brief list of some Span and Tween surfactants and where they fall on the HLB scale can be found in Table 2.

Table 2: Small Selection of Sorbitol Based Surfactants and their HLBs [34], [35]

HLB Value	*Application*	*Surfactants*	*Surfactant HLB*
2-3	Antifoaming	Span 65	2.1
3-6	W/O Emulsifier	Span 80	4.3
7-11	Wetting agents	Span 20	8.6
		Tween 65	10.5
8-18	O/W Emulsifier	Tween 80	15
		Tween 20	16.7

As mentioned previously, these surfactants can be mixed together, and they will both aggregate at the phase interface. In doing so, a combined HLB value will be made accounting for the properties of both surfactants. This is typically used for solubilizing different oils, or different combinations of oils which may require specific HLB values due to the presence of differing hydrophobic and hydrophilic moieties changing the solubility of surfactants. [35] The final HLB is simply the addition of each surfactants individual HLB, multiplied by the mass fraction each surfactant takes up of the combined surfactant mix. [37] An example equation for two surfactants can be seen below, but this can be extended for additional surfactants.

$$HLB_{Mix} = \frac{Mass_1 * HLB_1 + Mass_2 * HLB_2}{Mass_1 + Mass_2}$$

Equation 11: Combined HLB Value of Mixed Surfactants

Due to differences in solubility and self assembly at the interface, surfactants of different HLBs and different mixtures of surfactants can have varying effects on the interface between phases even at the same overall concentration. This can change the observed surface tension and can influence the overall emulsion stability. [34], [35], [38]

1.3 Therapeutic Cell Encapsulation for Regenerative Medicine

Regenerative medicine through the use of therapeutic cells is a growing option for treating damaged tissue resulting from chronic injuries such as, but not limited to, cutaneous wounds, [39] glial scarring from spinal cord injuries, [5] and heart infarctions that currently lack other effective treatment options. [2]

These therapies take advantage of the differentiation and paracrine signalling capabilities of various cells such as stem cells. Cells are harvested either autologously from the patient, or allogenically from a healthy donor. [40] In the case of engraftment, therapeutic cells are either injected at the site of the injury as a suspension where the present niche induces them to differentiate and fill in for the damaged tissue, [1], [7] or are grown in scaffolds that mimic basic tissue structure that can then be surgically implanted. [40] Paracrine signalling based therapies does not rely on the stem cells themselves, but the cytokines they emit that influence the existing tissue. [1], [41] These cytokines can induce the migration of healthy cells to the site of the injury, or counteract inhibitory growth factors given off by cells forming scar tissue. [1], [41], [42]

One particular area where stem cell therapy is under investigation is in regenerating the heart tissue after a myocardial infarction. [2], [43] After an infarction, there is an area of heart muscle that dies and forms scar tissue.[44] This scar does not regenerate and leads to a loss of function in the heart. [40], [45] Over time, to compensate for loss of function the ventricle begins to enlarge to maintain the same flow rate of blood. This stretches the scarred area, thinning it

which can eventually lead to heart failure. [44] The injection of Mesenchymal Stem Cells (MSCs) has been shown to reduce the size of the infarct scar and to help retain heart function, in both *in vivo* studies and randomized controlled trials.[2], [8], [40], [43]

The primary mechanism of this effect appears to be through "indirect" regeneration of tissue. The new regenerated tissue appears to be from the stimulation of endogenous repair from excreted paracrine factors rather than the injected cells directly forming the new tissue themselves. Injected suspensions of bare MSCs show low short term retention, and almost no long term retention with cells being almost completely absent by one month. [6] The amount of cells injected appears to have little impact, with the same ratio retention being found between orders of magnitude of injected cells. [7] Some of this appears to be due to clearance, as after injection, radiolabeled cells could be found throughout the body, especially in the lungs.[7], [46] The other contributing factor is that the site of an infarction is inhospitable to cells leading to cell deaths from oxidative stress and inflammation,[8], [47] or from anoikis due to lack of attachment from being injected as a suspension. [1], [2]

1.3.1 Stem Cells

Stem cells are defined by their ability to self renew, and to differentiate into the different functional cells that make up the types of tissues found in the body. There are many different levels of stem cells based on their multipotentancy. The cells found in a zygote are totipotent, able to turn into any type of cell. Over the course of gestation these differentiate into different multipotent lineages that stay present in the body, which differentiate into unipotent precursor cells, that eventually become somatic cells which provide a unique function but lack self renewal capabilities. Unlike somatic cells, stem cells can be harvested autologously or allogenically and be cultured in a lab, then frozen for later implantation in the body. [1], [40]

Stem cells are directly connected to their Niche, a collection of physical and chemical factors that influence their growth. Inside the body, cells are surrounded by networks of proteins referred to as "Extra-Cellular Matix" materials (ECM materials). The function of these EMC materials is to provide mechanical support and to provide cues for behaviors such as orientation,

growth and renewal. [48] Cells, both stem and somatic, also communicate by releasing cytokines through vesicles to mediate behavior. [40] This reliance on adherence to niche EMC materials is also the cause of anoikis, making replicating the niche an important part in utilizing stem cells. [2]

While not fully understood, differentiation in stem cells has been linked to many different aspects of the niche. As an example, mesenchymal stem cells (MSCs) are a type of stem cell found in bone marrow and are capable of differentiating into a wide variety of structural and connective tissue cells. [1], [49] Two common fates for these types of cells is osteogenesis and adipogenesis, turning into bone or fat cells.[49] Recent research has shown a competition between these two fates the ability to control this differentiation through multiple mechanisms. By inducing stresses on the cytoskeleton shape or by culturing them on stiff substrates or substrates with a grating with a 100 nm pitch osteogenesis could be routinely triggered, while softer substrates favoured adipogenesis. [50], [51] Replication of the niche is an important aspect of developing and improving cell based therapies, to promote the proper growth and behaviours in the therapeutic cells.

1.3.2 Encapsulation

Encapsulation of cells in scaffolds is a common method of enhancing cell therapy. By encapsulating cells, the scaffold provides structural support that can direct growth and aid in preventing anoikis, [2], [40], [52] while also providing an immunoprotected barrier to keep stem cells isolated from inflammatory effects. [3], [4], [53] Hydrogels are a common scaffolding material as their porous nature allows for the inward diffusion of oxygen and nutrients, and the outward diffusion of waste and therapeutic products.[3], [4] A graphical representation of this can be seen in Figure 6. Many hydrogels are made from naturally sourced materials such as polysaccharides, which come with biocompatibility, biodegradation and elastic properties that resemble various tissues, allowing them to act as substitute ECM for cells.[3], [4], [54]

The use of these scaffolds alongside MSCs and other stem cells in treating infarcted heart tissue has shown improvements in research and clinical trials. [55] Cells encapsulated in a scaffold

at the site of an infarction can be found alive weeks after insertion, while cells that were injected as a suspension are nearly non-existent. [6], [56] This longer residence shows a general trend of improving heart function in rats, with a visually apparent reduction in infarct size . [6], [8]

One area macro-scaffolds are deficient in is the diffusion of nutrients. In a thick hydrogel, oxygen forms a gradient that limits its reach to the innermost cells, meaning a scaffold can typically support cells in only 5-10% of its volume [3], [57] By instead encapsulating individual cells in micron scale hydrogel spheres, every cell is located near the surface of a scaffold due to the increase in overall surface area. This corresponds to a higher cell density in a given volume of scaffolding and faster diffusion due to the small size of the cocoons. [3], [13], [57]

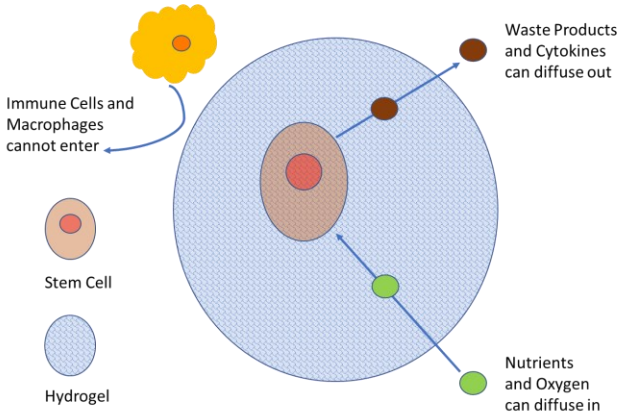

Figure 6: Concept of Microencapsulation. Porous hydrogel allows the diffusion of nutrients, waste and therapeutic products while protecting encapsulated cells from immune response at the site of injury.

1.3.3 Agarose

Agarose is a linear polysaccharide chain derived from seaweed. [3], [4] At low temperatures, the polymer chains undergo a sol-gel transition into a solid hydrogel that is biocompatible but not biodegradable. [4] In tissue engineering, agarose has been approved for testing as implants for various parts of the body, [3], [58] and has seen wide use as a material for cell encapsulation. [14], [52], [59], [60] Despite this, agarose has no moieties in its structures that allow cells to adhere, limiting the interaction between cells and the surrounding matrix. [4]

Agarose is a thermo-reversible hydrogel. At temperatures above the melting temperature, the chains exist in solution as random coils. As the temperature decreases, the structure changes to a double helix and aggregate through hydrogen bonding. [3], [4] The gelling and melting temperatures of agarose show a wide hysteresis, though the exact temperatures depend on the concentration of the gel, the length of the chains and the degree of sulfation of the chains. [4], [61] When agarose is heated above the melting temperature, cooling it to below the melting temperature will not turn it back into a gel. It must be cooled below a lower gelling temperature, and will then stay solid above the gelling temperature until it has again reached the melting temperature. [61] For the agarose used in applications with cells, the melting point can be above 50^{o}C, while the gelling temperature is below 20^{o}C. [62] This allows for encapsulation to be done at physiological temperatures to avoid stress on the cells, but then once gelled the agarose cocoons can be injected into the body without melting. [14], [59]

Previous research in the Godin Lab involving cell encapsulation has used agarose as the primary material for cell encapsulation due to its biocompatibility, robust thermal and physical stability, and its convenient rheological properties for use in microfluidic devices allowing for high viability of encapsulated cells. [15], [60], [63] Work is currently underway to promote cell adhesion to the cocoons, through the addition of ECM materials into the matrix such as fibronectin to remove one of the downsides to its use. [4], [52], [59] While the lack of biodegradability is somewhat on an issue *in vivo* as it can lead to the prolonged retention of empty agarose in the body it is seen as a benefit for experimental purposes at the current moment as it provides a stable scaffold for retaining cells to track metrics such as viability. [3] In the future, modification of agarose to include programmed degradation is potentially an avenue for therapeutic improvement.

In this thesis agarose serves as the outer layer of the hollow cocoons. “Ultra-low- Gelling Temperature, Molecular Biology Grade” agarose Type IX-A is the historical type of agarose used for encapsulation, but due to its more suitable thermal properties “Ultra-Low Gelling Temperature” Type IX agarose was substituted in for the formation of hollow cocoons. [62], [64]

1.3.4 Poloxamer

Poloxamers are block copolymers consisting of end group blocks of hydrophilic Poly(ethylene oxide) (PEO) and a center block of hydrophobic Poly(propylene oxide) (PPO), a visualization can be seen in Figure 7. [65] This structure makes the polymer amphiphilic like a surfactant with the ends of the chains favouring aqueous phases while the middle prefers organic phases, and poloxamers are sometimes used to stabilize emulsions. [66]

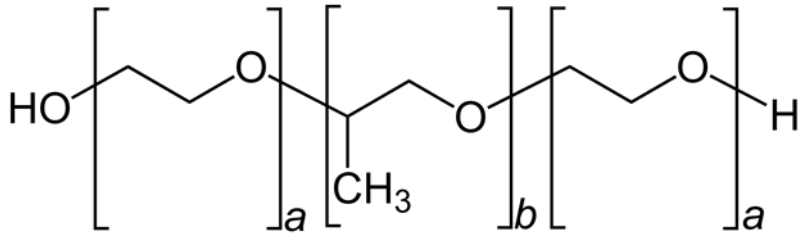

Figure 7: Composition of Poloxamers. "a" blocks are Poly(ethylene oxide), "b" block is Poly(propylene) oxide

The relevant application of poloxamers as it relates to this thesis is their ability to form thermo-reversible gels. At low temperatures, poloxamer chains exist in aqueous solution, with the water hydrogen bonding to the PEO blocks favoring an open conformation rather than sequestering the hydrophobic PPO block. There are however critical micelle concentrations (CMCs) and temperatures (CMTs) that transform the solution into a gel. At a given concentration, raising the temperature above the CMT will provide enough energy for the chains to favour the formation of micelles, which physically entangle forming a solid gel. Once formed, cooling the gel disrupts the stability of the gel, returning it into a solution [65], [67]

The temperature required to form a gel varies by both the concentration and the structure of the polymer blocks. Larger percentages of PEO blocks to the PPO block increase the temperature needed to form a gel due to the increasing hydrophilicity of the polymer. [65] For a given poloxamer, an increasing concentration lowers the needed temperature to form a gel. [68]

At least some poloxamers have been proven to be safe in use with cells, and have previously been used to encapsulate cells in hydrogel scaffolding. [69], [70] Pluronic F-127 specifically was chosen to undergo testing due to previous literature showing its use, and a CMT occurring

between 15-30°C for the working range of gelling concentrations which would allow it to gel at temperatures acceptable for maintaining cell viability. [68]

1.3.5 Gelatin

The other hydrogel used in this thesis to encapsulate cells is gelatin, a protein by-product of the hydrolysis of collagen that changes it from a triple helix to single strands. [4], [61] It is highly biodegradable and shows low to no immune response when implanted in the body, and has FDA approval for use in tissue engineering. [71]

Gelatin is another thermo-responsive hydrogel. The exact melting temperature is variable, depending on the concentration of the gel, the molecular weight of the chains and how long it has been gelled. [61], [72] It can also be influenced by the presence of sugars and polyols, increasing with the presence of sugars and glycerol but decreasing with methanol or ethanol. [73] Unless chemically crosslinked, this melting temperature is always less than body temperature making encapsulation of cells infeasible for purely gelatin cocoons. [61] The gelatin used was "Gelatin from porcine skin" (Sigma-Aldrich, Type A, 300 Bloom) as it was thought the high bloom would provide mechanical stability through the encapsulation process and because Type A gelatins are neutral at physiological pH to avoid electrostatic complications. [74]

1.3.6 Single Emulsions

One method of producing microencapsulated cells is through vortex mixing. This method involves adding liquid hydrogel with suspended cells to oil being vortexed before gelling the resultant emulsion. This method produces cocoons with high polydispersity and low encapsulation, [52], [75] which can be a problem when attempting to create consistent doses of encapsulated cells.

To produce more monodisperse samples, microfluidic channels can be used to generate emulsions using liquid hydrogel as the dispersed phase. While the increased viscosity limits the rate of cocoon generation when compared to simple W/O emulsion generation due to a larger Ohnesorge number, flow-focusing devices have been proven to still be able to generate hydrogel

cocoons at high throughputs. An example flow-focusing device was able to produce 55 µm cocoons at 250 Hz, and by tuning the flows also create 20 µm cocoons at 3900 Hz. [12] Work previously done in the Godin Lab was able to encapsulate cells in 80 µm cocoons at 200 Hz, and 60 µm cocoons at 600 Hz using the same device. [60]

The specific design and function of the flow-focusing encapsulation of cells done in this thesis will be further reviewed in the Methods section.

1.3.7 Poisson/Occupancy of Single Emulsions

In statistics, a Poisson Process is a random process where events randomly occur over specific time intervals, independent of whether an event has occurred previously. There is an assumed average rate that events occur, events cannot occur simultaneously and there is a small time offset between events. In this type of process, the probability of a number of events occurring with a certain average rate is given by:

$$P(x, \lambda) = \frac{e^{-\lambda}\lambda^{x}}{x!}$$

Equation 12: Poisson Process Probability for the Encapsulation Rate of Flow-Focusing Microfluidics

Where "x" is the number of measured occurrences in an interval and λ is typically the mean number of events multiplied by the time interval. [76], [77]

It has been shown that for the encapsulation of individual cells through passive processes like flow-focusing, the occupancy of cells in cocoons matches the Poisson distribution. In the flow-focusing geometry, there is a stream of cells in the dispersed phase that are randomly placed throughout the stream, which reach the nozzle at random times creating random independent events with a mean occurrence based on their concentration in the sample. Due to the monodispersity of flow-focusing there is a constant volume of sample extruded through the nozzle that makes up each cocoon, which represents the time interval of the distribution. Thus, for the cell encapsulation process, the λ term is found through the concentration of cells in the sample, multiplied by the volume of a cocoon. Due to this it is possible to calculate the percentage of cocoons that will contain no cells, one cell or any number of cells. [76]

1.3.8 Cell Egress

While microencapsulations containing single cells have been shown to improve retention, there are still inadequacies. Recently it has been found that over time cells will attempt to exit the cocoons, increasing the clearance rate of the cells as they become exposed to the environment outside. [78] While this behaviour might be beneficial for engraftment, as previously mentioned the primary effects of stem cells on the heart is through paracrine effects, meaning that for this purpose keeping cells encapsulated for the duration of their retention is preferred. [79] Additionally, un-encapsulated cells show high amounts of mechanical clearance from areas such as the heart, being distributed throughout other organs due to them washing away through the bloodflow. [7] This is especially important as therapeutic cells such as MSCs and Endothelial Progenitor Cells show higher cell egress rates, and lower viability amongst cells that cannot egress when encapsulated in agarose supplemented with ECM material. [14] While the exact mechanisms of egress are still unknown, cell proliferation appears to be a factor, with daughter cells appearing to be able to push out of cocoons. [14] Increasing hydrogel concentration and cocoon size are also able to control egress, with bigger cocoons or those with higher concentrations showing lowered egress rates. [14], [15] Additionally, cells are randomly placed throughout the cocoon when they are encapsulated and as such are often located near the edge of a cocoon. Cells located at edges have much thinner layers of hydrogel, allowing them easier escape. [80]

1.3.9 Double Encapsulation

As a way to better understand and control cell egress from cocoons, previous work in the Godin lab was to generate double encapsulations of cells. [15] One typical way to produce these encapsulations is through three phase emulsions, where instead of simply W/O or O/W emulsion, another outer phase is introduced creating a shell layer. These can be generated in microfluidic channels through the use of glass capillaries and coaxial flows to combine co-flow and flow-focusing geometries.[81], [82] Briefly, a glass capillary containing the innermost phase is surrounded by a co-flow of an immiscible middle phase. These two phases meet the outermost

continuous phase flowing in the opposing direction, and all three phases are flow-focused into a second capillary which breaks the co-flow into dispersed droplets. A visualization of this can bee seen in Figure 8. By putting these in sequence, this can begin to produce triple or further emulsions.[81]

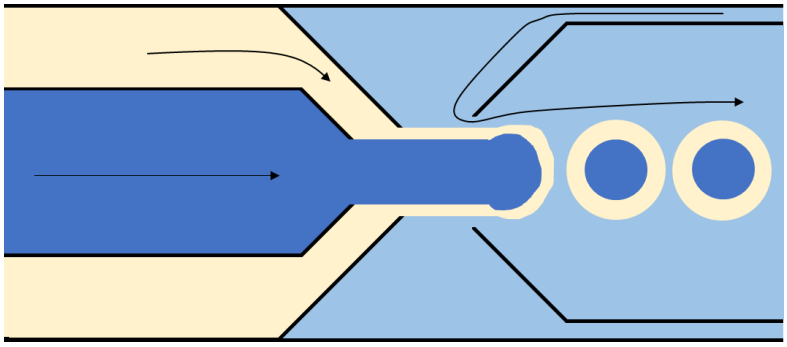

Figure 8: Co-Flowing Flow-Focusing geometry for double emulsion generation. The inner dispersed phase leaves a glass capillary to a second immiscible dispersed phase that then enters another capillary along with the continuous phase to form droplets.

For cell encapsulation purposes, this method has drawbacks in that throughput is necessarily low to keep the flows stable entering the second capillary, and in order to create solid droplets oil phases are encapsulated inside the cocoon as well. [82]

An alternate method is to do a two step encapsulation process, encapsulating cells in a flow-focusing geometry, purifying the sample and then re-encapsulating the generated cocoons in another layer. [83] The method used by the Godin lab was to re-encapsulate cells in a second cell-free layer of agarose so that no cells were located near the edge of the cocoon. It was found that the addition of a second layer drastically reduced egress, from 60% down to 20% when compared to single encapsulated 3T3 cells, with no significant comparative drop in viability over 48 hours. [15] Based on this result, the positioning of cells within the cocoon does appear to be a relevant factor in cell egress and a second encapsulation can be a viable way to mitigate this.

1.3.10 Hollow Cocoons

A modification on the double encapsulations that has been done previously are cocoons with hollow cores. As previously noted, encapsulated MSCs attempt to proliferate while encapsulated, but the lack of space in the solid hydrogel pushes the daughter cells through the cocoon. [14] The encapsulation in hydrogel in fact appears to suppress proliferation, which limits the amount of potential therapeutic cytokines that can be generated. [84] By instead producing hydrogel cocoons with hollow cores, the immunoprotective nature and the diffusion of nutrients and waste are still present but cells are now free to use the inner wall as an attachment site and can use the free volume to stretch and proliferate. [83], [84] Cells encapsulated in these style of cocoons have shown the tendency to form aggregates in the hollow volume with high viability, [85], [86] and encapsulated cells implanted next to tumours in mice showed reduction in tumour size showing the hollow cocoons can potentially be viable for therapeutics. [83]

Hollow cocoons have been generated using a similar system to the capillary based method for double encapsulations. Rather than relying on an inner oil phase to form the double emulsion structure, they instead use Aqueous Two Phase Systems (ATPS), or All-Aqueous-Phase Systems. [85], [87] These utilize high molecular weight hydrogels that phase separate at high concentrations leading to an outer shell phase that crosslinks, and a fluid core that later diffuses out of the shell when placed in aqueous media. These processes are cell friendly and can produce cocoons in a single encapsulation step with less than 10% polydispersity. However they require complex microfluidic devices and reagents to properly phase separate, and reported throughputs have been as low as 2 Hz. [85], [87]

A different method utilizes two encapsulation stages similar to the double encapsulation utilized by the Godin lab previously. [15] The first step encapsulates cells in a hydrogel such as alginate that gels with the addition of ions. After removing the continuous oil phase, the core cocoons are then re-encapsulated in a hydrogel with a different gelling mechanism such as thermo-responsive hydrogel to form the outer shell. After the outer shell is gelled, the core is liquified freeing the cells in the core. [83], [86]

The method of hollow cocoon production in this thesis shows similarities to the second method, but rather than using hydrogel cores that require later steps such as chelation to liquify the core, both materials are thermo-reversable for the minimum cell stress. As mentioned previously, agarose once gelled will not melt until above 50^{o}C making it stable at physiological temperature. Gelatin however melts when exposed to temperatures reaching physiological conditions, and poloxamers would melt when the cocoons were cooled to gel the agarose. By encapsulating cells in a less thermally stable hydrogel, then creating an agarose outer shell, hydrogel cocoons can be produced that later turn into hollow microcapsules without any additional processing just by placing them into an incubator or injection into an *in vivo* location.

A two step process was chosen for several reasons. ATPS typically require expensive and often custom synthesized polymers to make the phases, and due to their careful phase balancing currently operate under slow flow rates or require active droplet formation. Other one step processes will encapsulate oil along with the inner core. While two step processes require a sample purification step, they can be done with more common phases, less complex microfabrication and both stages can be high throughput potentially taking less time overall for both steps than a slow throughput single step.

1.3.11 Microfabrication

The prototyping cycle for designing microfluidic channels for cell encapsulation comes with inherent restrictions The materials need to be biocompatible, the process needs to be able to make high aspect ratio features such as pillars, devices need to be inexpensive and fast to produce while in a laboratory setting, and there needs to be fast turnaround between making an alteration to the design and making the next iteration of the device. [88]

For material selection, silicon, the traditional microfabrication material, is expensive and opaque. Glass is cheaper but requires milling or chemical etching to form channels and is difficult to bond with other surfaces to form a watertight seal. The microfluidic devices used in this thesis were made with poly(dimethylsiloxane) (PDMS), an optically clear elastomer that is biocompatible once cured. [89] The PDMS used in this thesis is Sylgard 184, a two part elastomer that cures when the dimethylsiloxane base is mixed with a crosslinking agent, and is exposed to

heat. [90] PDMS devices are typically paired with soft lithography processes, pouring uncured PDMS on a mold to form channels. [91], [92]

Photolithography is done through exposing a photosensitive polymer known as a photoresist to high intensity UV light through a photomask. Photoresists can be either “positive” or “negative” in nature and can greatly vary in their properties A positive photoresist breaks down under UV, while a negative photoresist crosslinks. After exposure, a resist specific “developer” solvent is used which washes away the unwanted resist leaving only the desired pattern. [88], [91], [92] In order to create a flat layer of photoresist, it is applied to a polished silicon wafer through spin coating. During spin coating a portion of liquid photoresist is applied to the center of the wafer, which is then rotated at hundreds to thousands of rpm. The rotation causes the liquid resist to flow outwards radially, with the final thickness dependant on the viscosity of the resist and on the rpm chosen. [93] After exposure, the resist undergoes a series of high temperature baking steps that removes the rest of the solvent and sets the mechanical properties of the resist, before chemical etching removes the excess resist leaving only the mold.[88], [94]

For this project, SU-8 2050 was used as the photoresist. It is a high aspect ratio, negative photo resist produced by Kayaku Advanced Materials that can fabricate the high vertical sidewalls of the channels and filter pillars required for the device. It crosslinks using an epoxy driven process under UV light, and can be deposited in thicknesses between 170 and 40 microns through spincoating. [94]

To finish microchannel fabrication, the PDMS was bonded to glass microscope slides using O2 plasma bonding. When surfaces containing silicon, such as PDMS and glass, are exposed to O2 plasma they develop silanol groups. When these surfaces come into contact, they dehydrate forming covalent Si-O-Si bonds, irreversibly bonding the two surfaces that can withstand 200-350 kPa of pressure. [91], [92], [95] Plasma treatment affects the surface wettability, decreasing the contact angle of water (θ) making it hydrophilic. One heated, the loose silanol groups are dehydrated once again making the surface hydrophobic. The full fabrication process of the devices used in this thesis are provided in the Methods section.

1.4 Working Parameters

When designing microchannels and producing emulsions there are a number of parameters that can be controlled or influenced. Table 3 is a summary of all the immediately relevant parameters that were directly controlled in this thesis. It covers the method of altering each parameter, when during the encapsulation process they can be influenced and their overall importance during droplet generation. This is a non-exhaustive list, and many other parameters can be implicitly affected outside of those listed here.

Table 3: List of Operating Parameters, what they affect and how they are controlled.

Parameter	*Relevance to Process*
Characteristic Length L	• Affects Reynolds and Weber Numbers, dictating cocoon size and stability. • Width of nozzle correlates to the minimum droplet size by constraining the flow column. Ex: 30 µm nozzle can make cocoons larger than 30 µm • Dependant on the width of the nozzle, which can only be changed when initially designing the microfluidic channel. • Increasing width can offset viscosity effects, allowing for monodisperse emulsions of larger cocoons.
Dispersed Phase Density ρ	• Influences Reynolds and Weber number, but little direct control on this parameter as hydrogel density varies little. • Can be modified during sample preparation, through concentration of hydrogel or by adding solutes to the solvent.
Dispersed Phase Flow Velocity u_d	• Major influence on Reynolds and Weber numbers. Directly related to size of produced cocoons and stability of emulsion and one of simplest parameters to alter. • Increase for larger droplet size, but also increases Weber number eventually causing jetting. • If the emulsion is jetting, reducing this parameter can allow return to monodispersity. • Controlled relative to the applied pressure to dispersed phase sample inlet. • Controlled in realtime using pressure-driven flow, or using syringe pumps.
Continuous Phase Flow Velocity u_c	• Major influence on Capillary number. Directly related to size of produced cocoons and stability of emulsion and one of simplest parameters to alter. • Increase to shrink droplet size and increase flow rate in channel, as well as Capillary number eventually leading to jetting. • Depending on cause of jetting, can increase or decrease this parameter to return to monodispersity. If Capillary number is too high, reducing this

	stops jetting. If Weber number is too high increasing this reduces the u_d and can break off the column sooner. Most effective method is to reduce this and u_d simultaneously to avoid having to determine cause. • Controlled relative to the applied pressure to dispersed phase sample inlet. • Controlled in realtime using pressure-driven flow, or using syringe pumps.
Flow Pressure Ratio R	• Strongest determining factor of cocoon size during an encapsulation, and the easiest to control throughout. • Ratio of u_d and u_c. • While not fully linear, simultaneous increases or decreases of the two flow rates maintains cocoon size. Increasing R increases cocoon size, decreasing it lowers cocoon size. • Maintaining R at higher absolute u_d and u_c allows for higher throughput. • When this value is too high or too low will cause streaming or backflow, stopping droplet production.
Dispersed Phase Flow Viscosity μ_d	• Influences Reynolds number, and thus the Ohnesorge number. • Increasing this drastically reduces ability to reach higher throughputs as jetting occurs at lower u_d due to higher Ohnesorge. • Can be altered during sample preparation through selection of the hydrogel concentration. • Improperly low device temperature can increase this value. • Lowering concentration or increasing nozzle size can mitigate issues.
Continuous Phase Flow Viscosity μ_c	• Influence on capillary number, increasing will cause jetting at lower u_c. • For typical mineral oils and range of surfactant concentrations this parameter shows minimal influence compared to γ. • Can be changed during sample preparation through selection of surfactant, surfactant concentration or any other additives to the continuous phase.
Interfacial Tension γ	• Vital influence on the Capillary and Weber numbers. Directly relates to the stability of the emulsion and the maximum flow velocity that cocoon production remains monodisperse. • If emulsion is coalescing, decrease this value through more surfactant to stabilize. • If jetting is an issue, reducing surfactant concentration can allow for higher throughputs by decreasing the Capillary and Weber numbers. • Can be changed whenever sample is prepared through selection of surfactant concentration and HLB. Higher concentration lowers γ, Increasing HLB appears to lower γ.
Hydrogel Diffusivity D	• Important when mixing fluids on chip, otherwise irrelevant to regular operation. • Slight ability to change through changing device temperature. Main influence is the selection of hydrogel. • Altered by chain length and other structural features of hydrogel chains, temperature and solvent viscosity. • Rather than attempting to change D, more workable solution is to change the channel length to allow longer diffusion time (L*Pe is

	theoretical mixing length). Other alternative is adding turbulent mixing geometries.
Channel Surface Wettability θ	• For best results the channel needs to be as hydrophobic as possible to prevent wetting. • If surface wetting is occurring, heat devices to 70°C for 24 to 48 hours. • Can be altered in microfabrication, or afterwards at least 24 hours before an experiment.
Cell/Cocoon Concentration C	• A high concentration directly relates to a higher occupancy. • Past a certain point a high concentration causes clumping and polydisperse cocoons • Directly controlled when doing sample preparation when mixing cell solution into hydrogel.
Cocoon Volume V	• As a parameter influences the occupancy of the final sample. A larger volume means less cocoons, but on average more cells per cocoon. • Controlled through the ratio of dispersed and continuous phase pressures.

1.5 Objective Statement

The investigation done to complete this project can be divided into four sections. First the formation of a monodisperse emulsion is tested with gelatin and poloxamer is tested, with gelatin ultimately being chosen due to its stability. This step continued with investigation into how surfactant concentration and hydrogel concentration affect gelatin emulsion generation, and the melting point of the produced cocoons to better optimize cocoon production. Secondly, a microfluidic platform for encapsulating the gelatin in a layer of agarose is created, with characterization of occupancy, monodispersity and throughput. Next, NIH 3T3 cells are introduced into both steps to determine any impact on viability in the process. Finally, the hypothesis on cell proliferation and viability in the hollow cocoons is tested in a cursory fashion. Should this project be a success it will show a proof of concept microfluidic platform to produce high throughput hollow cocoons using multiple hydrogel materials and demonstrate the impact these cocoons have on encapsulated cells.

2 Methods

2.1 Microfabrication

The microfluidic devices used in this thesis are based on soft photolithography processes adapted from previous processes. [15], [60], [88] Briefly, photolithography is used to create molds using SU-8 photoresist on 100 mm silicon wafers. PDMS is then poured onto the molds and cured, and then after the individual channels are cut from the mold they are then bonded to glass slides. Single encapsulations use refined versions of the devices used previously, but the formation of hollow cocoons required modified designs.

2.1.1 Single Encapsulation Design

The soft photolithography process begins with a photomask. Microfabrication processes requiring constant use and higher resolution are done using chromium on glass, but for this project's rapid prototyping needs, clear transparencies coated in an ink emulsion at 20K DPI was used, acquired from Cad/Art Services. The minimum feature size of these masks is 10 µm.

The photomasks are designed using AutoCAD®, an engineering drafting software that allows for 2D or 3D mock-ups to be made. Outlines are made in the software at real world scale, which can be transferred to the created photomask.

Most of the microfluidic encapsulation devices used in this project all follow a general layout adapted from previous work done in the lab by Nicholas Catafard and Ainara Benavente-Babace, an example of which can be seen in Figure 9, which is the current typical single emulsion flow-focusing device. The basic areas of this device being the Inlets, the Encapsulation "Nozzle", the Channel and Serpentine, and finally the outlet.

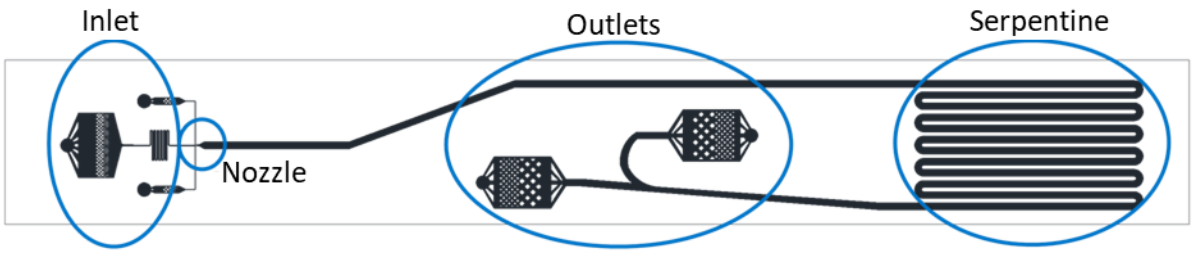

Figure 9: Design of Single Encapsulation Microfluidic Device. The dispersed phase enters at the large inlet, where it passes through a filter while the continuous phase enters though the two small inlets. An emulsion is created at the nozzle, before entering the wider and slower flowing visualization channel. Cocoons are gelled in the serpentine and exit from one of the two outlets.

Inlets start with a circular region with an outer diameter of 1/32'' which is the same diameter of the PEEK tubing that is inserted to supply the inlets. The following region then contains filter posts which block any large contaminants that may enter the device to avoid clogging. The width of the inlet, and the size and distance separating the posts are designed with the expectation of the size of what is to be filtered. For example, the oil inlets are small with a tight filter grid as there should be no solid contaminants, but if any exist they should not pass through to the nozzle. Meanwhile the sample inlet has a filter with sparser spacing as cells or cocoons need to make it through the filter, and the width much wider as any given space between posts is at greater risk of clogging, so a wider filter provides more avenues of flow.

The nozzle is where the oil (continuous phase) and the sample (dispersed phase) flows meet perpendicularly in a flow-focusing geometry to generate the monodisperse emulsion. A schematic of the most common flow-focusing nozzle used for typical single encapsulations in this thesis can be seen in Figure 10. The size of the inlet flows and the size of the nozzle partly determine what size range of cocoons can be stably produced by the ratio of the two flows. The nozzle diameter is a component of the channels hydraulic diameter that forms the characteristic length, influencing the Reynolds and Weber numbers. The primary nozzle size used in experiments in this thesis is 30 µm, but in some cases tests were done using a 50 µm variant.

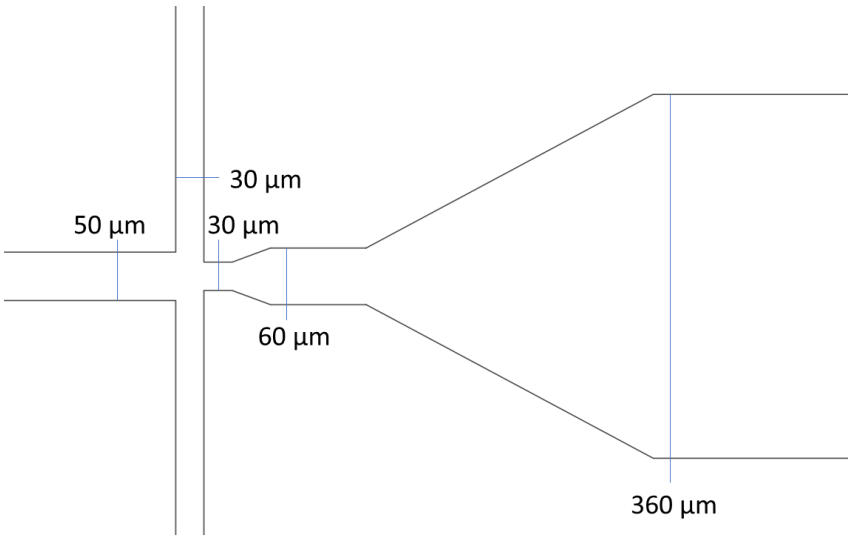

Figure 10: Flow-focusing nozzle for the generation of monodisperse 50 µm droplets.

The channel is largely meant to provide space between the two temperature controllers to produce a temperature gradient, the wider width compared to the inlets is to slow down the flow enough so the cocoons are visible in the channel after being made and to ensure the cocoons are in the serpentine long enough for gelation. The serpentine section is positioned over the cooling block, to gel the cocoons. This aspect of the design was largely static between designs barring channel width, though the gelling behavior of poloxamer means that when producing poloxamer cocoons the heating gradient was reversed.

The outlets posses another circular region for the outgoing PEEK tubing, as well as an array of posts meant to break up any clumps of cocoons that may have aggregated before they reach and clog the outgoing tubing.

When given space around the channel to allow a safety margin when constructing devices, each channel is 60 mm by 8.5 mm in size. This allows for 8 channels to fit in the working area of a 100 mm wafer, as seen in Figure 11.

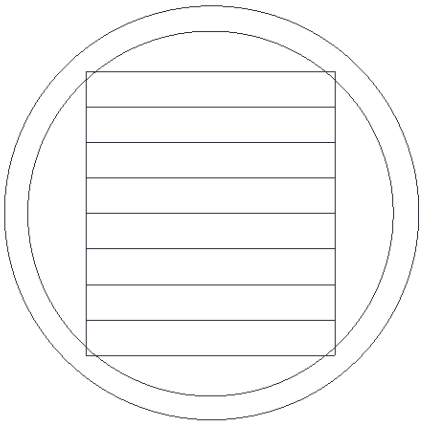

Figure 11: Placement of Microchannel Photomosk over a 100 mm Si wafer. Inner ring denotes the area unsuitable for microfabrication due to edge effects of spincoating photoresist.

For the “Double Emulsion” encapsulation devices used previously, [15] the overall design remains the same. All changes were made to enable the relatively large, roughly 50 µm cocoons from the previous emulsion to enter the device and pass through the nozzle. To this end, the dispersed phase inlet filter posts are more spaced out, the nozzle was increased from 30 µm to 90 um, and the dispersed and continuous inlets were scaled along with it to maintain flow ratios.

In order to generate hollow cocoons using gelatin in this project, a new photomask was needed in order to produce a microchannel that mixes previously generated cocoons and liquid agarose on chip before emulsification. The new photomasks possess two dispersed phase inlets, one a double emulsion filter, which meet and mix in a serpentine before the nozzle that is based around the double emulsion devices. A more detailed examination of these features and their outcome will be given in the Results section, but the new inlet design can be seen in Figure 12.

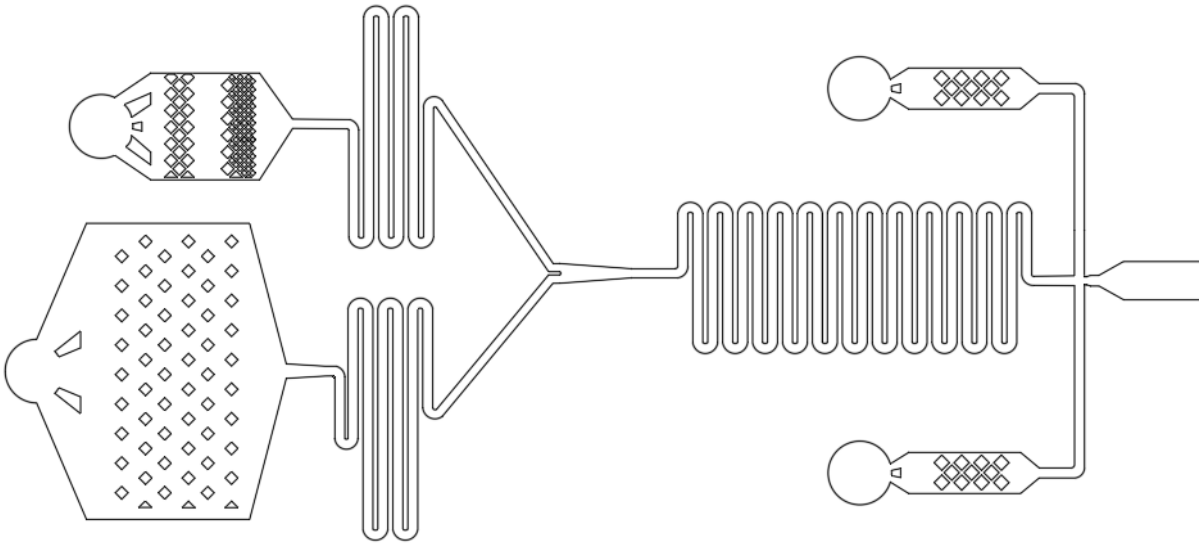

Figure 12: Inlet design for hollow cocoon generation Larger inlet has wider filtration to allow for cocoons to enter the device, smaller inlet is meant for agarose.

2.1.2 Photolithography

Once a photomask is acquired, the next step is to make a master mold that will be the basis of fabricating the channels. This mold is made though photolithography, where the design on the photomask is transferred to a layer of photoresist. Due to the size of the features, dust can be a major cause of defects should it fall onto a feature, so all microfabrication should be done within a Cleanroom. [88]

The substrate of the mold is a simple silicon wafer, 100 mm in diameter and 500 µm thick, polished with a <100> orientation. These were procured from University Wafer. The photoresist was Su-8 2050, and the developer was SU-8 specific 1-Methoxy-2-Propanol Acetate and was procured from Kayaku Advanced Materials. [94]

Plasma cleaning was done using air plasma in a Glow Research, Autoglow quartz plasma chamber. The spin coating of the resist was with a Laurell Technologies Corporation Model WS-400BZ-6NPP/Lite spincoater. The UV exposure was done using a OAI Hybralign Series 200 mask

aligner with a model 2110C2 Illumination Controller that exposes using a mercury bulb with 15.3 mW/cm^2. All steps were completed in a Class 1000 Clean Room to avoid contaminants.

The following steps in creating a master mold were adapted from the parameters in the SU-8 2000 series datasheet created by MicroChem, for use in this project. [94] Parameters shown here were chosen for a thickness of 100 µm. For devices of different thicknesses parameters were adjusted following the datasheet as needed.

- First a new silicon wafer is rinsed with acetone, isopropyl alcohol and ethanol to clean the surface, then dried by N2 air. The wafer is then exposed to 200 W plasma for 10 minutes to further clean off any contaminants, then finally dehydrated on a hotplate at 200^{o}C for 10 minutes before being placed centered on the spincoater.
- Roughly 1 mL of SU-8 2050 is poured onto the wafer, then the spincoat recipe for the thickness is initiated:
- Ramp to 500 rpm at an acceleration of 100 rpm/sec, for 10 sec to evenly spread the SU-8 on the wafer
- Ramp to 1700 rpm with an acceleration of 399 rpm/second, for 30 seconds to reduce the SU-8 layer to 100 um
- Ramp back to 0 at a rate of -399 rpm/sec
- Next a “Soft Bake” is done to remove solvent so the SU-8 Layer remains uniform and can be placed in contact with the Photomask. This involves a 5 minute prebake at 65^{o}C to limit thermal stresses, and the soft bake at 95^{o}C for 16 minutes.
- Next is the UV exposure. The photomask is attached to a glass cover, while the wafer is laid on a platform with a ball-vac. The platform can be adjusted to level and center the wafer beneath the photomask, and then raised to create contact to improve the aspect ratio of the features. For 100 um, the wafer needs to be exposed by 230 mJ/cm2, so exposure lasts roughly 15 seconds.
- Following exposure is the “Post Exposure Bake” which helps finalize crosslinking before development. There is again a prebake step at 65oC, lasting 3:35 minutes, and the bake at 95^{o}C that lasts 9 minutes and 15 seconds.

- After the wafer cools, it is developed to remove excess photoresist. During development the wafer is fully submerged and is constantly agitated, removing any unexposed SU-8. For 100 µm the development time is 9 minutes. Post development, the residual developer is washed off using isopropyl alcohol.
- To guarantee that the thermal response of the SU-8 is completely stable, there is a final "Hard Bake" which consists of heating gradually to 150oC, baking there for 5 minutes then turning off the hotplate to gradually cool down. The gradual nature prevents the difference in thermal expansion rates from lifting the SU-8 from the wafer, and reaching such a high temperature means the SU-8's thermal properties will not change during PDMS curing, as well as helping seal any cracks that may have formed during the development process.

The final step in producing a mold is "silanation". By producing a monolayer of silane on the SU-8 and the silicon surface, it is easier to remove PDMS without putting excess force on the SU-8, extending he lifetime of the mold. (TriDecaFluro-1,1,2,2-TetraHydroOctyl)TriChloroSilane acquired from Gelest is used. [96] To silanate, the wafer and 2 µL of silane are added to a vacuum chamber. The vacuum is initiated then the chamber is sealed off, leaving the contents under vacuum without removing any additional air. This induces the silane to vaporize and coat the wafer. This process only needs 2 hours but is typically left overnight until the vacuum bleeds off. [88]

2.1.3 PDMS

Once the master mold is finished, the channels can be cast using PDMS. The wafer is fitted with ring with a roughly 100 mm inner diameter and 5 mm height, cut from an acrylic sheet to serve as the vertical section of the mold to limit wasted material. The PDMS acquired from Ellsworth is Sylgard 184 which comes in two components, the Dimethyl Siloxane base and a crosslinker. [90] These components are mixed in a 10:1 ratio to begin the crosslinking process. This mixture is poured onto the wafer, constrained by the ring.

After pouring, degassing is needed as the mixing introduces air bubbles which can form on the SU-8 features, potentially ruining the devices. The wafer with PDMS is placed in a vacuum chamber and is kept under vacuum until all air bubbles have left the surface. This typically lasts roughly 30 minutes but can be longer for the initial use of the wafer.

After degassing the wafer is placed into an oven at 70^{o}C for 2 hours to cure the PDMS. Too little curing will leave the PDMS tacky to the touch, causing issues peeling it from the mold, ruining visibility and potentially leeching uncrosslinked Siloxane into the fluid flow. Too much stiffens the PDMS to the point where it can fracture when the inlets and outlets are being created, causing leaks.

After curing, the PDMS is cut along the edge of the ring using a scalpel and is gently peeled off the SU-8 features. The devices are then cut from the bulk PDMS, and a biopsy punch, size 0.75 mm, is used to punch holes for the inlet and outlet PEEK tubing using a microscope for alignment.

2.1.4 Plasma Bonding

The final step in preparing the microfluidic devices is bonding the PDMS to a solid flat bottom surface to create a watertight channel. [88] For these devices, VWR Vistavision Microscope slides (75x25x1 mm) were used. They were precleaned by sonicating in acetone then ethanol for 10 minutes each to remove any residues that could taint the surface chemistry.

Plasma treatment occurred in a Glow Research, Autoglow quartz plasma chamber using air generated oxygen plasma. The surfaces were exposed to 36 Watts of plasma for 36 seconds, at a vacuum of 500 MTorr to guarantee a strong bond. [95]

Post exposure the devices were placed in an oven at 70^{o}C for several days. This is initially to provide the thermal energy to complete the bonding reaction, but also removes water vapor and the silanol surface groups so that the interior of the channel is hydrophobic to prevent wetting of the dispersed phase in the channel. A finished channel can be seen in Figure 13.

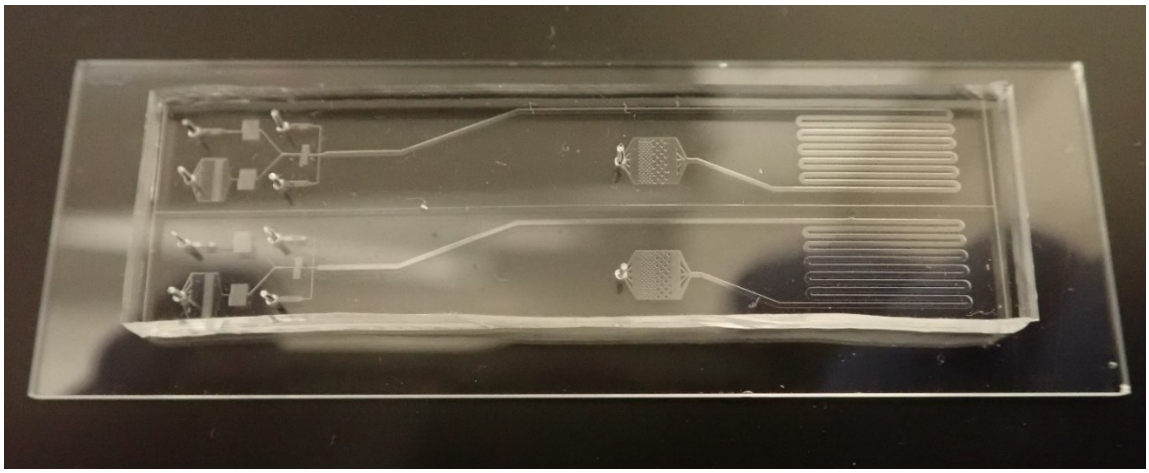

Figure 13: Picture of a finished microfuidic channel. The transparanct PDMS and Glass allow for viewing on a microscope. Two channels fit on a single slide to reduce the amount of time spent switching devices from the holder.

2.2 Encapsulation

2.2.1 Hydrogel Preparation

The Ultra Low Gelling Temperature agarose acquired from Sigma comes as a powder that must be dissolved into a gel before use. [64] Higher concentrations of agarose, those reaching 3% and above, gel easily at the working temperature, and have higher viscosities that negatively impact the formation of a dispersed phase while lower concentrations approaching 1% tend to be too weak to properly encapsulate cells upon gelling due to the sparse networks that form. [60] For this reason, the agarose used to encapsulate cells in this project falls between 1.5 and 2%.

When preparing agarose, a higher concentration of 2.7% is made to allow for mixing in a suspension of cells to reach the proper concentration. A larger stock of 3 mL is produced at a time which is stored at 4^{o}C until needed. To make, agarose powder is added to sterile PBS in a falcon tube. The tube is placed in a beaker of water in the microwave, and alternating heating and vortexing steps are done until the agarose reaches the edge of boiling and all the agarose is dissolved, typically within 1 to 1.5 minutes of heating in increments of 10 seconds. When stored at 4^{o}C, the stock will gel but upon heating to above 65^{o}C it will melt into a usable state.

If this agarose is meant to be a single emulsion, some of the sterile PBS should be replaced with OptiPrep Density Gradient Medium to ensure that the cells do not settle before entering the device to avoid clumping. [97] For the 3T3 cells used in this project, 20% of the volume should be replaced, but this value is cell dependant as they have differing densities.

The gelatin acquired from Sigma comes in the form of a powder and must be dissolved before use. [74] The acquired gelatin has a high bloom strength at 300, which means the gelling point is fairly high even at lower concentrations. [72] In order to guarantee that the cocoon melt under physiological conditions, 10% or lower gelatin is used for encapsulation. This has a secondary benefit as higher concentrations began to show streaming behaviour even at low pressure, potentially due to decreasing surface tension of higher gelatin concentrations as well as the influence of the increasing Ohnesorge number on the break up of the flow cylinder. [98]

To prepare gelatin stock, powdered gelatin should be added to sterile PBS in a falcon tube to make a 15% concentration. Heat a beaker of water on a hotplate and add a stirbar to the falcon tube. Heat the gelatin and mix until all the powdered gelatin is dissolved, and then store at 4^{o}C. When needed, the stock can be heated to 40^{o}C to melt it to a usable state. Similar to agarose preparation, if cells are to be used, an appropriate amount of PBS should be replaced with Optiprep. If the melting point needs to be adjusted, glycerol can be added to increase the melting temperature. [73] Glycerol is primarily cytotoxic through osmolality mismatch, with little to no loss of viability for concentrations below 3 mol/kg, especially if preloaded to avoid swelling stress allowing for up to 17 mol/kg. [99] A working guideline found in this experimental process was that every 15% addition of glycerol volume, or roughly 2.7 mol/kg, equated to a 2.5^{o}C increase in bulk gelatin melting point.

The poloxamer used in this study is Pleuronic F-127, which comes in a powder and must be dissolved before use. To allow for the formation of a gel while not being too viscous in the liquid phase, concentrations between 20% and 30% were used in forming the emulsion. [68]

To prepare the poloxamer stock, powered poloxamer should be added to sterile PBS in a falcon tube to make the required concentration. As poloxamer is soluble in cold temperatures, the tube should be added to an icebath on top of a cool hotplate with a stir bar. Mix the powder

until fully dissolved, then store at room temperature to avoid the polymer chains settling from solution. When needed, the poloxamer can be cooled in a fridge or ice bath to melt the gel.

2.2.2 Device Preparation

Outside of the channel, there are external components that build around the glass slide to control the temperature and fluid flows on chip, and to visualize what is happening in the channel.

Devices are first set into a specially designed apparatus consisting of an aluminum horseshoe heatsink that maintains temperature through water flowing from a heated water bath. On either end of the horseshoe there is a Peltier pump and an insertion point for a thermistor and there are two insertion points in the top of the horseshoe for the sample and oil vials. The device fits into the holder with each end placed under a Peltier pump, as can be seen in Figure 14. The temperature of each end of the device is controlled by custom LABVIEW Software using feedback from the thermistors using a Wavelength Electronics HTC Temperature controller that communicates through a National Instruments USB Multifunction I/O. [100] To further control temperature, an insulated acrylic box can be placed over the whole apparatus to keep the air temperature stable, heated by the heatsink based on the temperature of the water bath allowing for isolation from any environmental changes in the lab.

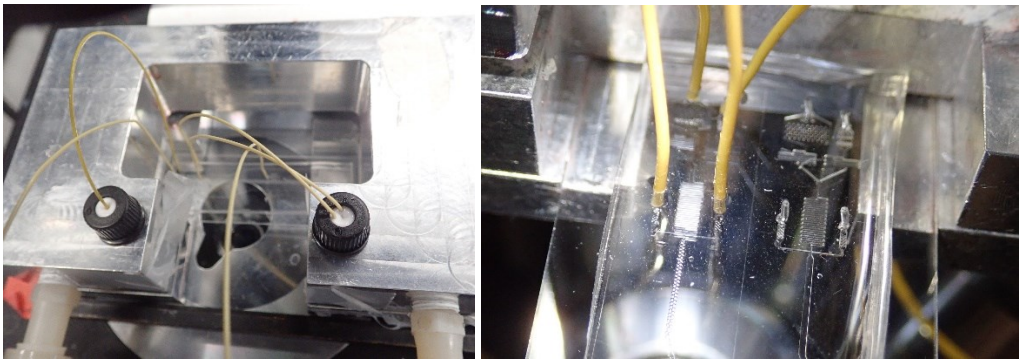

Figure 14: (Right) Aluminum heatsink with sample vials in holders. (Left) Glass slide sits with ends held near peltier pumps, and the channel above objective lens of inverted microscope.

Sample and Oil are brought into the device using PEEK tubing with an outer diameter of 1/32'' and an inner diameter of 0.007''. Flow is pressure driven and controlled by a mix of pressure regulators and solenoid valves. Manual pressure regulators control the pressure that each phase is driven by allowing for control over the ratio, and all are split off from the same source so any potential fluctuations in air flow will affect all inlets, improving stability. The range of these valves are from 34 kPa to 172 kPa for the continuous phase, and 34 kPa to 152 kPa for the dispersed phase, though the actual gauges are delineated with PSI. When a third pressure flow is needed, there is another pressure gauge that allows for 30 kPa to 400 kPa, but the available maximum airflow that can pass through it in reality is closer to 200 kPa. These flows pass through a solenoid valves that are controlled by custom LabVIEW software. Flows can be turned on and off individually or simultaneously. Due to the flow-focusing encapsulation mechanism, the oil pressure regulator applies pressure through two oil PEEK inlet tubes the same time. At the outlet, additional PEEK tubing brings the cocoons into an outlet holding vial containing DMEM in an ice bath. An additional pressure regulator can be used to pressurize the outlet should a shallower pressure gradient be required, but this was not used in this project.

To monitor the size and uniformity of cocoons, this apparatus is mounted on the stage of a VWR Inverted Microscope, seen in Figure 15 with a Point Grey 60 FPS colour USB camera connected to SpinView software to provide real time video of the device. The stage includes XY mobility allowing for panning, and a number of objective lenses allow for various views. A contrast filter can also be applied over the light source to provide more information on features such as agarose gelling.

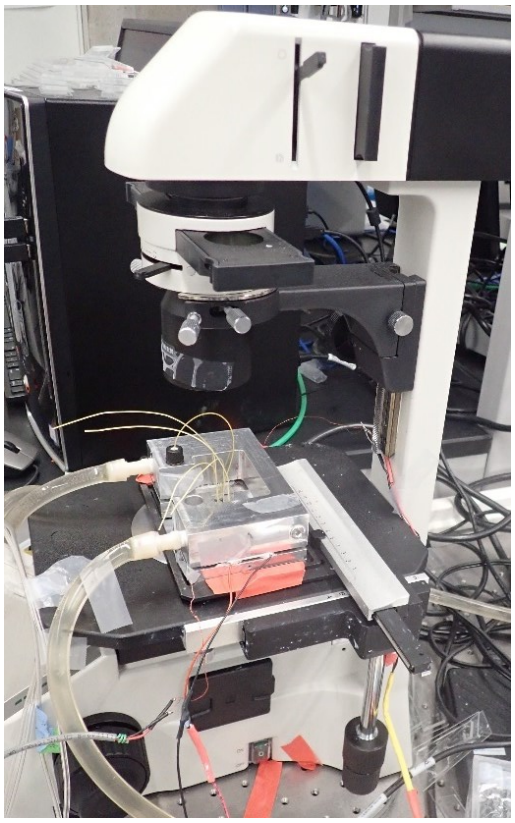

Figure 15: Picture of set-up on inverted microscope

Before beginning encapsulation, an emulsion with sterile water and oil should be made on the device. This serves several purposes. It allows for any leaks or flaws in the device to be made apparent before any vital sample is wasted, and any device to device variation can be accounted for by monitoring the response of the emulsion to changing the pressure ratio. The oil used is a sterile Mineral Oil specified for molecular biology purchased from Sigma-Aldrich. [101] In order to support the creation of water-in-oil droplets for the encapsulation, the continuous phase is typically supplemented with 1.5% Sorbitane Monooleate (Span 80), a low HLB value surfactant that has low cytotoxicity at values lower than its critical micelle concentration. [102] Making this phase was simply micropipetting the correct volume of Span 80 into the aliquot of mineral oil then vortex mixing to ensure that it disperses. In the case that a higher HLB value is needed, a portion of the Span 80 can be replaced with Tween 80, which is a different Sorbitan Monooleate with Polyethylene Glycol as a moiety. To support the emulsion 1.5 mL of oil/span mix is added to

a 2 mL screwcap glass vial with a PTFE Laminated Disk serving as the insertion point for the inlet tubes.

To prepare the device, the glass slide first needs to be placed in the apparatus and all the PEEK tubing needs to be inserted into the proper inlets and outlets. Using the LabVIEW software the temperature needs to be set, and the pressure valves need to be set to a low value, typically 35 kPa on each for consistency to track the size of the generated emulsion between devices. The oil pressure is the first to be turned on to check if the flow is symmetric from both inlets, and to "wet" the hydrophobic channel with oil. After turning the oil pressure off the water pressure is then turned on, then off. If no issues are apparent, then both flows are activated and minor adjustments are made until a stable emulsion is generated, as seen in Figure 16. If the dispersed phase flow is too high then streaming will occur or in more serious cases backflow of the oil inlet, too low will cause the oil to backflow up the dispersed inlet. Once stable, this flow should be left running while final sample preparation is occurring, to allow the water phase to fully wet the sample inlet filter and to allow the temperature to stabilize. The outflowing end of the outlet PEEK tubing is placed in a microcentrifuge tube designated for waste.

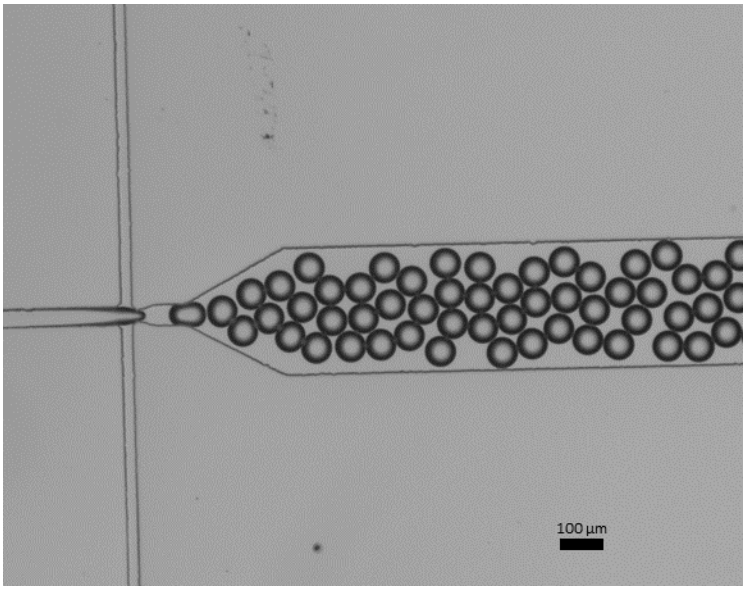

Figure 16: Stable W/O emulsion made with DI water, and Mineral Oil with 1.5% Span 80 surfactant.

2.2.3 Dispersed Phase Sample Preparation

While the O/W emulsion is flowing, the hydrogel sample is then prepared. First the stock hydrogel needs to be melted through heating on the heating block. Agarose is heated to 70°C while gelatin is 50°C to guarantee that the sample is properly melted. After this, the temperature is reduced to 40°C so that cells can be added without loss of viability. The size of the vials used takes a maximum of 200 µL, but 150 fits comfortably after inserting the inlet tube. For agarose, 150 µL of 2.7% stock is introduced with 52 µL of either PBS if it is meant as the outer encapsulation, or DMEM cell suspension to produce 8.5 million cells/mL for a traditional 2% agarose single encapsulation. For gelatin, 130 µL of 15% stock is mixed with roughly 70 µL of PBS or cell suspension to form 10% gelatin. Finally, 150 µL of sample is added to a 5mm CS100 glass insert, which is placed in a glass vial filled with water for better heat transference and capped with a PTFE Laminated Disk for the PEEK tubing.

2.2.4 Cocoon Formation

Once the water/oil emulsion has fully stabilized and the sample is made, the dispersed phase inlet needs to be replaced. This is accomplished by stopping flows, unscrewing the sample vial. inserting the PEEK tubing into the glass insert containing the sample and then restarting the flow.

To increase throughput, the pressures now need to both be increased, adjusting the ratio to account for the change in viscosity and surface tension of the hydrogel. Once at a reasonable throughput, adjusting the sample pressure allows for fine tuning of cocoon size. Exact measurements can be done by taking a snapshot with SpinView and using ImageJ software to measure the diameter of a cocoon in relation to the known channel width. Once the proper size is attained, the outlet tube is switched from the waste outlet, to the proper DMEM filled outlet microcentrifuge tube, placed in an ice bath to maintain cell viability. The size of the cocoons should be monitored throughout the encapsulation process, with adjustments made to the pressure as needed to maintain consistent size.

2.2.5 Post run Purification

After the encapsulation is finished, the oil phase needs to be removed from the sample, as it would interfere with any subsequent encapsulation and is not appropriate for therapeutic purposes. This is done through use of a microcentrifuge. Centrifuging at 0.3xG for 3 minutes is enough to move the cocoons from the oil phase to the aqueous phase and pellet the cocoons, while not reducing cell viability. After centrifuging, the oil phase is removed using a micropipette and the process is repeated. After this second time, the pellet is broken up and the aqueous phase is moved to a new vial as oil will still be coating the surface of the initial vial. This sample is then kept on ice until any further encapsulation or testing.

2.2.6 Double Cocoons

In the case of making a typical double layered cocoon, the methodology is highly similar to creating the initial single cocoons. While the sample purification is ongoing from the initial run, the single encapsulation device is replaced by a double encapsulation device. The set up for this is identical, the major difference being the on chip geometry, with the nozzle increasing from 30 µm to 110 µm to allow for the cocoons to pass. [15]

After sample purification finished, producing the new sample of agarose to inject into the device is very similar. The number of produced cocoons is calculated using a hemocytometer, and the sample is again centrifuged. The supernatant is removed and replaced with an amount of DMEM such that 52 µL of suspension will create a 2% agarose solution with 1.5 million cocoons/mL. [15] This lower concentration is due to the larger size of the cocoons compared to cells causing increased risk of clogging, and the increased size of double encapsulated cocoons reducing the throughput and final number of produced cocoons.

2.2.7 Hollow Cocoons

The process of generating hollow cocoons being described in this report shares general similarities to the previous single and double emulsions, but due to some inherent limiting features is much more involved. The initial encapsulation of cells is identical to a single encapsulation involving gelatin described previously. The goal size is 130-150 µm, to balance occupancy and ease of encapsulation. The differentiation begins to occur after sample purification.

As mentioned previously, the design of the microfluidic devices involves two dispersed phase inlets. As individual control of each of these is desired, a third pressure gauge controlled by a solenoid valve is needed, as well as a third inlet vial and PEEK tubing. When starting the initial oil and water emulsion, the two dispersed phase inlets need to be balanced to prevent backflow. Due to the different inlets, changes in oil flow tend to cause backflow primarily in the cocoon inlet channel, so balancing the flow tends to require careful adjustments to all three gauges to find an equilibrium. To find proper initial values, food colouring can be used with a throwaway device, to colour one inlet flow for easier visualization. An example of a proper co-flow of two water samples can be seen in Figure 17. These values can then be used on any devices of the same design, with only minor adjustments needed for variation in set ups.

For the cocoon sample, the number of produced cocoons is calculated using a hemocytometer, and the concentration of cocoons is adjusted using DMEM to 850,000 cocoons/mL. The sample vial is stored in an icebath to maintain cell viability and cocoon integrity. The agarose used to produce the shell is 2.7%, which is diluted when mixed with the cocoon inlet flow to roughly 1.5%.

Due to gelatin having a higher density than the DMEM, and the porous nature of the cocoons limiting the use of Optiprep, the cocoons begin to settle in the sample vial. Due to this, another PEEK tube connected to a vial containing only air can be used as a “bubbler” to agitate the cocoons, or the vial can be periodically agitated by hand in order to keep a consistent cocoon concentration flowing into the device.

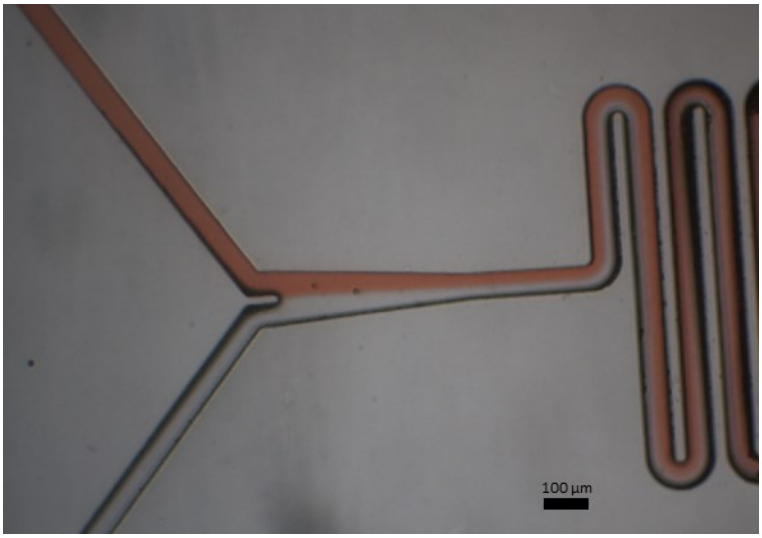

Figure 17: Balanced flow of the two inlet channels, visualized with food colouring to find proper pressure values

Once the sample is prepared, all flows are stopped simultaneously and the two water filled inlet vials are swapped to those containing the samples. When the flow is resumed, the agarose inlet pressure is increased as the added viscosity of the agarose lowers the flow rate. Then all three inlet pressures are increased at the same ratio to improve throughput. By slightly adjusting the agarose flow pressure, the ratio of cocoon and agarose flow in the mixing channel can be adjusted, allowing for more control over shell concentration. Once stable, the outlet tube should be moved to the final sample vial kept on ice.

2.3 Cell Culture

Due to the complex culturing and other requirements associated with stem cells, NIH 3T3 mouse fibroblasts were used as a substitute to model the behavior of cells when encapsulated in hollow cocoons. These cells are sturdy, adherent and replicate rapidly allowing for frequent tests involving cells. An adherent layer can be seen in Figure 15. Culturing protocols were adapted from the CFF guidelines to better fit the resources available. [103]

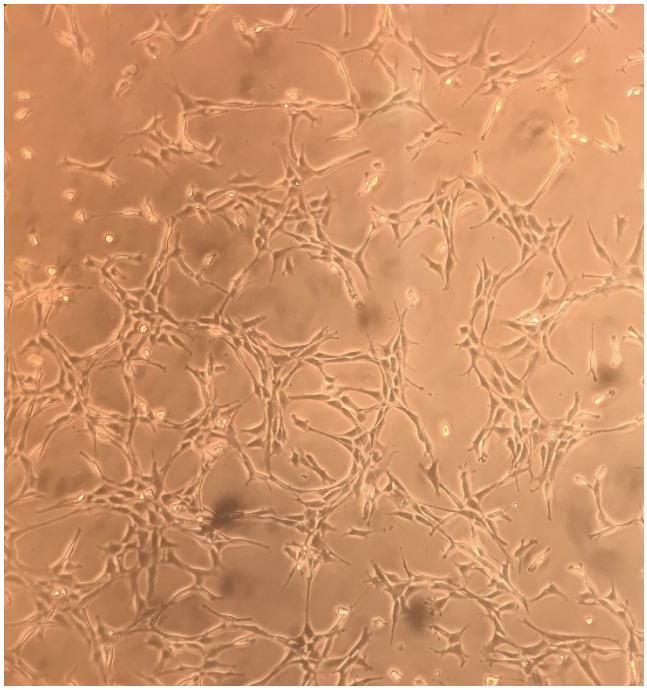

Figure 18: Adherent Layer of NIH 3T3 mouse fibroblasts.

The reagents used are:

- Dulbecco's Modified Eagle's Medium, a nutrition medium for adherent cells
- Penicillin/Streptomycin, an antibiotic mix to avoid bacteria growth
- Fetal Bovine Serum, additional nutritive additive
- Trypsin-EDTA, an enzyme meant to detach adherent cells
- Phosphate Buffered Saline, a pH buffer for washing cells

When starting cell culturing, a batch of growth media need to be prepared. 450 mL of DMEM, 50 mL of FBS and 5 mL of the Penicillin/Streptomycin mix are mixed. From this point forwards unless stated otherwise, “media” refers to this mixture.

3T3 cells come frozen in cryovials stored in liquid nitrogen. This frozen pellet is added to 5 mL of media to unfreeze and resuspend cells, diluting away the DMSO used to aid in freezing that would begin to kill thawed cells. This suspension is centrifuged at 1000 RPM for 3 minutes, the supernatant is aspirated and then the pellet is resuspended in 2 mL of media. This suspension is added to a T75 cell culture flask already containing 13 mL of media, and then the flask is placed

in an incubator overnight. The incubator should be set at 37oC, with 5% CO2 to create proper cell growing conditions.

Media should be changed every 2 to 3 days, if cells are not being passaged. This is simply done by aspirating the existing media and replacing it with a fresh amount of the same volume.

When cells become 80% confluent on the surface, as in they cover 80% of the bottom of the flask or petri dish, they need to be passaged. This involves lifting the cells from the flask, counting them then adding a small fraction into a new flask or petri dish, with the remaining amount being disposed of or used in experiments.

To passage, first the media is aspirated, then the cells are washed with PBS. This removes any remaining media. Next the cells are coated in 3 mL of trypsin and are placed in an incubator to lift off of the bottom of the flask. When the cells are off the surface, 6 mL of media is added, and the suspension is moved to a falcon tube. 10 µL is taken for hemocytometer counting, and the tube is centrifuged for 3 minutes at 1000 RPM. To continue the cell line, a new flask or dish should be filled with media and enough cells to regain 80% confluency after 2 days. For timelapse or time point, well plates should be filled with 2 mL of media, and enough cells should be taken to make an 8.5 million/mL suspension. Any remaining cells should be bleached and properly disposed of.

2.4 Quantification

2.4.1 Fluorescence

While brightfield is useful for visualizing the presence of cells in cocoons, and phase contrast for highlighting the difference in diffraction, neither can easily show the viability of the encapsulated cells. Stains such as trypan blue can be used to determine whether cells are alive or dead, but testing during this thesis showed that it can also stain the gelatin cocoons making the determination of cell viability difficult. An example of this can be seen in Figure 19.

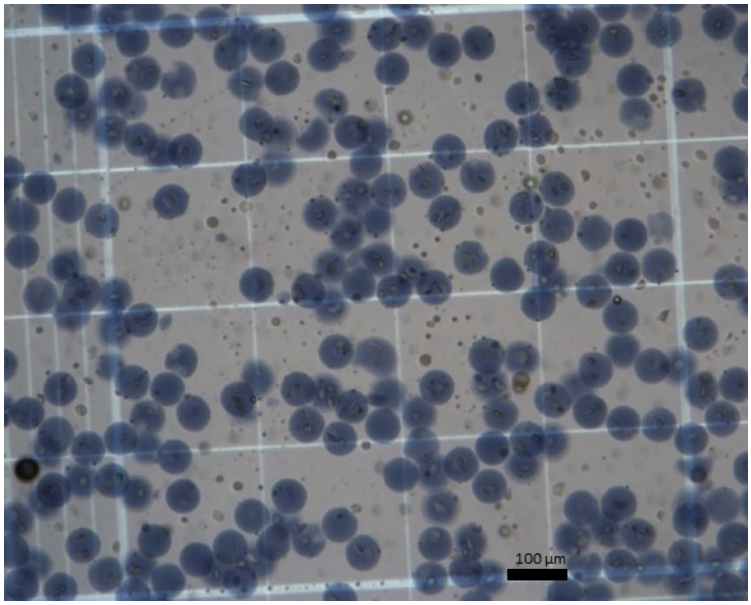

Figure 19: Gelatin Cocoons stained with Trypan Blue

Additionally, different wavelengths can be used to pair the method with fluorescent dyes to better determine cell viability. This works by pairing two fluorescent dyes that emit on different wavelengths and are tied to different cellular activities. Calcein is a green dye that is converted into a fluorescent material by enzymes in living cells. Ethidium Homodimer-1 is a dye that is excluded by living cell membranes but fluoresces when it binds to DNA. This means that using image processing it is possible to stack images of the two fluorescing dyes on top of a brightfield image to create an image where live cells are clearly marked as green, and dead cells are clearly marked as red, an example of which can be seen in Figure 20. [104] To stain cells, the two dyes are mixed in at a concentration of 1 µM, and incubated for 30 minutes before imaging.

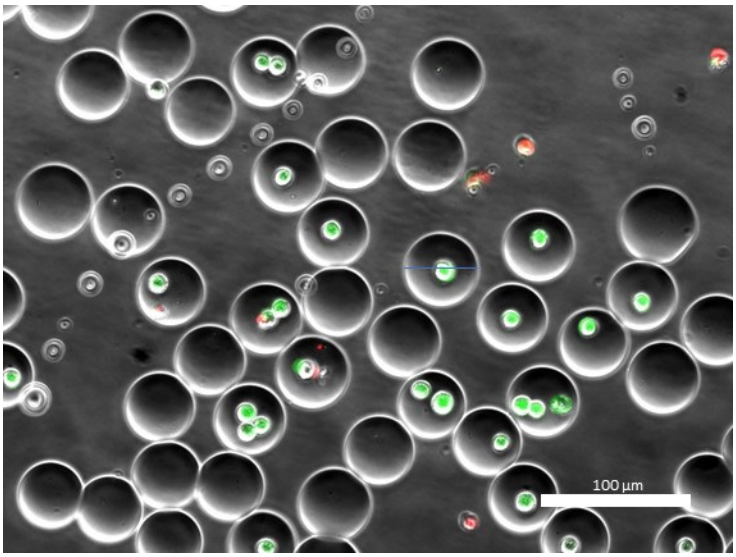

Figure 20: Live/Dead staining of cells in gelatin cocoons

The occupancy of cocoons is simply the number of cocoons containing cells over the total number of cocoons, and cell viability is the number of living cells over the total number of cells. These are found by counting the cocoons and cells seen during fluorescence spectroscopy images. While counting can be done using software, in this case it was done manually taking note of cocoon numbers, the number of cells with cocoons, the number of cells and the number of living cells and dead cells.

2.4.2 Timepoint

To determine the statistics of how cell viability and egress occur over longer periods of time, a series of fluorescence/brightfield images taken over the course of 48 hours can be taken and compared, typically every 12 or 24 hours. This length of time is chosen as after this, the media begins to run low on nutrients and replacing it would cause losses and disruption to the loose cocoons.

Cocoons are added to a series of wellplates filled with media, each containing roughly 20,000 cocoons each. At each time point, 5 images from each well are taken and the occupancy and viability are calculated from these images.

For occupancy, cocoons containing cells are counted, differentiating between cocoons that have 1 cell or more than 1 cell. Occupancy is then the occupied cocoons divided by the total number of cocoons. For hollow cocoons an adjustment can be made to account for the creation of pure agarose cocoons without a gelatin core. This would be the occupancy of "hollow" cocoons that actually contain a hollow core, and also the occupancy of cells in hollow cocoons compared to total number of truly hollow cocoons.

Egress can be defined by the change in occupancy over time. After calculating the occupancy at two time periods, the egress is the change in occupancy divided by the initial occupancy.

Viability is simply the number of remaining living cells compared to the total number of cells. In the case of cells egressing, this number can be adjusted by only taking the cells found inside cocoons into account, depending on the metric being investigated.

2.4.3 Hemocytometer

A hemocytometer is a grid based measuring system to calculate the number of cells in a volume based on a 10 µL subsample. The hemocytometer consists of a series of lines that create a grid of precise nine 1 mm^2 squares subdivided into further sections of 1/25 mm^2. When 10 µL of sample is added between this grid and a coverslip there is a precise volume that can be used to extrapolate the entire sample. [105]

The process for this is to count the number of cells, or cocoons, in each of the four large corner squares and average them. This number is then multiplied by the volume of total sample there in mL, then by 10,000 to account for the hemocytometer volume to get the total number of cells in the sample.

The throughput of the production of cocoons was found using this system. By marking the start and end times of sample collection, and then measuring the number of produced cocoons the average number of cocoons made per second across the entire sample run can be found. This has some limitations, a significant number of cocoons need to be produced in order to be accurately counted so taking throughput "snapshots" using this method was not possible.

When cells are not encapsulated in gelatin cocoons, hemocytometers can also be used for cell viability. Trypan Blue is a dye that is cannot cross the cell membrane of living cells, while dead cells become perfused with. By incubating cells with trypan blue for 5 minutes and counting with a hemocytometer dead cells are immediately visible allowing for viability to be measured.

2.4.4 Poisson Encapsulation Statistics

As mentioned previously, ideally the flow-focusing encapsulation process should follow a Poisson distribution (Equation 12) in regards to the occupancy of cells in cocoons. Using the initial concentration of cells as 8.5 million/mL , and the size of generated cocoons, the probabilities of how many cells can be found in a given cocoons can be generated. The results of this can be found in Table 4.

Table 4: Probability that a cocoon will be occupied by a cell given 8.5 million cells per mL

Diameter (µm)	*30*	*50*	*70*	*90*
% Unoccupied	88.7	57.3	21.7	3.9
% 1 Cell	10.7	31.9	33.2	12.6
% 2 Cells	0.6	8.9	25.3	20.5
% 3+ cells	0	1.9	19.8	63.0
% Occupied	11.3	42.7	78.3	96.1

Based on this, the goal size of the cocoons is between 50 and 70 µm, to have the greatest occupancy of single cells without generating cocoons so large that multi cell encapsulations become favoured.

Similar calculations can be done with the encapsulation of cocoons to make hollow cocoons, with some slight variation of λ (the mean number of events in a time interval) due to the increased volume of the cocoons compared to cells. For cocoons, λ is the ratio of the volume fraction of cocoons to the sample volume, over the volume fraction of the single encapsulation cocoons to the second encapsulation volume. [76] Table 5 shows the theoretical occupancy of various sized hollow cocoons when encapsulating 50 µm sized cocoons at a concentration of 850,000/mL. Should the flow of gelatin cocoons into the nozzle act as a Poisson process, producing cocoons at a size range approaching 150 µm should then allow for similar occupancy rates as in the existing cell encapsulation.

However, while this is a theoretical ideal, factors such as cell clumping and settling can lead to deviation from the assumptions of a Poisson process. By using the previously described quantification methods the actual measured results can be compared to the theoretical output to compare the encapsulation efficiency. Should the number of encapsulated cells or cocoons be too much lower than what was predicted, it is likely that there is some issue in experimental set up that might need to be addressed for improved encapsulation quality.

Table 5: Probability that a Hollow Cocoon will be generated, with a cocoon concentration of 850,000 per mL

Hollow Cocoon Diameter (µm)	*130*	*140*	*150*	*160*
Inner Cocoon Diameter (µm)	50	50	50	50
% Unoccupied	37.6	29.5	22.3	16.2
% 1 Cocoon	36.8	36.0	33.4	29.4
% 2 Cocoon	18.0	22.0	25.1	26.8
% 3+ Cocoon	7.6	12.5	19.1	27.5
% Occupied	62.4	70.5	77.7	83.8

2.4.5 ImageJ for Measuring Cocoon sizes

ImageJ is an open source image processing program made with Java by the National Institute of Health, and the Laboratory for Optical and Computational Instrumentation at the University of Wisconsin. It possesses numerous features for editing and analyzing images, and supports the inclusion of plugins to provide custom functionality. The image processing abilities of ImageJ were what was used to generate the stacked fluorescence images mentioned in Section 2.4.1.

One of the basic features of ImageJ is pixel based measuring. (Figure 21) By setting each pixel to be worth an amount of real distance it is possible to measure the size of features from collected images. This is the method used to measure the size of cocoons as they are being made in the microchannel. The width of the microchannel is known and is present in all images where cocoons are being measured, and as such acts as the guiding scale to determine the length that each pixel corresponds to. Lines are then made bisecting the cocoon, taking measurements of each. Due to a blurred "halo" surrounding the cocoons due to their relatively fast speeds, the accepted accuracy of these measurements are 1 µm.

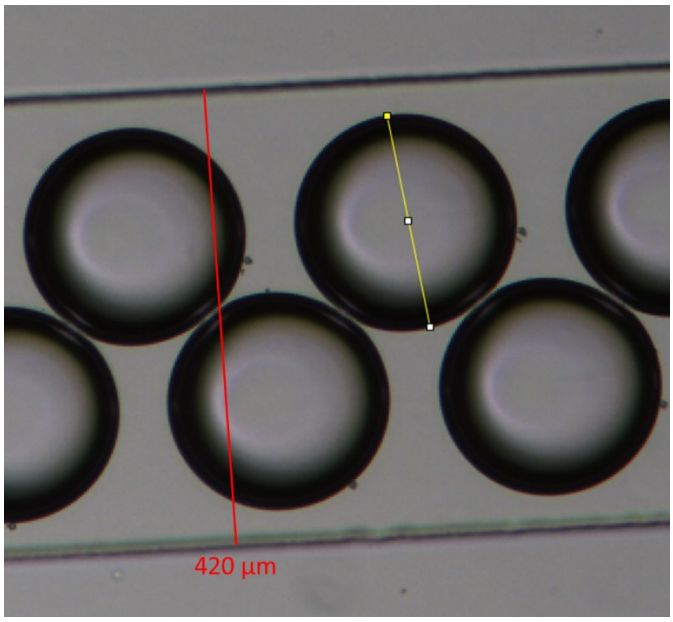

Figure 21: ImageJ method of measuring cocoon size. First a line would be made over the position of the added red line, which sets the number of pixels in that line to be equivalent to 420 µm. Next lines such as the yellow line are made that bisect each cocoon to provide the measured size.

Cocoons can be made at different sizes, either intentionally due to the selection of different pressures, due to size drift from conditions in the channel changing over time or from polydispersity where produced cocoons in a selected time frame vary around an average value. As a 1 μm variation in size leads to much more polydisperse cocoons for a sample that are 10 μm than 100 μm, comparisons of monodispersity are made though use of the Coefficient of Variation, which is a percentage made through the ratio of the standard deviation to the mean for a sample of cocoons to normalize the value for comparisons.

3 Results

The purpose of this research project is to investigate the effects that encapsulating cells in hollow hydrogel capsules has on their viability and proliferation. The hypothesis is that by giving cells an open volume that is still contained within an immunoprotective barrier, the cells viability and proliferation will improve while not significantly increasing premature cell egress. In applications relying primarily on paracrine based regenerative pathways, the early egress of cells from the cocoons can lead to premature clearance *in vivo* reducing the therapeutic effectiveness of the dose. Improved viability and proliferation would maintain, or potentially increase, the number of living therapeutic cells at the recovery site allowing for a dose to prolong its effectiveness. Should this hypothesis hold up, these hollow cocoons could represent an improvement in cell based regenerative therapies over current methods using solid hydrogel cocoons.

The goals in this project to test this hypothesis include developing a method of fabricating hollow cocoons in a cell friendly process, designing a microfluidic channel to carry out these encapsulations, characterizing the resulting cocoons and monitoring encapsulated cells to determine any effects on viability and egress.

Firstly, two thermoreversable hydrogels, gelatin and poloxamer, were investigated for their behavior when used in a flow-focusing geometry and the subsequent stability of the generated microparticles. Then the process and conditions of generating these particles at high monodispersity and throughput values is investigated, determining the proper concentration of the hydrogel as well as the concentration and HLB of the surfactant to best create a stable emulsion. After this, the previously explored method of creating double emulsions is modified with exploration of alternate device geometries, leading to the generation of hollow cocoons, the process of which is further optimized. [15] Finally, Fluorescence Live/Dead stains were used to determine cell behaviour in timepoint studies.

3.1 Hydrogels

The production of single emulsion droplets for encapsulating cells is done using the device laid out in Figure 9. While the use of agarose in these devices is well studied in this research lab in terms of generating a stable monodisperse emulsion, the behavior of other hydrogels is largely unknown. [60] To this end, investigation into creating hollow cocoons began with determining whether poloxamer and gelatin were suitable for creating the inner cores. There were some basic criteria for this determination. First was the ability to form droplets at a monodispersity under 3%, so that produced samples were as uniform as possible for dosing purposes and for consistency when used in subsequent encapsulation. The target size for these cocoons was between 50-70 µm, as that size correlates to a peak in throughput of the current devices, shows high occupancy at the cell concentration previously used for production of *in vivo* samples (Table 4), and be small enough to pass through a microfluidic nozzle with a diameter similar to those previously investigated. [15], [60], [106] Cocoon production throughput was needed on the order of 100s of cocoons per second to be able to generate over 1 million cocoons in less than an hour, so as to be able to produce doses for *in vivo* testing at a reasonable rate and to limit the stress placed on the cells. The last was for the cocoons to properly gel and to be physically sturdy enough to make it through the sample purification steps without breaking apart.

3.1.1 Poloxamer

Starting with poloxamer, the initial attempts were to try to form an emulsion using the same parameters as the typical agarose encapsulation but with poloxamer specific hydrogel concentrations. This was a device with a 30 µm nozzle, Span 80 surfactant at 1.5% (HLB 4.3), with gel concentrations between 20% to 30% to judge the viscosity of the poloxamer. It was quickly decided that 30% poloxamer was too viscous. While it formed a stable monodisperse emulsion, with a monodispersity of 2.1%, it required the maximum pressure of the dispersed phase and the minimum pressure of the continuous phase to generate roughly 45 µm cocoons. Given that no such issues occurred with lower concentrations, the higher viscosity of the 30% is assumed to bring the Ohnesorge number above the critical value, affecting the formation and breakdown of

the flow cylinder. Due to the extremely low continuous phase flow rate, estimated throughputs were as low as 1/s. (Figure 22)

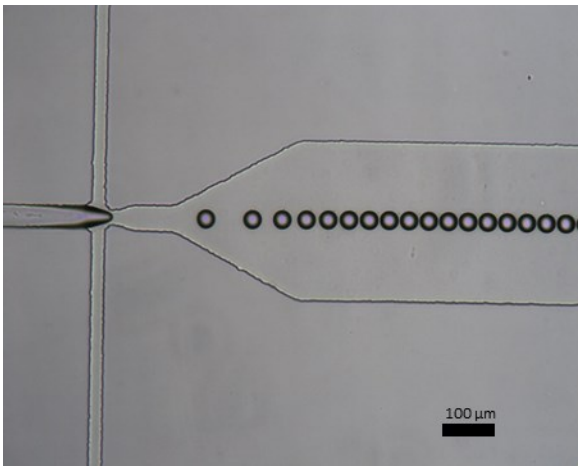

Figure 22: Emulsion formed from 30% poloxamer at maximum limits of pressure ratio.

Lowering the concentration to 20% poloxamer using otherwise the same conditions allowed for a more typical emulsion to be made. Size monodispersity of these emulsions were typically 2.5% and production throughput was vastly improved. The largest possible stable cocoon size made was only 21 µm, with anything larger turning into jetting and streaming. Conversely, this behavior also allowed for extremely small cocoons to be produced, smaller than could be accurately measured. Examples of these emulsions can be seen in Figure 23.

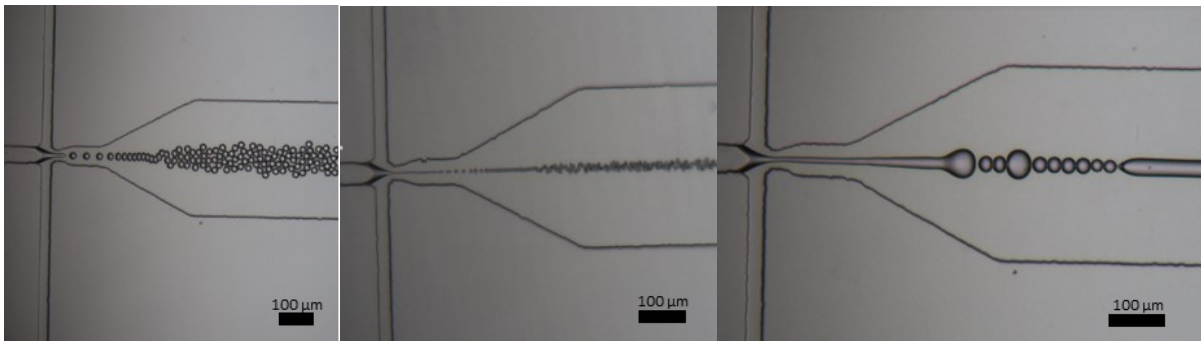

Figure 23: 20% poloxamer emulsion modes from left to right: Monodisperse, Small Dripping and Jetting.

Given that the poloxamer emulsions available size range was far smaller than the typical agarose emulsions using the same device, a design with a larger 50 µm nozzle was used for all future poloxamer tests, as the larger characteristic length would lower the Ohnesorge number and allow for a larger dispersed phase flow cylinder at lower flow rates. This immediately showed promise, as emulsions between 50-80 µm were easy to achieve at moderate flow rates, with moment to moment monodispersity typically achieving 1.5%, and often going beneath 1%. The emulsions size was not stable however, Figure 24 shows a single emulsion at times separated by roughly 30 seconds between each picture. The size rapidly shifted from 70, to 55, to 85 to 60 µm with no external disruptions.

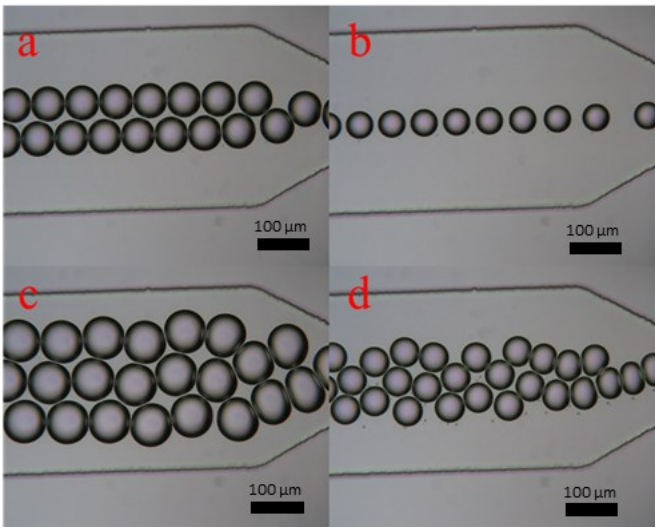

Figure 24: Varying emulsion size at constant pressure ratio: a: 70 µm b: 55 µm c: 85 µm d: 60 µm

By adjusting the HLB of the surfactant to 6, the size of the emulsion became much more stable, indicating that the previous issue was likely due to the surface tension between the poloxamer and oil phases. Cocoons between 50 and 70 µm were produced at a monodispersity of 1%, and after leaving the emulsion without any adjustments for 25 minutes, the size of the generated emulsion drifted only 2.5 µm, an amount that is easily accounted for through active adjustment throughout a run.

While upstream generation of the emulsion was successful, the poloxamer cocoons struggled with the final criterion as it proved difficult to collect solid poloxamer cocoons. There appeared to be two main issues, both potentially relating to poloxamer chains amphiphilic nature and the

nature of micelles. The first issue was the formation of droplet interface bilayers (DIBs). DIBs are an issue typically found with lipid surfactants where the tail groups of the surfactants show a greater affinity with other tail groups than the oil layer, which leads to a “bridge” forming between droplets. [107] An example of this with the poloxamer beads can be seen in Figure 25. As this is not a typical occurrence with Span and Tween surfactants, it seems likely the micellar nature of poloxamer gels is relevant to this issue. Unlike chemical or physical crosslinking, micellar gels are not static. Chains can move between micelles and the solvent even when gelled, and if the amphiphilic poloxamer chains also prefer to integrate with the Span and Tween surfactant chains, this could be what is causing the formation of DIBs. [67]

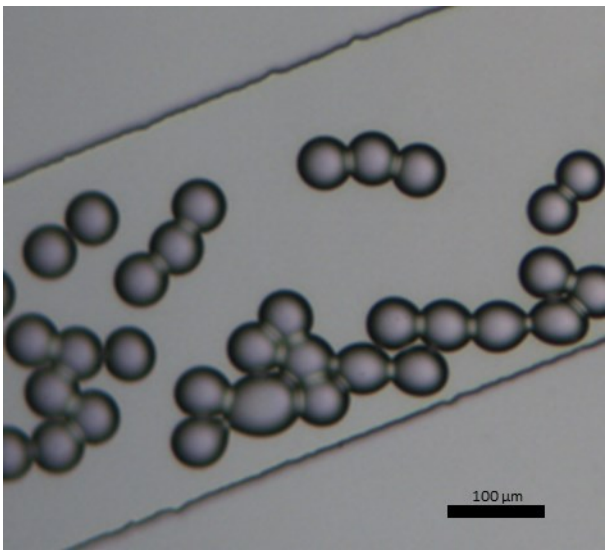

Figure 25: Poloxamer emulsion breaking down due to the presence of DIBs.

The second issue is that the poloxamer cocoons seem to be inherently unstable in an aqueous phase. After purification, no cocoons were ever found in the collection vessel. Before purification, they could be seen in the oil phase, albeit as an agglomerated mass likely due to the progression of the DIB merging the micelles, but not even those were visible after centrifuging. (Figure 26) This is again likely due to the micellar nature of the gel. Once in the aqueous phase, the micelles are in a solvent not yet containing any poloxamer. As poloxamers are only physically entangled when gelled, and formation of the gel relies on the concentration in the solvent being higher than

the CMC, the micelles break apart to diffuse throughout the solvent. Due to this issue, it was decided that the prudent option was to table poloxamers and begin investigation into gelatin.

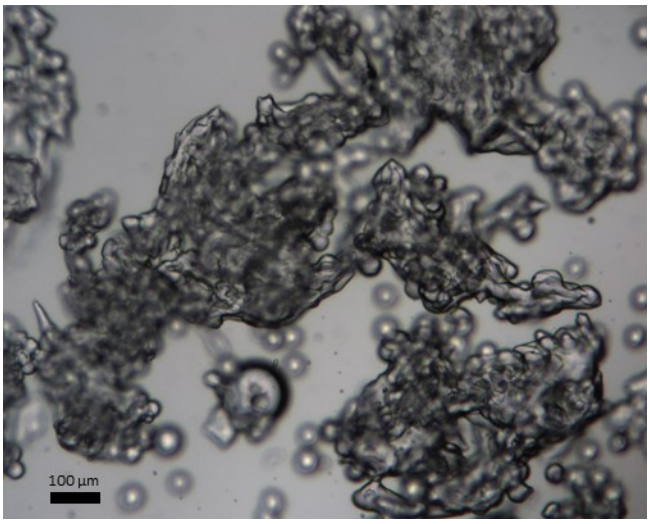

Figure 26: Poloxamer cocoons in oil phase, agglomerating so few individual cocoons remain.

3.1.2 Gelatin

For the initial tests with gelatin, emulsions went back to being generated with the 30 µm nozzle and original 1.5% HLB 4.3 surfactant. Concentrations between 10% and 20% were tested to find a balance between physical stability of the gelled cocoons and a low viscosity for the emulsion formation. Very quickly it was determined that 20% gelatin was too viscous, showing similar dripping behavior to 30% poloxamer. (Figure 27) Additionally, due to the high viscosity, secondary wavelengths formed in the Rayleigh-Plateau instability, and these cocoons formed numerous satellite particles alongside the main droplet.

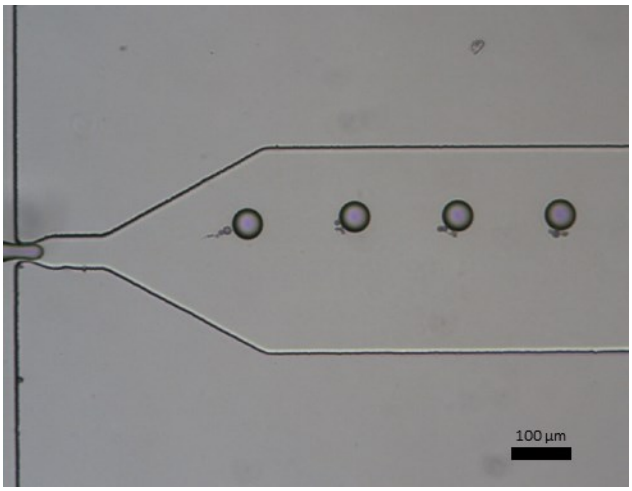

Figure 27: 20% Gelatin droplets showing satellites

Lower concentrations of gelatin showed far better results. Both 10% and 15% gelatin created emulsions of roughly 50 µm at moderately high flow rates and monodispersities below 1.5%. While monodisperse, the size of cocoons was not perfectly stable, showing drift in the size as time progressed. The 10% gelatin droplets began at a size of 45 ± 2 µm and over 45 minutes without outside adjustment to the pressure gauges increased to 52 ± 2µm. The 15% started at 52 ± 3 µm and over 45 minutes decreased to 40 ± 2 µm. (Figure 28)

These slow drifts are not uncommon when making cocoons and are something that can be mitigated by active monitoring of size and adjustment of the pressure ratio. They are typically attributed to slow changes in the conditions found in the device that develop over the course of a run. One common issue, especially with higher concentrations, is build up of partially gelled hydrogel. It is often noticed that in long runs the flow of the dispersed phase can become minorly obstructed due to gel building up of the walls of the inlet tube. This typically breaks off and becomes trapped in the inlet filter, but over time can lead to minor decreases in cocoon sizes. Size increases are less documented, but are thought to be due to factors such as the gradual attemperation of the sample inlet tube lowering the viscosity of the hydrogel, or the development of a small pressure leak in the PTFE rubber seal that the inlet tubes pass through into the sample vial reducing the continuous phase flow.

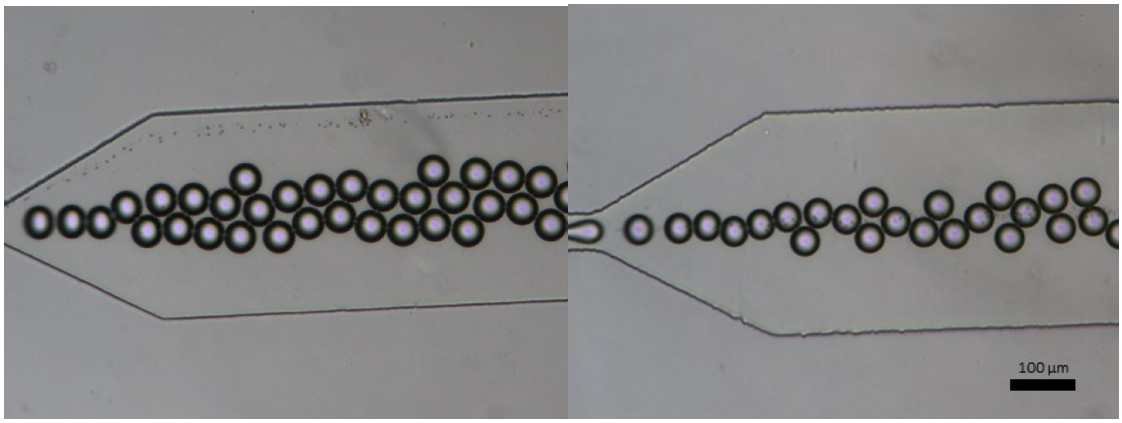

Figure 28: 10% Gelatin (Left) and 15% Gelatin (Right) emulsion

Unlike the poloxamer, the centrifugation steps that are typically used with agarose cocoons were able to properly move the cocoons from the oil phase into the aqueous phase while keeping their integrity. (Figure 29)

Based on the success of both being able to generate a monodisperse emulsion of the target size, and then gelling and retrieving the generated cocoons, gelatin was chosen as the hydrogel used to generate the temporary inner core of the hollow cocoons and thusly underwent more stringent analysis of its behavior.

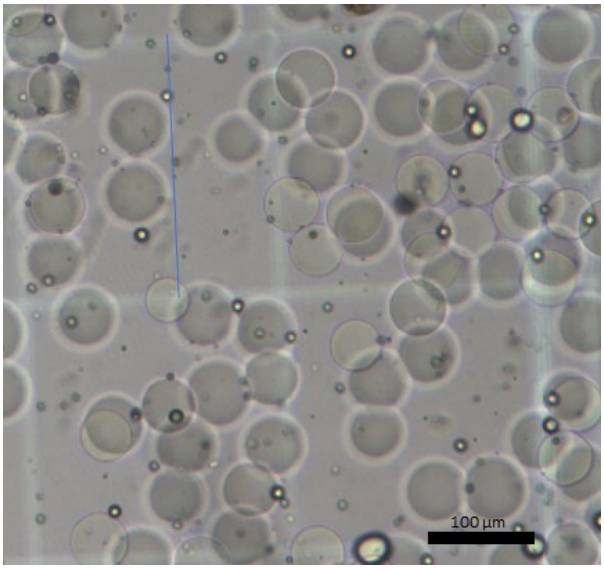

Figure 29: 10% Gelatin Cocoons on hemocytometer

3.1.3 Gelatin Melting Temperature

When producing hollow cocoons, there is a brief period when gelatin cocoons are on the heated section of the microfluidic channel, but not yet encapsulated in the agarose shell. If the melting point of the gelatin is too low, this heating might disrupt the mechanical strength of the cocoon causing it to shear before encapsulation. As mentioned earlier, concentration and the addition of polyols such as glycerol can affect the melting point of gelatin. [73] To gain an understanding of the profile for the gelatin used in the project, an experiment to determine the melting temperature of bulk gelatin for varying concentrations and glycerol content was undertaken.

Initially, 20% gelatin hydrogel was produced, and portions were diluted to 10 and 15% using PBS and Glycerol for 0 to 30% glycerol content. Subsamples of 0.75 mL of hydrogel were then pipetted to microcentrifuge vials and allowed to cool in a 4^{o}C fridge. To determine melting point, a heating block was used to apply a temperature ramp of 0.25^{o}C with each new temperature help for 3 minutes to allow for attemperation. To show when the gel had melted, small metal bearings roughly 2 mm in diameter were placed on top of the gelled hydrogel. The bearings were of higher density than the hydrogel, but not large enough to penetrate the stiff gel and so would only sink when the physical gel structure disappeared at the melting temperature. When a bearing broke through the surface of the hydrogel, it was marked as being melted at the applied temperature value. While crude, the results give a low granularity overview of the hydrogel behavior that shows the working range of the hydrogel.

It was found that increasing gelatin concentration by 5% increased the melting point by about 1-1.5^{o}C, which appears to follow previous literature showing a somewhat linear relationship between concentration and melting point temperature. [72] The addition of glycerol also appears to have a roughly linear effect on increasing the melting temperature of the gelatin, with a roughly consistent 2.5^{o}C increase per 15% glycerol content which can be seen in Figure 30.

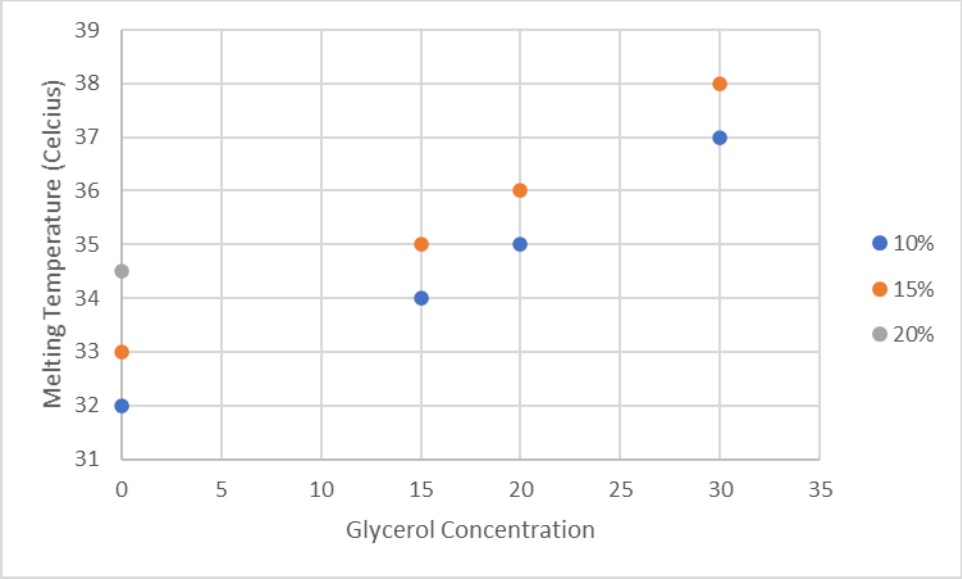

Figure 30: Gelatin and Glycerol Concentration relationship to Melting Temperature

Based on these results, it was decided to begin with 10% and 15% gelatin cocoons without glycerol to see if they could mix into the agarose on chip without melting for the sake of cell viability. Due to diffusion of glycerol out of the cocoons once in the sample collection vial, it is suspected that even cocoons encapsulated with 30% or more glycerol would still melt at physiological temperatures, allowing for glycerol to be held as a contingency should the cocoons be unable to hold their shape in the device before being re-encapsulated.

3.1.4 HLB Value Testing for Gelatin

While initial experiments showed that producing monodisperse gelatin cocoons was possible, there was still little knowledge of the optimal conditions for generating the emulsion. Reaching higher throughputs of cocoon production reduces the time required to produce a sample, which is beneficial both in a logistical sense and for reducing the stress placed on the cells. However, higher throughputs require higher flow rates, which increases the Weber and Capillary numbers eventually leading to a loss of monodispersity. [29], [30] By changing the surfactant concentration and HLB, the interfacial tension of the emulsion can be increased,

allowing for higher throughputs, so long as it doesn't rise so much that the emulsion loses stability from the dispersed phase attempting to coalesce, requiring a balance.

The goal of this stage of experimentation was to identify a surfactant concentration in the mineral oil based continuous phase that would allow for the creation of monodisperse gelatin droplets in the 50-70 µm range at the highest possible flow rates. As mentioned previously in Section 1.1.7, and later shown in Figure 23, higher flow rates can lead to "jetting" behavior as the Weber number scales by the second power. Additionally, when the dispersed phase flow outstrips the continuous phase there is no longer any breakup of the dispersed phase into droplets causing streaming, while the opposite leads to backflow of the continuous phase into the dispersed phase channel. By setting the continuous phase pressure and varying the dispersed phase, one can mark the transitions between these types of flow. When done across the range of continuous phase pressure a "flow profile" reminiscent of a phase diagram can be produced which shows the limits of monodisperse flow for a given emulsion. (Figure 31). Surfactant mixtures that produce a monodisperse region of the flow profile at higher pressures indicate a higher potential throughput and are thus the best candidates for future production of the gelatin cores.

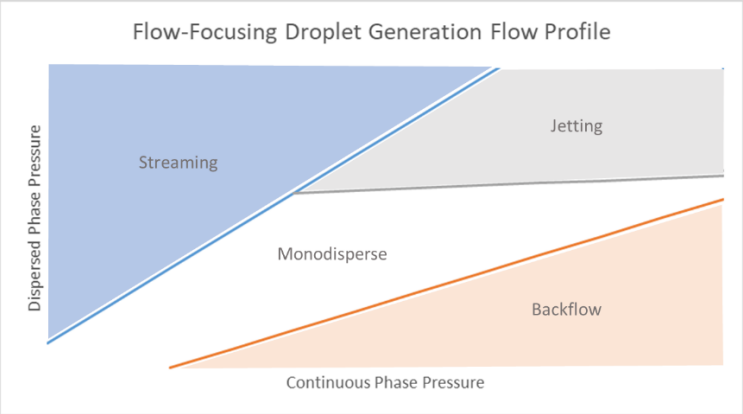

Figure 31: Example flow profile of a flow-focusing microfluidic device. The white region is where monodisperse droplets can be formed, which is held between streaming and backflow of the dispersed phase. At higher flow-rates monodisperse droplets become impossible due to jetting behaviour.

3.1.4.1 Determination of Flow Profiles for Gelatin

In order to cover a range of emulsion properties, surfactant/mineral oil mixtures of HLB 4.3 and HLB 6, chosen due to being the HLB of pure Span 80 and the higher end of the W/O emulsification range, were made in concentrations of 1%, 1.5% and 2%. Previously 1.5% Span 80 was found to be the optimal concentration for producing monodisperse agarose emulsion. [60] Gelatin of 10% and 15% was emulsified using these surfactants to generate the flow profiles.

When generating these graphs, two runs of each type were done, to ensure a measure of reproducibility in case of a bad sample or device. Each experiment consisted of one channel, with a pairing of a gelatin concentration and a surfactant mix. Starting from the lowest possible continuous phase pressure, the dispersed phase was slowly changed to find where backflow began, then increased to find the streaming and jetting transitions. As all of these points needed to be found in 150 µL of dispersed phase sample, the entire phase diagram could not be explored so continuous phase pressures at specific points were investigated, along with some additional nearby points to find the onset of the jetting regime if needed.

Throughout this process, sizes were monitored as well, though measurements were cursory and done mainly to locate pressure ratios at higher pressures that produced monodispersed cocoons in the 50-70 µm range.

Immediately it was determined that a full test involving 1% surfactant would not be viable. All attempts using both HLB 4.3 and HLB 6 mixtures suffered from various amounts of wetting on the surfaces of the channel. In the case of HLB 4.3 the wetting was mostly contained to the side of the nozzle, but while a monodisperse emulsion could be technically created, the consistency of the results is suspect. The HLB 6 emulsion showed worse wetting, with increased wetting of the main channel causing pockets of dispersed phase to gather on the walls, merging with droplets that passed near them. (Figure 32) The hypothesis for this behavior is that the interfacial tension between dispersed and continuous phases was at a level that could sustain the emulsion, but was higher than the interfacial tension between the dispersed phase and the glass slide where it appears the wetting occurred. While inconvenient, this does not occur at higher surfactant concentrations and as such has not been further explored.

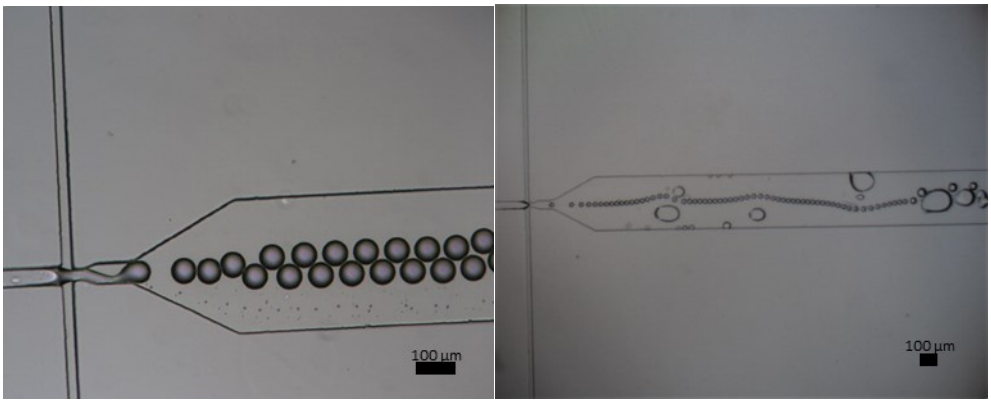

Figure 32: 1% Surfactant emulsion tests causing wetting: (Left) HLB 4.3 showing wetting of the nozzle with an otherwise monodisperse emulsion. (Right) HLB 6 showing wetting of the channel surface

For the other surfactant mixes monodisperse emulsions were able to be made for at least part of the available pressure range available from the gauges, a max of 172 kPa for the continuous phase and 140 kPa for the dispersed. Graphs of their behavior can be seen in Figure 33, outlining the limits of monodisperse flow.

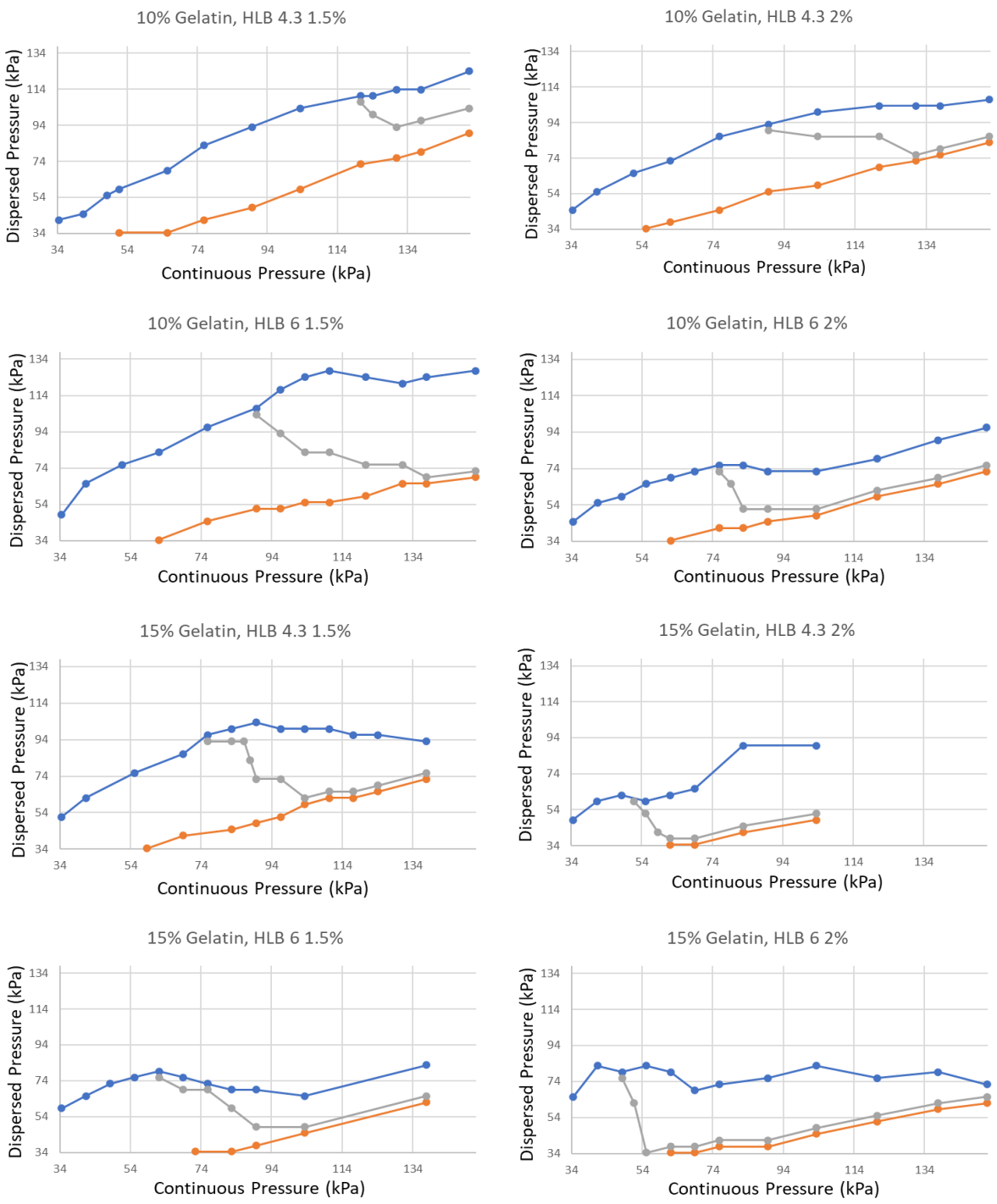

Figure 33: Graphical Flow Profiles of 10% and 15% Gelatin using 1.5% and 2% Surfactant at HLB 4.3 and 6. The blue line represents streaming behavior, the orange is backflow of oil into the dispersed phase channel, and grey is jetting behavior causing polydisperse emulsions. The area below the blue and grey lines but above the orange is the pressure ranges that lead to monodisperse emulsions. The line is for visual convenience and not to imply anything about the data between points

3.1.4.2 Results of Flow Profile Analysis

Based on these experiments some general behaviours were found regardless of the surfactant HLB or concentration. In lower to moderate continuous phase pressures without jetting, there is a roughly linear increase in the minimum dispersed phase pressure needed to prevent backflow and the maximum dispersed phase pressure before streaming occurs. Once pressures reach a point that jetting behaviour develops, the maximum dispersed phase before streaming occurs loses this relation, often showing decreases or other disturbances.

The concentration of gelatin used for the dispersed phase was shown reduce the monodisperse range of emulsion generation. When using the same surfactant HLB and concentration, 15% gelatin routinely showed the onset of the jetting phase at continuous phase pressures of roughly 2/3 the magnitude of the onset pressures seen in 10% gelatin. This behaviour is likely to do with an increase in the Ohnesorge number due to the increase in viscosity of the higher concentration gelatin. The density of hydrogels changes little with increased concentration meaning the Weber number should be largely the same value. [108] This means that at the same flow velocity, the only parameter that should have changed is the viscosity meaning the critical Ohnesorge number causes the transition to jetting occurs at a lower flow rate.

Similarly, increased surfactant concentration also caused jetting to occur at lower continuous phase pressures, due to the decrease of interfacial tension increasing the magnitude of the Capillary and Weber numbers. This behaviour is predicted by the resulting increase in those numbers and indicates that any benefit gained from a stable emulsion at higher pressures due to the decrease in surface tension is not enough to outweigh the negative impacts on monodispersity.

Increasing the HLB number of the surfactant showed a similar result, indicating that the surfactant mix was lowering interfacial tension. This might indicate that utilizing surfactants with lower HLB values, such as a mix of Span/Tween 85 to produce a HLB value of 3 may be a method of increasing throughput in the future.

While the appearance of polydisperse droplet generation was determined by the magnitude of continuous phase pressures, it also impacted the available size range of the generated emulsion. For 10% gelatin with 1.5% HLB 4.3 surfactant near 35 kPa in the continuous phase pressure, the lowest size of droplet feasible to produce was 50 µm while the size created right before streaming was over 100 µm. By the time the continuous pressure reached 105 kPa, the largest cocoon that was produced is 60 µm. By 140 kPa, due to the constraints of jetting the only feasible cocoon size that could be produced is 30 µm. Monodispersity does not seem to be affected by this change in behavior, as all measured monodisperse emulsions held monodispersity values of under 2%, with most emulsions with pressure ratios away from the jetting and streaming phase lines falling closer to 1.5%.

The outcome of this investigation was that 1.5% HLB 4.3 surfactant was the current best choice as it allowed for the highest range of pressures for the highest throughput. For both 10% and 15% gels, the highest flow rate pressures that produced 50 µm cocoons were found using the chosen surfactant. For 10% gelatin 121 kPa continuous pressure and 100 kPa dispersed pressure produced emulsions between 50-55 µm depending on device, with a throughput of 300-350 droplets/s. For 15% gelatin the highest was 85 kPa and 85 kPa, producing emulsions at 48-53 µm and due to the lower pressures had throughput at 150-170 droplets/s.

Due to these results, moving forwards the main production of gelatin cocoons would be done with 10% gelatin and 1.5% HLB 4.3 Span 80 surfactant, with 15% gelatin cocoons held as a reserve should a higher gel strength be needed at the cost of higher throughput.

3.1.5 Gelatin Cell Encapsulation

With the optimal emulsion components and processes settled, the next step was to recreate the previous process of encapsulating cells but with gelatin cocoons instead of agarose. Based on the previously mentioned flow phase diagrams, 10% gelatin and 1.5% HLB 4.3 surfactant were used this combination allowed for the highest pressures to generate cocoons that were still monodisperse. Before encapsulation, 15% gelatin was diluted with cell media containing 1.7 million cells to produce 200 µL of 10% gelatin with 8.5 million cells/mL. After reconfirming the

previous results that a continuous pressure of 121 kPa and a dispersed pressure of 100 kPa create cocoons at 50-55 µm, this pressure was chosen to produce cocoons as it was the highest available pressures to produce cocoons at that size while still being monodisperse. To test this, five samples of gelatin cocoons were produced to determine the nature of gelatin encapsulation of cells on cocoon size and throughput, and cell occupancy and viability, the results of which are collected in Table 6.

Table 6: Results of Cell Encapsulation in Gelatin.

Sample	*Cocoon Size (µm)*	*Throughput (/s)*	*Occupancy %*	*Cell Viability %*
1	54 ± 2	346	46.7	97.1
2	52 ± 2	370	56.0	98.7
3	52 ± 2	454	51.4	98.3
4	55 ± 2	290	51.2	98.7
5	54 ± 3	376	49.3	96.2

3.1.5.1 Gelatin Cocoon Monodispersity

The addition of cells did little to affect the emulsion generation. As with previous experiments with agarose, the individual cells flowed through the filter, with a small build up of cells over time that did not appear to greatly affect flow. The cells passed though the nozzle with random spacing, leading to the expected rate of producing occupied cocoons. (Figure 34)

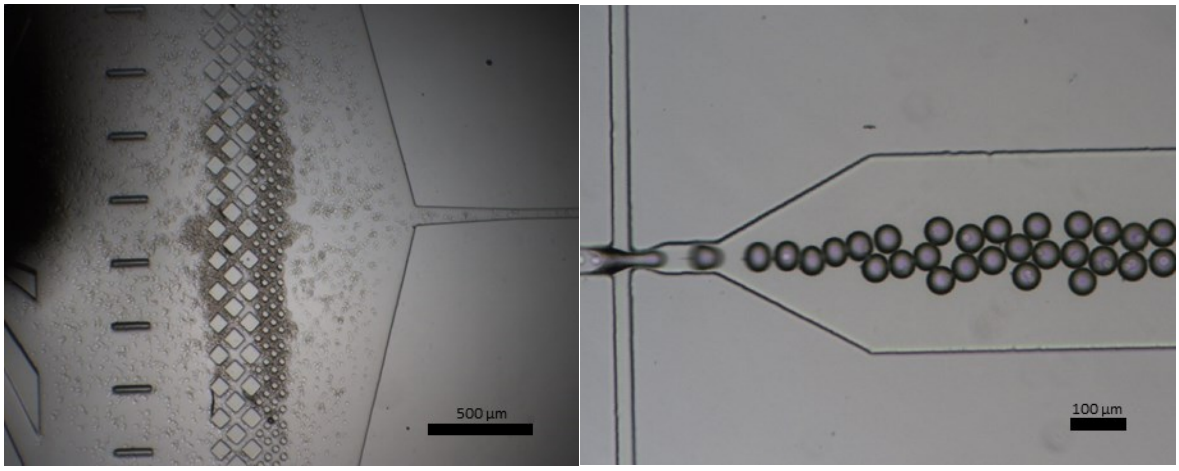

Figure 34: (Left) Cells passing through inlet filter partway through encapsulation. Cells are beginning to agglomerate in the filter. (Right) Encapsulation of cells in monodisperse gelatin cocoons.

The presence of cells did appear to have some impact on the cocoon monodispersity. For cocoons produced without cells the majority of emulsions had monodispersities that were typically around 1.5% no matter the generated size or throughput, with emulsions that approach the threshold of jetting behavior being slightly more polydisperse at 2%. For emulsions generated with cells this is slightly higher, ranging from 2-3%, likely due to the disruptions caused by the 10-15 µm cells in the dispersed phase flow column. Average sizes of the cocoons at the constant pressure were less stable over the length of the experiment. While the moment to moment sizes of the cocoons were monodisperse, the average size tended to slowly fluctuate by up to 1 to 2 µm. The second column of Table 5 shows the range of cocoon sizes using the standard deviation of the measured cocoons. In comparison an additional experiment using the same conditions, but with active monitoring of cocoon size and active pressure adjustment created cocoons of the same monodispersity but with a lower size range of 49 ± 1 µm.

3.1.5.2 Gelatin Cocoon Throughput

The throughput of producing these cocoons was seemingly much more variable. Three of the values were relatively close together at 370 cocoons/sec while Sample 3 was far higher, and Sample 4 far lower. To an extent the throughput of an emulsion should depend on the size of the cocoons being produced. There is a given volume of dispersed flow and if it is producing larger cocoons it should make them at a slower rate as the instability breaks down at a lower frequency to account for the increase in cocoon volume. This however seems to not be the determining factor as aside from Sample 4 being the largest cocoons on average with the lowest throughput there otherwise does not appear to be any size based relation occurring.

The throughput was calculated using a hemocytometer, taking a small subsection of the sample to extrapolate the whole number of cocoons produced. This has a small flaw when it comes to counting cocoons, as they begin to settle almost immediately. If the cocoons are not evenly distributed when taking a subsample, that subsample would not be representative of the whole and as such could skew the throughput higher or lower depending on whether the cocoons were too dense or sparse. To try to confirm how realistic the measured throughput values were, calculations comparing the measured values to theoretical expected values were carried out in

Table 7. Each of the samples consisted of 100 µL of gelatin, which was completely utilized aside from some untraceable transfer losses. Based on this and the average cocoon volume, the expected number of cocoons could be found, which could then be compared to the measured number of cocoons and the timeframe of the experiment to see if the throughputs align.

Table 7: Theoretical throughput compared to measured values.

Sample	*Cocoon Size (µm)*	*# Cocoons Calculated*	*# Cocoons Measured*	*Time (min)*	*Calculated Throughput (/s)*	*Measured Throughput (/s)*
1	53.5	1240000	1330000	64	325	346
2	51.7	1380000	1043400	47	490	370
3	52.1	1350000	1254000	46	469	454
4	55.3	1130000	870000	50	376	290
5	54	1210000	1143750	56	360	376

Before comparing the results of Table 7, there are some potential reasons why the number of cocoons in a collected sample may not match the theoretical value. There is some loss at the beginning of an encapsulation run when the size of the droplets is being adjusted and are not being collected in the sample vial. Similarly, there are cocoons lost at the end of an encapsulation inside the channel when the flow is stopped. Finally the sample purification process involves several sample transfers, which can lead to some loss of sample. This may account for why the measured number of cocoons were almost nearly always lower than the theoretical value. Without deeper investigation and additional experiments there is no way to determine the losses from these sources. As multiple subsamples were not taken at the time of the experiments, there is also no way to judge the heterogenicity of the subsampling method at this time to try to create a more accurate value of the true number of cocoons in the sample vial at the time of measuring.

That said, between the theoretical and the measured throughputs there is good reason to believe that production of these cocoons meets or exceeds the required cocoon production rate. Given the reoccurring lower bound throughput value of 370/s from both the calculated and measured throughputs, 1 million cocoons could be produced in 45 minutes which based on previous experience is well within a reasonable timeframe for an encapsulation run.

3.1.5.3 Gelatin Cocoon Cell Occupancy and Viability

For the occupancy and viability, as well as cell egress, fluorescence microscopy images were used to count cocoon numbers, cell locations and cell vitality. Typically cocoons would be monitored over several days to judge changes in the proportion of living and dead cells, and the decrease in occupancy that correlates to cells egressing the cocoons but due to the desired thermo-reversible nature of the gelatin cocoons incubating them for any length of time would melt them. Longer term measurements would not be wholly relevant anyways as the cells are only to be encapsulated in the bare gelatin for at most one to two hours before they are all re-encapsulated in hollow agarose shells.

For the five samples, initial egress was almost non-existent as expected. There were occasionally free-floating dead cells, but in low enough number to state that directly after encapsulation cells are firmly inside the cocoons. Similarly, viability of the cells is at 97.8 ± 2% for the five samples. This is if anything higher than previous experience with encapsulating cells in single layers of agarose of similar size. [15], [60] This seems to indicate that encapsulating cells in gelatin as a transitional step to hollow cocoons is a cell safe method and should provide a high starting viability for hollow cocoons.

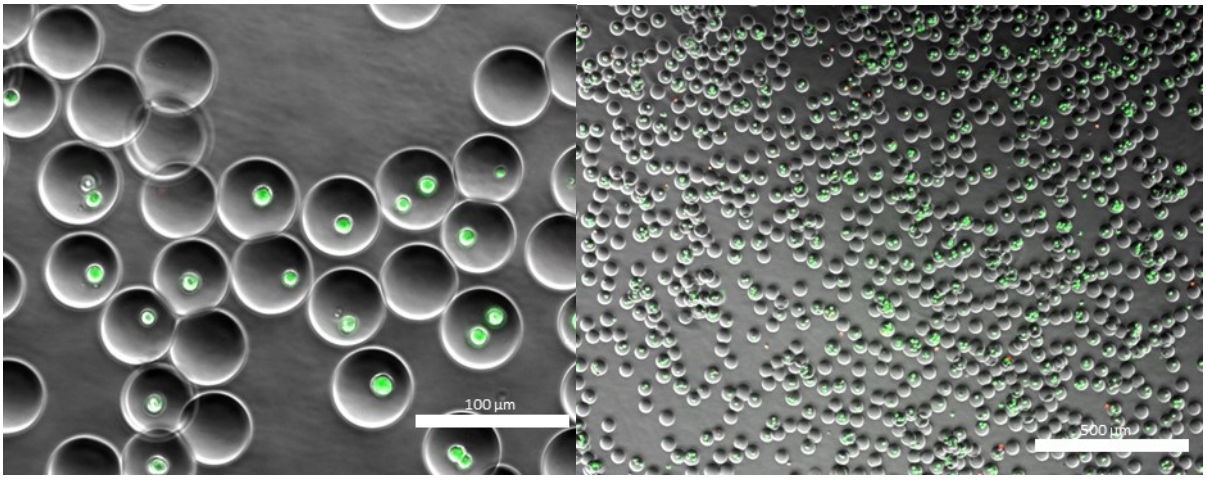

Figure 35: Cells encapsulated in gelatin cocoons. Green indicates a living cell, while red is a dead or dying cell.

The average occupancy of the five samples was 51 ± 6%. This range covers right where the Poisson occupancy estimate of 52% for cocoons between 50 and 55 µm with a cell concentration

of 8.5 million/mL. That said, there is an abnormal amount of cocoons with three or more cells which should normally make up less than 3% of the total cocoon amount. Based on this it seems likely that the concentration of cells mixed into the sample is biased at a higher concentration than 8.5 million/mL but potentially some clumping behavior of the cells helps maintain the overall occupancy. To clarify, if cells are clumping then they are moving towards the nozzle non-independently breaking the assumption of the encapsulation being a Poisson process. However if the clumps are still entering the nozzle independently the overall occupancy rate can remain mostly the same, as the higher concentration of cells begins to appear like a lower concentration for the purposes of the encapsulation due to the clumping. This currently does not have much bearing on the success of producing hollow cocoons or analysing the behavior of encapsulated cells, as the main priority at this time is encapsulating them as a proof of concept, but this is something that will need attention at a later date to create consistent doses should *in vivo* experiments become likely.

3.2 Hollow Cocoon Microchannel Design

The method of re-encapsulating hydrogel cocoons in another layer of hydrogel using microfluidic flow-focusing devices is something that has already undergone some investigation by members of the Godin Lab. [15] This process uses a channel design similar to the one shown in Figure 9, but with modifications to the nozzle area shown in Figure 10 to account for the flow of cocoons in the inlet and for the production of larger emulsions. A schematic of the channel can be seen in Figure 36. The main differences compared to the single encapsulation channel are a wider post spacing in the dispersed phase inlet to allow cocoons to flow, along with a wider inlet channel. There is a wider nozzle to increase the size of the generated cocoons to over 100 µm at high throughputs, and wider continuous phase nozzles to reduce flow resistance allowing for higher continuous phase flow to balance out the increase in dispersed phase flow from the larger inlets.

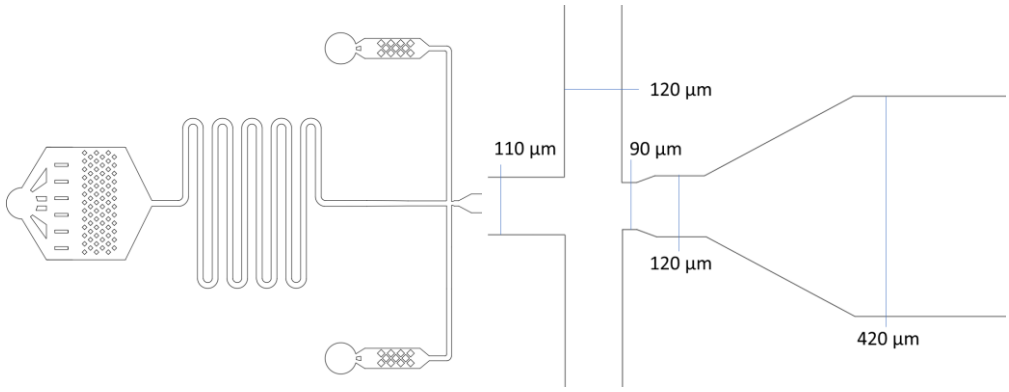

Figure 36: Inlet Design for the production of double emulsions. Compared to single emulsions, the inlet channels and the nozzle are increased in size, and the inlet filter is looser to allow cocoons to pass.

This design is not suitable for the re-encapsulation of gelatin cocoons however, as previously mentioned if the gelatin cocoons enter the device in the liquid agarose, they will have melted in the heated sample vial long before reaching the nozzle. An additional concern would be that the agarose chains would diffuse into the gelatin cocoons, leaving behind an agarose gel in the hollow once the gelatin melts. One potential solution for this was a design proposed for mixing a crosslinker into a polymer solution on chip before encapsulation. In this design there were two inlets that met in a co-flow Y-Junction, that leads into a mixing serpentine before the nozzle. (Figure 37)

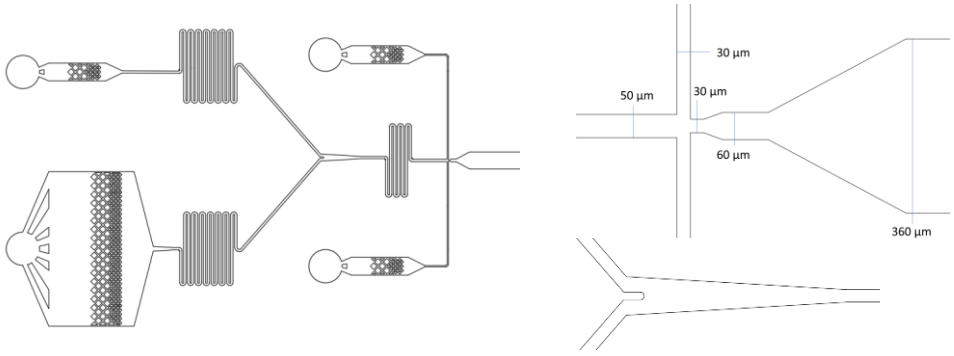

Figure 37: Crosslinker Mixing Inlet Channel Design. The nozzle area is the same as a regular single emulsion channel. Main addition is the second sample inlet and Y-Junction to mix samples into single dispersed phase on-chip.

By combining the mixing geometry with the already established re-encapsulation nozzle geometry, it was hypothesized that the gelatin cocoons could be mixed with agarose on chip and be encapsulated before the gelatin loses cohesion in the hot agarose in order to produce hollow cocoon structures.

In order for the designed channel to produce hollow cocoons there were numerous elements and channel functions required in order to succeed. Those that were specific and novel to the new hollow cocoon microfluidic channel could mostly be grouped into three main design goals. Gelatin cocoons need to be able to flow into the nozzle, without clogging or melting, the two dispersed phase inlet streams need to properly mix before the nozzle while allowing proper flow rates for both inlets, and finally the nozzle need to create monodisperse droplets with good occupancy of gelatin cocoons.

The final iteration of the design used in this thesis was derived from the design in Figure 37, which can be seen in Figure 38. While there are still elements of the design that still need to be addressed due to the results shown in this thesis, this design was found to be capable of forming monodisperse hollow cocoons to allow for early testing of encapsulating cells.

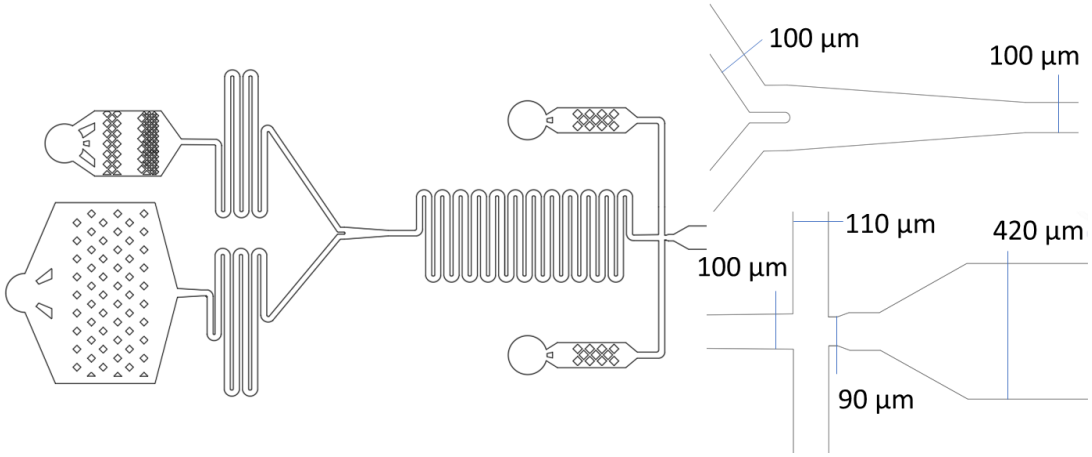

Figure 38: Final design of the inlet for the microfluidic device producing hollow cocoons. The nozzle is based off of previous work in re-encapsulating agarose cocoons, while the Y-Junction, mixing serpentine and inlet filters of the crosslinker device were enlarged to support the flow of gelatin cocoons.

3.2.1 Gelatin Cocoon Flow

To ensure the flow of cocoons, the first major design update was the sample inlets. The filter used for encapsulating cells in agarose or gelatin have a spacing of 20 µm at the smallest, which helps to break up clumps of cells while blocking any gelled hydrogel clumps. This design was kept as is for the agarose inlet, seen as the top inlet in Figure 38. As the cocoons flowing in this inlet were intended to be 50-70 µm in diameter, this spacing was increased to 160 µm. The gelatin structure is stiffer than that of a cell membrane, so the wide spacing and alternating posts were designed to influence cocoon separation without causing a clog to occur. Figure 39 shows the results of this design, with cocoons successfully passing through posts, with clumps gradually separating. This additionally helped show the ability for 10% gelatin cocoons to pass through the hottest part of the microfluidic channel, held at 30°C initially, without melting showing a lack of need for the use of glycerol or other methods to keep the gelatin solid.

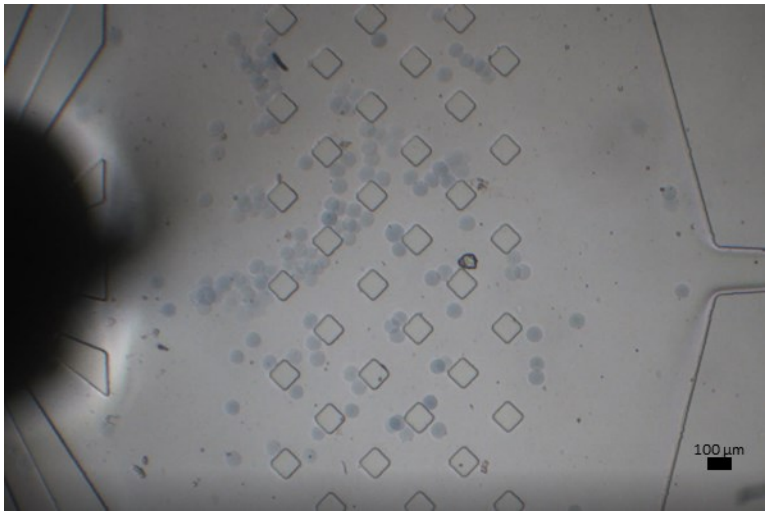

Figure 39: Trypan Blue stained gelatin cocoons passing through filter without clumping or melting.

Inlet channels into the Y-Junction were increased to 100 µm. This diameter was chosen to allow cocoons to flow in the inlets without clogging, and for better flow into the nozzle area for more stable emulsion production. Experimentation with smaller 70 µm nozzles showed clogging behaviour even with smaller 50 µm cocoons. (Figure 40)

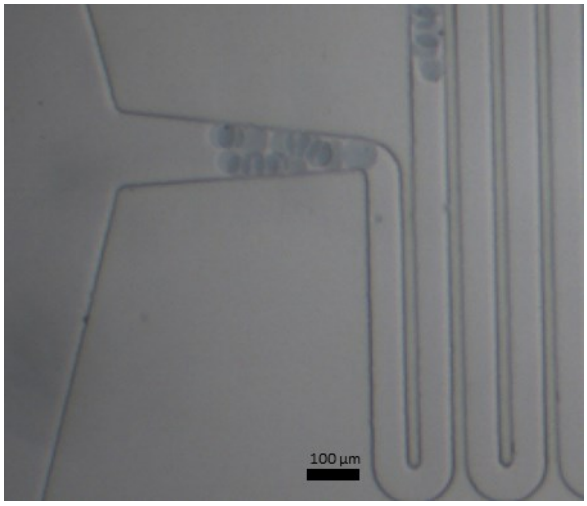

Figure 40: Clogging of gelatin cocoons in 70 µm channel.

3.2.2 Mixing of the inlet

The main alteration made in order to properly mix the two inlet phases for the final design of the channel was to increase the length of the mixing serpentine after the nozzle. As mentioned previously in section 1.1.5, the Peclet number is a measure of the time it takes to mix two phases. After increasing the width of the channel the characteristic length is also larger and so the Peclet number is increased. To accommodate the increased mixing time the channel length was increased. While a 60% increase of the characteristic length would theoretically only require a channel that is an additional 60% as long, extra length was added to help ensure faster flow rates would still mix in time. Figure 41 shows a co-flow of 2% agarose and PBS buffer, that over the course of the mixing serpentine became a homogeneous mixture.

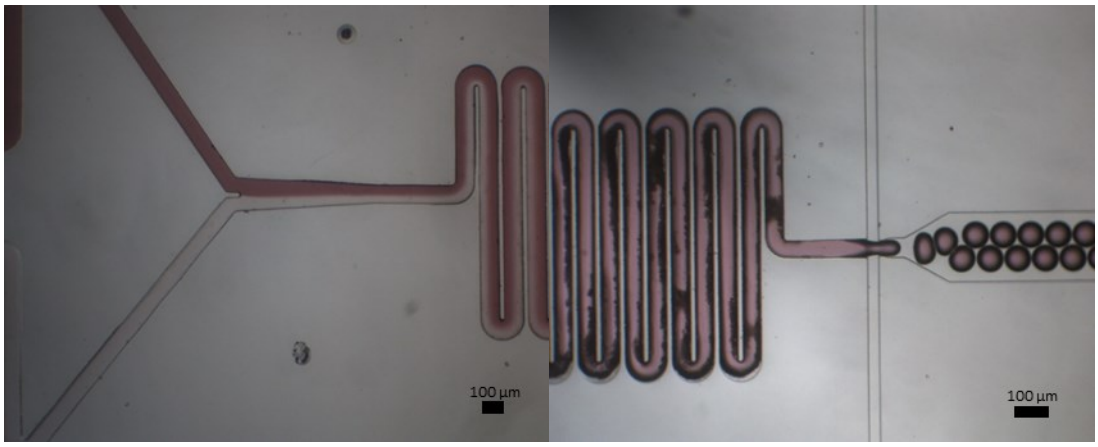

Figure 41: Monodisperse emulsion generated from hollow cocoon device after mixing the two 100 µm inlets. Dispersed phase flow mixed with red dye is agarose.

With the mixing criterion fulfilled, the second consideration was the flow rate. When two phases of equal viscosity meet in a Y-Junction, the fraction of the channel they take up before diffusion is their flow rate over the combined flow rate. However if a more viscous fluid is injected at the same flow rate, it will take up more of the channel, while the less viscous fluid flows faster to compensate. [23], [24] As Figure 42 shows, balancing the two inlet flows led to the agarose flow taking up the majority of the flow channel. This balance is somewhat delicate, with changes of only a few kPa drastically swinging the balance of the two flows leading to the backflow of one of the two inlet channels. The required balance was consistent between devices however, and so became easier to initiate with practice. Most importantly, when properly balanced the two flows can reach all the way to the maximum pressure of 140 kPa available for the dispersed phase without disruption and with homogeneous mixing.

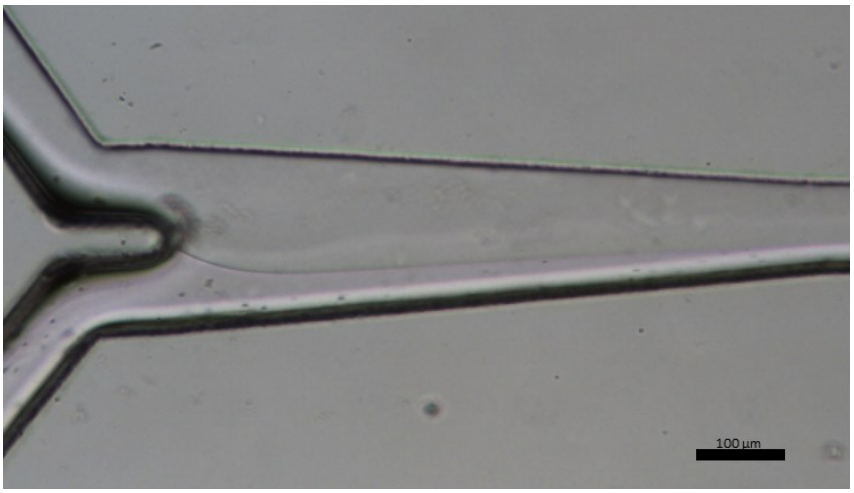

Figure 42: Agarose/PBS flow balancing. Agarose flow is the top flow intruding on the flow of the PBS.

3.2.3 Forming Monodisperse Emulsions

The design of the nozzle that was best able to create monodisperse emulsions was similar in design to the one meant for double emulsions. [15] The nozzle diameter of 90 µm was chosen to prioritize the formation of droplets larger than 100 µm. As the inlet channel was necessarily at least 100 µm due to the requirements of cocoon flow earlier in the inlet, continuous flow channels of 110 µm were found to be the best at stabilizing the flow through the nozzle to form monodisperse emulsions. To accommodate for the larger cocoon size, the height of the channel was adjusted during spincoating to be 150 µm rather than 100 µm. This lead to a necessary minor adjustment in the serpentines, increasing the spacing from 35 µm to 55 µm as the higher aspect ratio was leading to underdevelopment of the channel walls. (Figure 43)

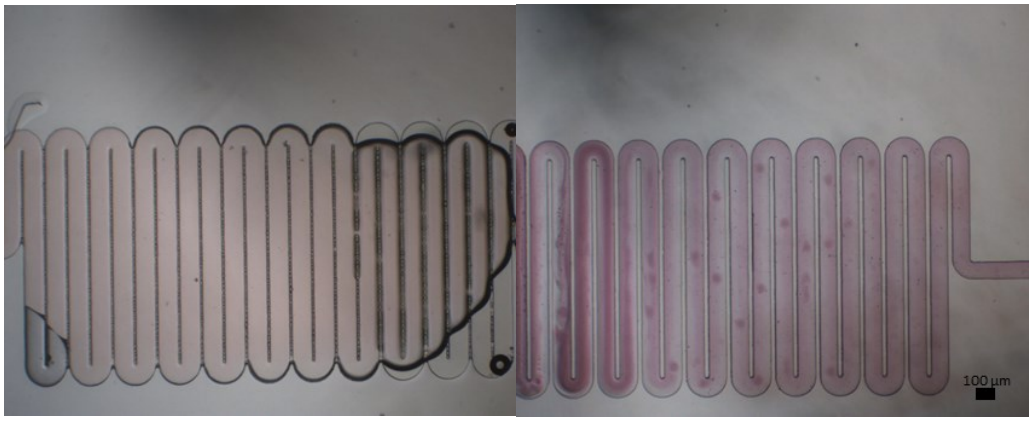

Figure 43:Underdeveloped mixing serpentine due to high aspect ratio causing unformed serpentine walls. (Right) New wider spacing provides easier to produce functioning channel.

Monodisperse emulsions similar to those seen in Figure 41 made with this design were able to be produced from continuous pressures of 70-140 kPa. Flow profiles like the ones made for gelatin were not produced for these devices, due to the complexities of balancing the two dispersed phases. The size of the cocoon was not based only on the ratio of the dispersed phase to the continuous phase in this design, but also on the ratio of the two dispersed phases. This is partly due to the impact of viscosity when the flow column breaks into droplets. When adjusting the relative flow rate of the two dispersed phases, it alters the final viscosity of the mixed dispersed phase depending on the final concentration of agarose. Observationally this means that in certain circumstances decreasing the agarose flow pressure increased cocoon size slightly as even though the overall flow rate is lower, as the lowered viscosity has a greater impact on the size. Given that ideally the concentration of the agarose shell should remain constant, the attempt was made to keep the two flow rates as equal as possible, which was mostly done visually to produce a fraction such as in Figure 42.

Cocoons made in this way ranged in size from 110 to 180 µm (though anything larger than 150 µm is constrained in the z axis due to the height of the channel, so true diameter is unknown) with low monodispersities ranging from 1-1.5%. Smaller cocoons were possible, down to roughly 90 µm but at this point droplet production was a slow drip and not suitable for producing cocoons and the dispersed flow was nearly stagnant. Size fluctuations over time were still present in this larger design and are seemingly more impactful due to changes in inlet flow balance changing

the viscosity of the dispersed phase on top of existing sources of change. Cocoons of 131 µm were produced at a continuous pressure of 140 kPa, and over the course of 10 minutes drifted to 136 µm. Constant monitoring of cocoon size, and the balance between the two inlet phases, is thus considered necessary for the time being barring future improvements.

3.3 Hollow Cocoon Production

With the ability to produce monodisperse emulsions of the target size consisting of a homogeneous mix of the inlet phases, and the successful flow of gelatin cocoons into the nozzle, the next goal in this project was to create hollow cocoons. The ideal outcome was the production of cocoons with a monodispersity of less than 3%, at a throughput acceptable for the production of cocoons on the order of 100/s, with occupancy of gelatin cores at least somewhat approaching the theoretical Poisson values of 60% for a 130 µm cocoon up to 84% for a 160 µm cocoon.

The end result of this experimentation was a conditional success. While emulsions consisting of only hydrogel and PBS were largely stable, the introduction of cocoons into the inlet introduced an infrequent but disruptive tendency for the balance of the two inlet flows to fail. During periods where the flows were balanced, the three goals were met, and in some cases surpassed. However, overall occupancy and the monodispersity of the final samples were greatly impacted by the periods of instability.

Additionally, two other major issues in the creation of hollow cocoons were present. Due to the higher density of gelatin cocoons than the PBS buffer they were suspended in, cocoons would begin to settle over the course of a run leading to a concentration too high for the device to handle. The other issue was at higher flow rates the larger cocoons began to have their shape distorted from the shear of the cooling serpentine, limiting the maximum throughput of the cocoons. The issue of settling cocoons was mostly mitigated through the use of an agitation system in the sample vial, but until new serpentine designs are produced the ability to produce hollow cocoons at the highest available pressure ranges is currently cut off.

Overall this phase of experimentation showed the potential of this device geometry to produce hollow cocoons, and future improvements to the design should be able to greatly reduce the impact of the current issues. In the meantime it was decided that the current rate of hollow cocoon production was at a high enough occupancy and throughput that investigation into the behaviour of encapsulated cells would be possible.

3.3.1 Emulsion Generation and Hollow Cocoons

Cocoon concentrations in the sample vial were set to 850,000 cocoons/mL, an order of magnitude lower than the concentration for cell encapsulation, which were estimated from the Poisson calculation in section 2.4.4 to produce good occupancy in cocoons of the 130-150 µm cocoons size range that were so far consistent to produce using these devices. The agarose in the inlet was at a concentration of 2.7%, which previously was on the higher range of concentration before the viscosity began to cause flow problems in the channel.

While generating the emulsion using the finalized device, gelatin cocoons flowed into the nozzle at a consistent rate for large periods of the encapsulation runs. (Figure 44) During these periods, monodispersity was still at 1.5% when producing cocoons between 140 and 160 µm in diameter, and occupancy of the moment to moment snapshots varied from 35% to 100%, with most images showing roughly 60% of cocoons being occupied.

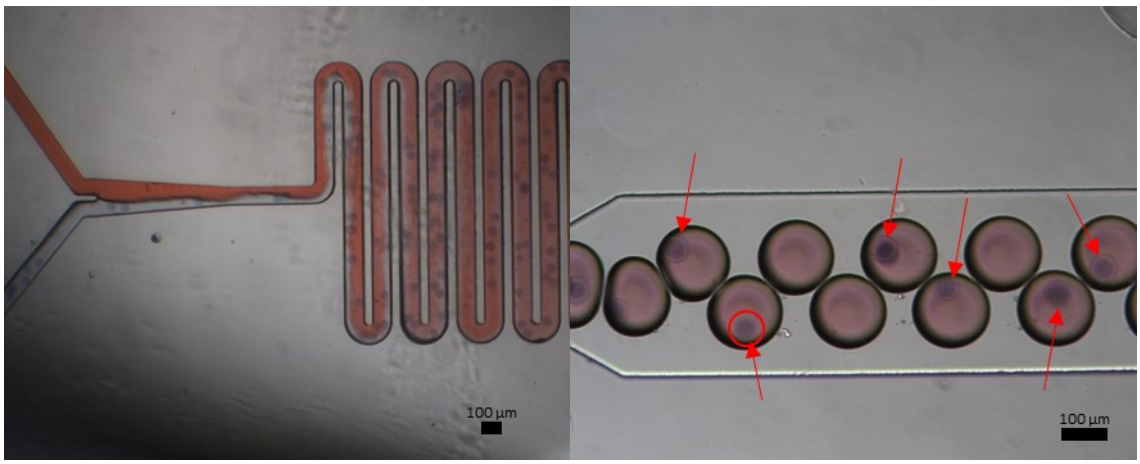

Figure 44: (Left) Cocoons flowing in Y-Junction and mixing serpentine. (Right) Monodisperse droplets containing encapsulated gelatin cocoons.

At moderate flow rates with a continuous phase pressure of roughly 100 kPa, the throughput of hollow cocoons of 140 µm size were in the range of 150-200 cocoons/s. While not as efficient as single emulsions, this lower throughput is expected due to the much larger volume of the produced cocoons.

To test whether the generated droplets could form hollow cocoons, after purification samples were placed onto a hemocytometer to view their physical structure. When taken straight from encapsulation without heating, Trypan Blue stained gelatin cores could be clearly seen in the cocoons. Upon heating to 37°C for 5 minutes, the gelatin cores were no longer present leaving behind what appear to be hollow agarose structures. (Figure 45) While further testing will be needed to fully confirm that they are in fact hollow, one indication is that after melting the cores the addition of further Trypan Blue after cooling down the cocoons does not lead to re-staining of a gelatin core which seems to show that the gelatin has left the inner hollow.

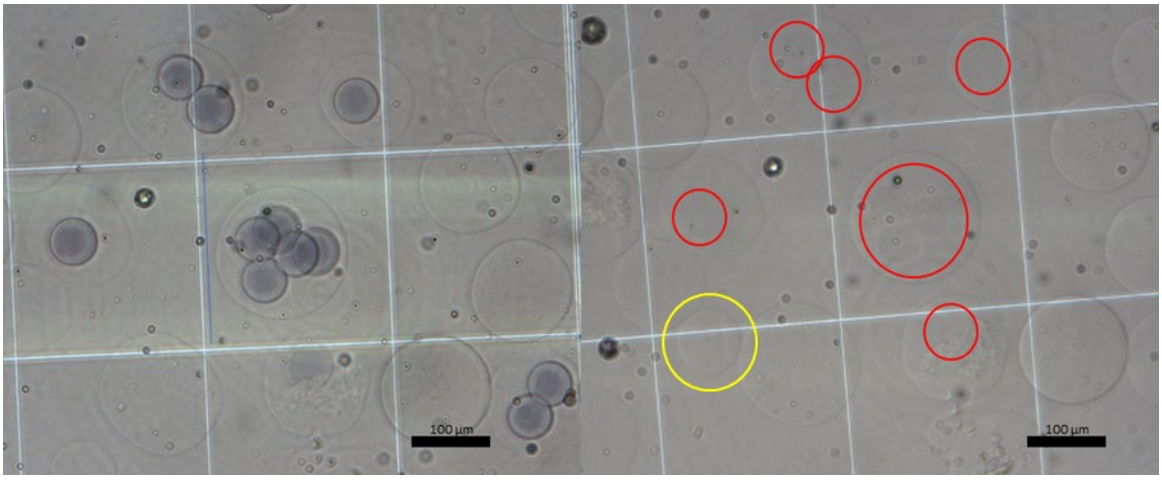

Figure 45: (Left) Trypan Blue stained gelatin cocoons inside agarose shells. (Right) Same cocoons after heating to 37°C for 5 minutes leaving open hollows in the shells. (Hollows highlighted within red circles due to low contrast) The yellow circle shows a smaller pure agarose cocoon.

3.3.2 Hollow Cocoon Occupancy and Occupancy Issues

When examining the resulting cocoons on the hemocytometer, the calculated occupancy of the hollow cocoons was typically between 30-40%. The results of hemocytometer analysis of three successive encapsulations done during the same day from the same sample of gelatin cores

can be seen in Table 8. This is much lower than both the calculated Poisson estimate of 70% occupancy, and the average observed occupancy of cocoons leaving the nozzle at a moment to moment basis. The samples also tended to be far “messier” than those seen in encapsulation of single layers of hydrogel. Alongside the monodisperse cocoons there were often large amounts of loose gelatin cores, agarose shells with what appeared to be missing gelatin cores before heating, and smaller cocoons made of pure agarose without gelatin cores. The reason for this lower occupancy, and for the increase of garbage in the sample is likely linked to two main factors.

Table 8: Occupancy of Three Hollow Cocoon Encapsulation Runs

Sample	*Average Occupied*	*Average Total*	*Occupancy*
1	10.5	25.25	41%
2	12	33	36%
3	5	17.25	29%

The first cause is one that is not directly related to the emulsion generation, but instead is egress of the gelatin cores. This appears to be similar to the egress of cells investigated in the Godin Lab previously. Based on the appearance of the affected cocoons, occasionally gelatin cores will be located too close to the edge of the agarose shell upon gelling and will exit the cocoon during the centrifugation step of sample purification. [15] This does not make a true hollow cocoon, but instead a concave structure that would not be counted when measuring occupancy with the Trypan Blue stained gelatin cores. The presence of these loose cores represents a loss of occupancy from the cocoons observed leaving the nozzle. (Figure 46) The issue of cores egressing was not previously seen during production of agarose cored double emulsions, so this new issue is potentially due to a lower connection between the gelatin core and the shell. Previously the agarose cores would be sitting in the same vial as the liquid agarose before encapsulation on the device, so potentially the entangling of polymer chains in the agarose cores pore structure created a stronger link preventing the cores from egressing that is not present in the quick mixing and gelling of this encapsulation method. [15]

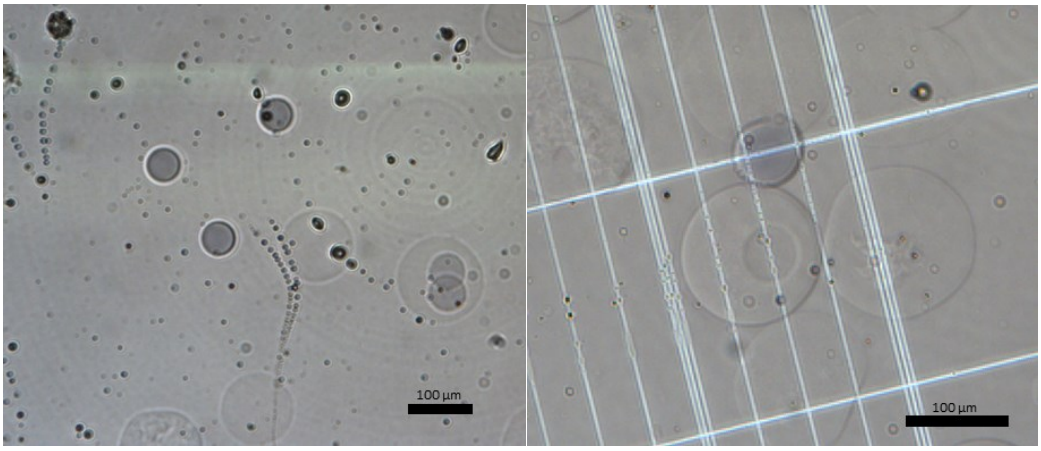

Figure 46:(Left) Loose gelatin cores. (Right) Loose gelatin core next to Agarose cocoon with a missing core. Likely not hollow but possessing a concave divot in the surface of the cocoon.

The other cause is an irregular disruption of the typical monodisperse flow. While the emulsion produced was predominantly the monodisperse droplets shown above in Figure 44, there were occasionally periods where the flow of agarose would overtake the other inlet of the Y-Junction causing backflow into the cocoon inlet. As mentioned in Section 3.1.2, the inlet flows can occasionally drift due to pressure leaks or build up of material in the path of the inlet flows. As these flow issues are only present during the encapsulation of cocoons, it is possible that build ups of cocoons cause small clogs reducing the PBS flow. During these periods, the more viscous agarose entering the nozzle leads to the production of smaller cocoons without any gelatin cores, an obvious example of this can be seen in Figure 45, outlined in yellow.

These interruptions happen quickly, often without warning. Though they are easily fixed by a small pulse of increased cocoon inlet pressure, these short periods of purely empty cocoon production last at least 10 seconds even when caught immediately and the production of empty cocoons begins to add up over the course of a run. As there is not a simple method of separating out these cocoons when counting, their presence lowers the overall occupancy.

That said, a 30% rate of hollow cocoons being produced, with the 50% occupancy of cells in the gelatin cocoons would still theoretically mean 15% of produced cocoons would be hollow cocoons containing cells. While not acceptable long term, in order to begin investigating the behavior of cells encapsulated in hollow cocoons this was deemed high enough to continue on, with the optimization of the encapsulation to be held off for a later date.

3.3.3 Cocoon Density and Clumping

Initial attempts at generating the hollow cocoons showed far worse results. Due to the density of cocoons, they quickly began to settle in the sample vial, leading to an excessive concentration of cocoons flowing into the device leading to early clogs. (Figure 47) As hydrogels are porous, density gradient mediums such as Optiprep would diffuse into the cocoons, limiting them as a solution. One potential solution would be to increase the viscosity of the media to slow the cocoons settling, but this would need to be done with a cell compatible material and may have impacted sample flow so it was not yet explored.

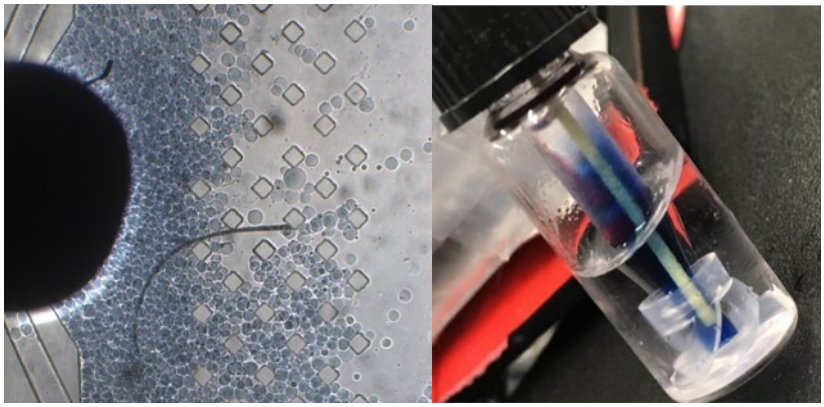

Figure 47: (Left) Mass clogging of cocoons, right away the flow of cocoons lead to stacking preventing most of the flow from passing through the filter. (Right) Settling of cocoons in sample vial, as shown by the lack of Trypan Blue near the top of the vial with an excess near the bottom near the opening of the Peek Tubing.

As an attempt to mitigate this problem in the short term, the idea of agitating the cocoons to prevent settling was put into place. Either manual agitation of the sample was carried out every few minutes to keep the cocoons suspended, or a “bubbler” tube was inserted into the sample vial. The bubbler was PEEK tubing connecting the sample vial to a sterile vial that was otherwise empty. (Figure 48) The airflow from the solenoid valve would pressurize the empty vial, causing airflow into the sample vial creating air bubbles that agitated the cocoons every few seconds. As the sample inlet PEEK tubing was kept lower than the bubbler tube, no air bubbles ended up in the device.

Figure 48: To fix settling an agitation mechanism was added, the pressure flow began in a separate vial filled with air, which then connected to the sample vial with PEEK tubing. Air bubbles in the sample vial led to agitation preventing settling.

Both the manual agitation and the bubbler proved adequate in homogenizing the cocoon concentration to the point of preventing obvious clogs in the inlet, but settling of cocoons may still be the cause of the periodic disturbances in the flow noted in the previous section. A more robust method of dealing with this issue is on the agenda for future improvements.

3.3.4 Droplet Integrity at High Flow Rates

The issues surrounding the shear of droplets in the cooling serpentine were a new occurrence arising from trying to maximize the throughput of the very large cocoons. As mentioned previously, pressure driven flow in the laminar flow regime possessed a gradient of flow speed, with the maximum speed in the middle of the channel slowing down to the speed of the channel wall due to “no-slip” conditions. [20] This means that something as large as the cocoons experiences different flow rates across its surface as it travels down the channel, though due to surface tension typically only causes minor deformation in the shape. In serpentines, the pathlength of the flow lines changes between the inner wall and the outer wall causing a sharper gradient and greatly increased shear on larger droplets. Due to the shear and the confinement of the microchannel, when producing droplets at continuous flow pressures above 100 kPa, it was noticed that in the bends of the serpentines droplets became elongated, and at longer sizes began to actively break apart. [17], [109] At more moderate flow rates, with smaller droplets, the

emulsion showed some minor elongation but due to the lower flow rates there was not enough shear to cause breakup and the droplets maintained their shape. Examples of this behaviour can be seen in Figure 49. While unfortunate, the 150-200/s throughput at 100 kPa is still adequate for the time being, though new serpentine designs made to lessen the shear on the droplets are being considered.

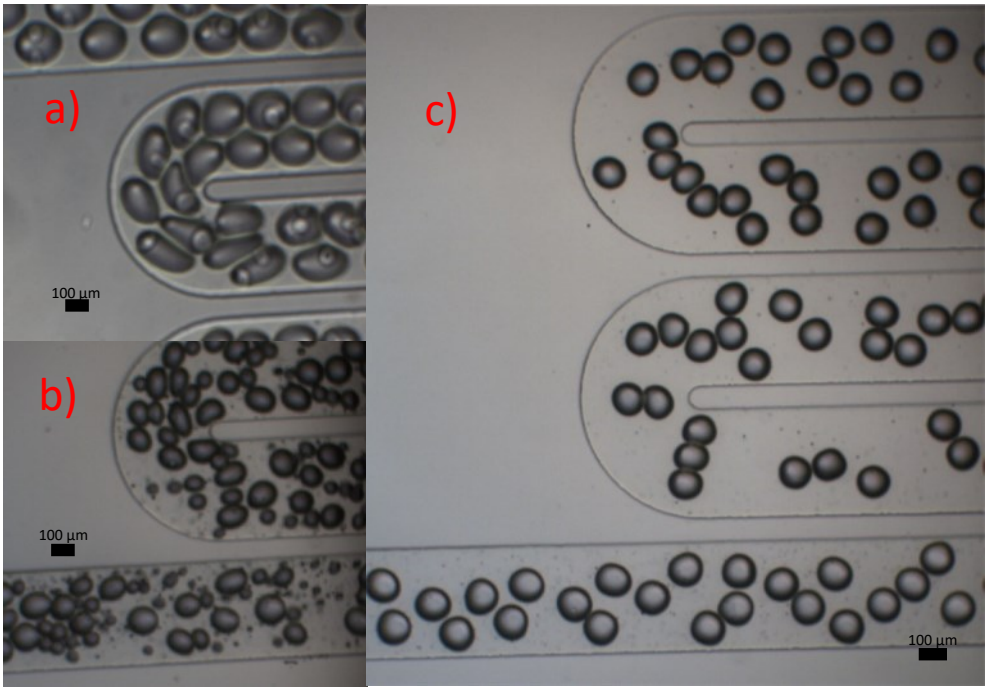

Figure 49: a) Cocoons at 140 kPa entering serpentine. b) Cocoons at 140 kPa exiting serpentine. c) Cocoons at 100 kPa exiting serpentine

3.4 Cells in Hollow Cocoons

With a working microfluidic device and a process that was able to produce hollow cocoons as a third of the total sample fraction, the next step was to encapsulate gelatin cocoons with encapsulated cells. Ideally this process of cocoon production would have similar monodispersity, throughput and occupancy values for the hollow cocoons as before, while occupancy of cells in successful hollow cocoons would approach the 50% occupancy of the cell occupation in gelatin. Once encapsulated, the goal was to show that encapsulated cells maintained high viability, and to investigate potential indications of cell egress, adherence and proliferation within the cocoons.

Experiments done to attempt to encapsulate cells in hollow cocoons began with all the previously established parameters and conditions. 10% gelatin cocoons 50 µm in size were created encapsulating an 8.5 million/mL cell concentration. These cocoons were purified from oil, then resuspended in DMEM cell media at 850,000 cocoons/mL and were kept in an ice bath in the sample vial. In the most current microfluidic channel design, 2.7% agarose and the suspended gelatin cocoons were introduced into the 30^{o}C inlet to form an emulsion with a 100 kPa continuous phase pressure. Due to issues with cocoon stability, the inlet temperature was reduced to 25^{o}C. It was at this point that Type IX agarose came into use, due to its lower gelling temperature compared to IX-A agarose, and overall resistance to gelling between the sample tube and device inlet.

Once produced, samples of cocoons were prepared for timepoint studies using the method explained in the sections 2.4.1 and 2.4.2. Fluorescent images were taken over the course of two days, to track the progress of encapsulated cells.

3.4.1 Encapsulation of Cells Encapsulated in Gelatin

When beginning the attempt to encapsulate gelatin cocoons with encapsulated cells, immediately upon beginning the flow of gelatin cocoons into the device the cocoons began to melt and shear, becoming a dilute solution of gelatin containing cells. This was not an expected result, as the temperature in the inlet was kept at 30^{o}C which was shown to be successful in section 3.2.2. In appearance, the shearing behavior was similar to a previous exploratory test of injecting cocoons into a device heated to 40^{o}C. When injected into a inlet that is above the melting temperature, cocoons enter mostly spherical as per usual, but quickly become elongated by the shear as the flow in the inlet increases near the beginning of the inlet channel and the cocoons begin to melt. (Figure 50)

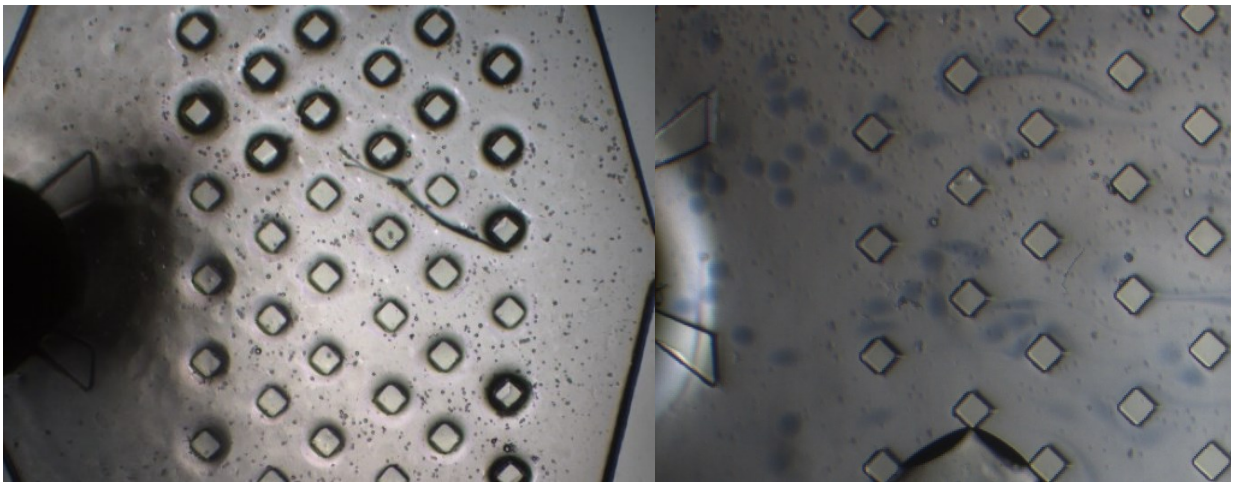

Figure 50: (Left) Gelatin cocoons melting upon entering a device held at 30°C. (Right) Empty gelatin cocoons melting while flowing into a device heated to 40°C.

There were two changes in the conditions between the earlier tests and those with cells. The first is the switch of the dispersed phase from PBS to DMEM, while the second was the presence of cells inside the gelatin hydrogel structure. Some investigatory tests were done to determine the impact of either of these changes.

First, gelatin cocoons without cells were suspended in DMEM, to be used to attempt to flow into the microfluidic device. This was not suspected to be the cause, as the sugars in the DMEM would be more likely to increase the gelling temperature than reduce it. [73] As expected, the left image of Figure 51 shows solid gelatin cocoons flowing in DMEM in the inlet without melting.

To see if the presence of cells was affecting the structural integrity of the cocoons, gelatin cocoons containing cells were flowed through PEEK tubing directly onto a hemocytometer that was heated to 30°C, emulating the injection onto the device without the subsequent flow in the channel. The right image of Figure 51 shows that the cocoons maintained their solidity. This seems to indicate that the cells are not disrupting the gelatins physical crosslinking to the extent that the shear from the PEEK tubing flow can disrupt cocoons, nor is it lowering the melting temperature of the gelatin so that heating it to 30°C is suddenly enough to melt the cocoons.

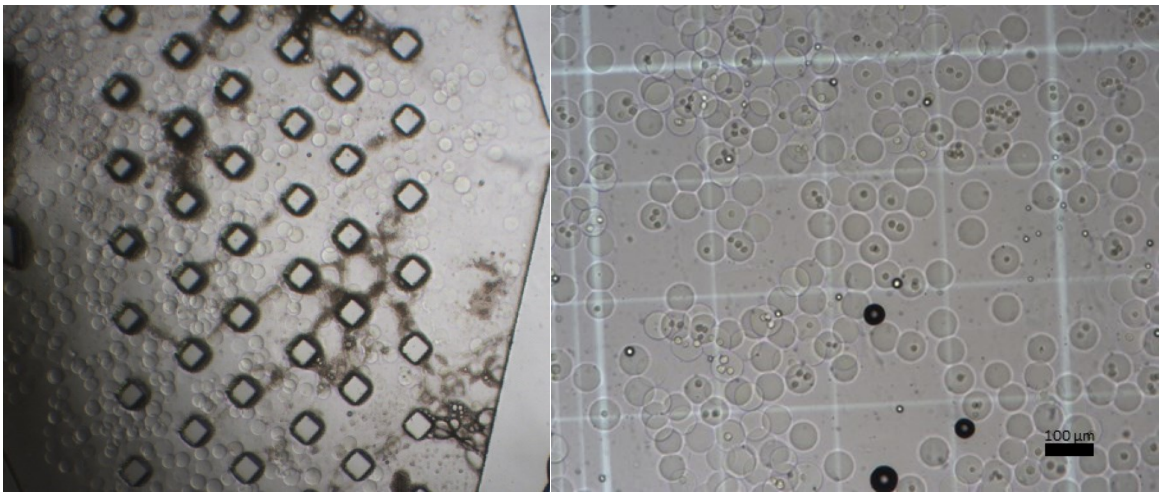

Figure 51: (Left) Cell-less gelatin cocoons flowing in DMEM without melting in the inlet. (Right) Cocoons containing cells holding form at 30°C after flowing through PEEK tubing onto a hemocytometer.

Before potentially compromising cell viability with the backup strategy of the addition of glycerol to increase melting temperature, or throughput by using a higher concentration of gelatin, an attempt was made to further decrease the inlet temperature. In exploratory testing the new Type IX agarose had shown far greater working temperature ranges than the Type IX-A agarose used previously, with negative effects of the initiation of gelling in the inlet only beginning to onset below 20°C.

When gelatin cocoons with encapsulated cells were injected into the inlet with a temperature of 25°C there were no longer any issues of cocoons melting in the device. (Figure 52) Based on this result, the presence of cells appears to reduce the Shear Modulus of the gel at temperatures approaching the melting temperature. When flowing from the ice bath to the channel or when in the channel at a lower temperature there is no shearing, but at temperatures approaching the melting temperature there is shearing. When there is no flow, such as on the hemocytometer, cocoons do not melt even while sitting at 30°C for minutes longer than cocoons are present in the inlet. One possibility for this may be an enzyme given off by the cells preventing the stabilization of the physical crosslinking structure of gelatin at higher temperatures so that the cocoons can be sheared even while being slightly below their melting point, but without further study the exact cause of this behavior is unknown. [61]

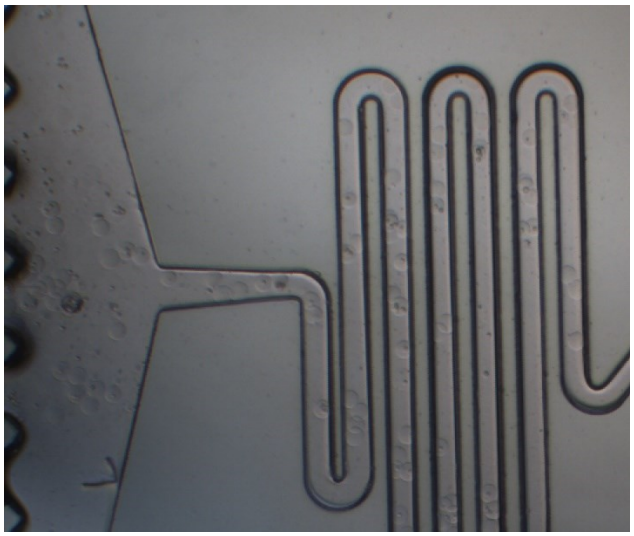

Figure 52: Gelatin cocoons flowing into the inlet without shearing at 25^{oC}.

Once the issue of the gelatin cocoons melting was bypassed, attempts to encapsulate the cell occupied cocoons resumed. Using similar pressures and elements such as the bubbler, emulsions of up to 150 µm with 1.5% monodispersity were produced. Observations of cocoons being produced puts occupancy as varying between 40-60%. Similar to before, there were semi-frequent disruptions to the production of monodisperse cocoons due to sudden shifts in the balance of the inlet flows that needed manual correction. On top of this disruptive behavior, there was an added issue. Cocoons containing cells appear to be "sticky" or otherwise more likely to adhere to each other during flow. This would cause build ups of cocoons in the inlet, that would periodically let go and flow into the inlet. During these periods, occupancy would become excessively high due to the number of cocoons, distending the cocoons shape and causing polydisperse cocoons. (Figure 53) This did not appear due to there being too high a concentration of cocoons in the inlet sample, as even at lower concentrations of 500,000 cocoons/mL the build up of cocoons still occurred, just with lowered occupancy of produced cocoons in periods between the surges of under 40%.

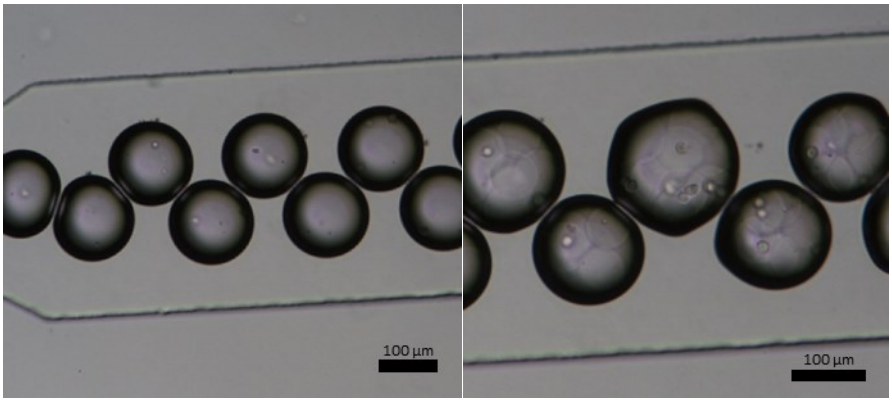

Figure 53: (Left) Typical monodisperse flow with gelatin cocoons containing cells in roughly half the droplets. (Right) Droplets during a period of high occupancy. Droplets are polydisperse, and often not perfectly spherical due to presence of too many cocoons distending the shape.

Due to these factors, while many hollow cocoons containing cells were produced the overall sample is filled with loose cores, shred of broken cocoons and polydisperse cocoons of pure agarose in proportions worse than the similar mess found in samples of the previously made cocoons without cells. Correctly made hollow cocoons are a minority in the sample, present but in low enough numbers that attempts of statistics on the occupancy of the cocoons would be highly biased from the heterogenicity of the sample. (Figure 54)

Due to time constraints the presence some amount of cells inside of a hollow agarose shell was deemed enough to move onto fluorescence microscopy, but long term there is a clear need to optimize the encapsulation process before using hollow cocoons in any subsequent experiments.

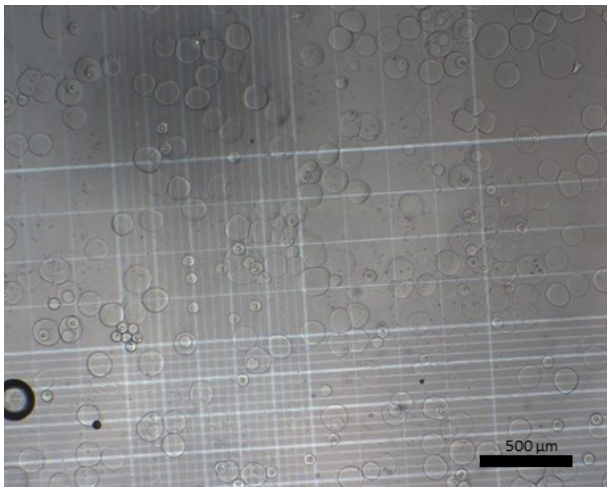

Figure 54: Example of the resulting sample on a hemocytometer. Aside from the presence of a few well formed hollow cocoons, most of the sample is polydisperse agarose and free floating gelatin cores that egressed from poorly formed cocoons.

3.4.2 Fluorescent Cell Viability Analysis

After hollow cocoons were produced, the sample was split into three portions and placed into three 35 mm petri dishes for cell culture alongside 1 mL of DMEM. Two of the dishes were marked for 24 and 48 hour time points, while one was prepared with the fluorescence dyes for immediate imaging. Due to the sparse number of cocoons in each sample and the messy sample overall this analysis is unfortunately unable to meet the requirements to generate statistical evidence of cell viability, egress or proliferation. Rather than random sampling, hollow cocoons were actively sought out to image in the dish, meaning a non-random selection of the hollow cocoon population was sampled. Instead this analysis is making note of general trends, marking oddities and reoccurring features for future experiments involving encapsulating cells in hollow agarose cocoons.

3.4.2.1 Fluorescence Timepoint 2 Hours Post Encapsulation

Immediately after encapsulation cell viability was high. Across five attempts of encapsulating cells that proceeded to fluorescence, dozens of hollow cocoons containing cells were imaged and there was not a single instance of finding a dead cell encapsulated in a cocoon. Based on the encapsulation of cells into the gelatin cores routinely having a viability of above 95%, it appears

that the encapsulation and purification steps for hollow cocoons do not show significant stressors on the cells causing their immediate death. (Figure 55)

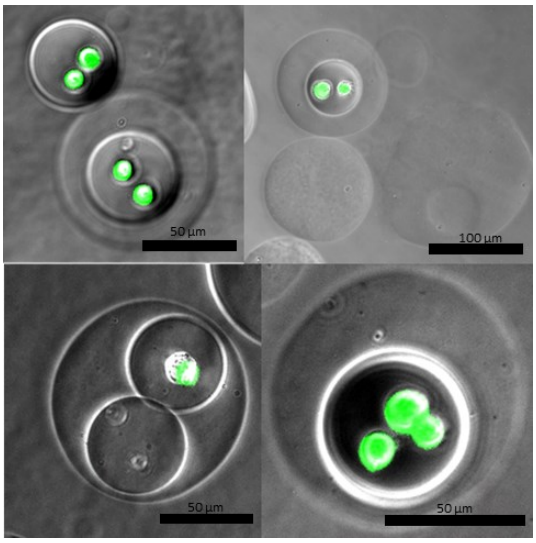

Figure 55: Examples of Hollow Cocoons before heating. From top left to bottom right: Hollow cocoon contrasted with free floating core, Hollow Cocoon contrasted with agarose bead with egress divot, Double occupancy Hollow Cocoons, Hollow Cocoon with Trypan Stain

Imaging the sample after heating showed a visual change, both removing the contrast line glow caused by the gelatin core and allowing cells to group with each other on the wall of the hollow. An interesting feature of note is that several individual and groups of cells were seen seemingly looking to adhere to either each other or the walls of the channel, with the appearance of the extensions of cytoplasm rather than the mostly spherical shape seen when cells remain encapsulated. (Figure 56) This behavior is the other major indication that the cocoons are truly hollow, as the cells drift to the bottom of the hollow and begin to move without impediments.

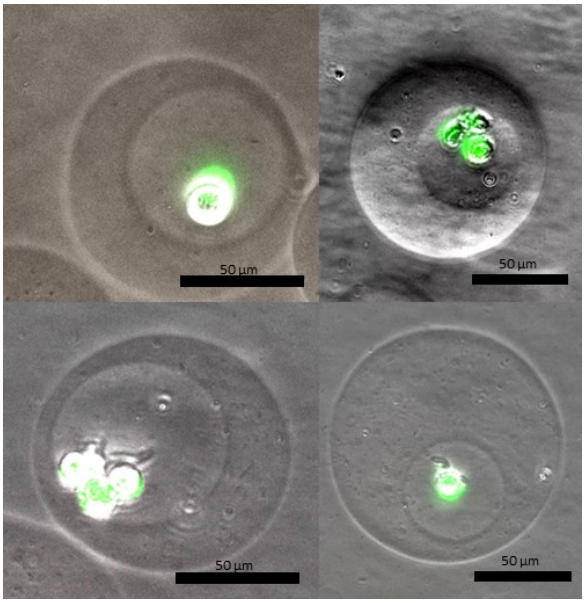

Figure 56: Examples of Hollow Cocoons after heating. From top left to bottom Right: Single cell in hollow cocoon, Cells in Hollow Cocoon adhering together, Adhering cells with cytoplasm extending, Single cell with extending cytoplasm.

3.4.2.2 Fluorescence Timepoint 24 Hours Post Encapsulation

After 24 hours there were some small visible changes in the samples. Cells that were originally in free floating gelatin cores post encapsulation that were freed when the cocoons melted had all adhered to the bottom of the dish. Their presence makes it difficult to ascertain if cells are egressing the hollow cocoons through observational means. Typically in timepoint studies, changes in occupancy between samples would be the method of tracking this, but due to the low number of cocoons this would not be statistically relevant.

That said, several cocoons showed extremely thin walls separating cells from the outside surface of the petri dish. Previous research into cell egress tied egress to both distance from the edge, and proliferation pushing daughter cells out of the cocoons. [14], [15] The continuing presence of these cells still in the cocoons even when separated by less than 5 µm from the more favourable petri dish surface may indicate an inability for the cells to leave. (Figure 57) Anecdotally, there did not appear to be significantly more empty cocoons, or cocoons showing some kind of visible sign that would indicate a breach of the cocoon wall.

There were far fewer cells showing any kind of adherence to the surface of the cocoons. Cells continued to be grouped together, but showed at most minimal attempts to interact with the

surface of cocoons. As agarose is not a naturally cell adherent material, after initial attempts to adhere encapsulated cells may have ceased attempts to spread on the surface of cocoons. [4]

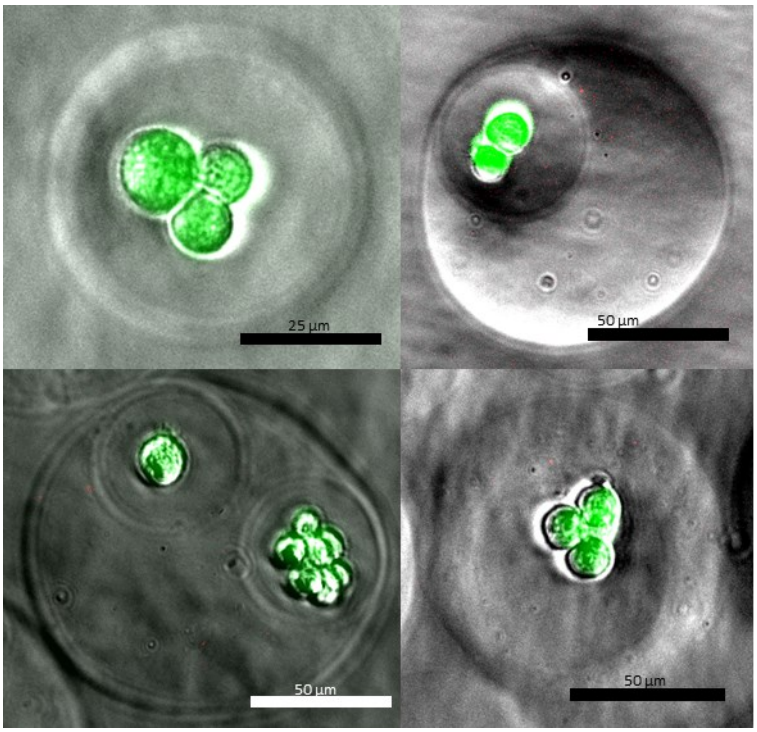

Figure 57: Hollow cocoons after 24 hours. From top left to bottom right: Encapsulated cells still alive, Cells remaining in cocoon despite thin wall, Hollow Cocoon with one hollow containing numerous cells, Hollow Cocoons where one cell is potentially making an attempt at adherence with surface of the inner cocoon.

While the majority of cells in cocoons remained perfectly viable, a new feature was present in a small number of cocoons. The way that the Live/Dead stain operates is that calcein is metabolized by living cells to fluoresce, while EthD-1 is excluded by living cells but in dead cells can enter the membrane to bind to DNA to fluoresce. In some cocoons, the cells themselves still fluoresce green indicating they are alive, but the whole hollow of the cocoon is fluorescing red indicating DNA is present. Some examples of this can be seen in Figure 58. This may be an indication that a cell has died, from either from anoikis causing apoptosis or something causing necrosis, releasing DNA fragments while the remaining cells remain alive. [1] Another option could be extracellular vesicles being released containing DNA, in which case would indicate the cells are healthy, despite the negative visual impact of the stain. [106]

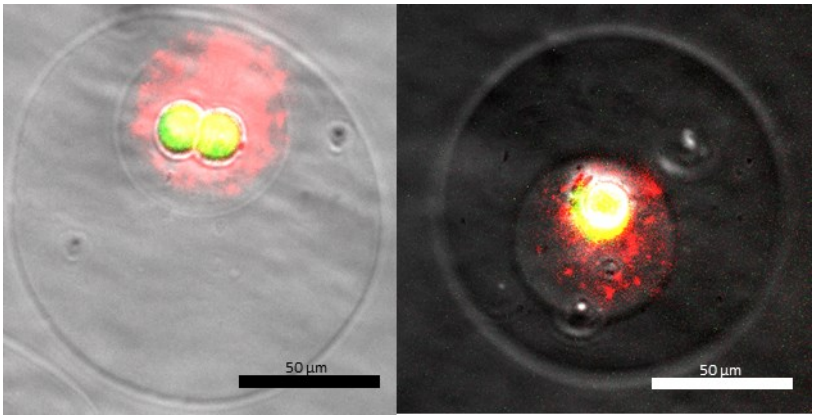

Figure 58: Hollow Cocoons showing novel ETHD-1 staining. (Left) Two living cocoons with dead stain filling entire hollow. (Right) Image edited with higher contrast to highlight the particulate nature seemingly spreading from the "Live" cell.

3.4.2.3 Fluorescence Timepoint 48 hours Post Encapsulation

Conditions in the sample after 48 hours were not much different than after 24 hours. The majority of cells within hollow cocoons remained clearly viable, and no obviously dead cells could be seen barring one cocoon where a cell or a group of cells was potentially undergoing apoptosis, as small beads that could be apoptotic bodies could be seen. Figure 59 shows an image of this occurrence, where there is a larger mass of green fluorescence showing a living cell, with small offshoots that appear to be in the process of disconnecting from the mass.

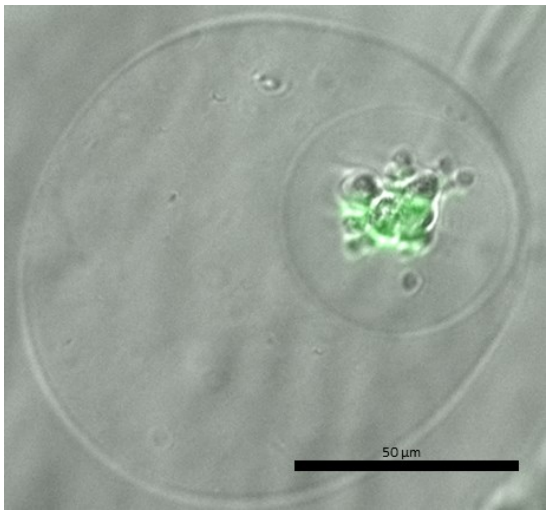

Figure 59: Potential apoptosis underway in hollow cocoon.

Some cells appeared to maintain small amounts of adherence to the walls of the cocoons. While not the full spreading seen in a petri dish, small attachment sites could often be seen

underneath groups of cells where they touch the cocoons. An example of this can be seen in the top left image of Figure 60.

Inference on whether cells were proliferating in cocoons is still unclear. While there were still many cocoons with only a single cell, some contained far more cells than should be possible from encapsulating a single cocoon. In one particular outlier, cells appeared to fill nearly the entire hollow as can be seen in the top right of Figure 60. In this case it seems unlikely that a gelatin cocoon containing that volume of cells would have survived to be re-encapsulated, even if that many cells were able to be encapsulated to begin with, so it is possible that at the very least some proliferation occurs in instances where enough cells are present to form an adherent surface for one another.

Instances of the Ethd-1 dye fluorescing around living cells continued, though they did not appear more numerous. There was one novel cocoon where the fluorescence of the two dyes are both perfectly contained in the cells but not yet in the rest of the hollow. This can be seen in the lower left of Figure 60, where it shows in the combined image as green fluorescing cells with a red outline. This may be the beginning stages of the earlier noted instances of the hollow cocoon being filled with DNA. Due to the calcein fluorescence, metabolism in the cell is ongoing but the membrane is in some way unable to keep out the EthD-1 indicating some issue with the membrane that may lead to the dispersal of DNA.

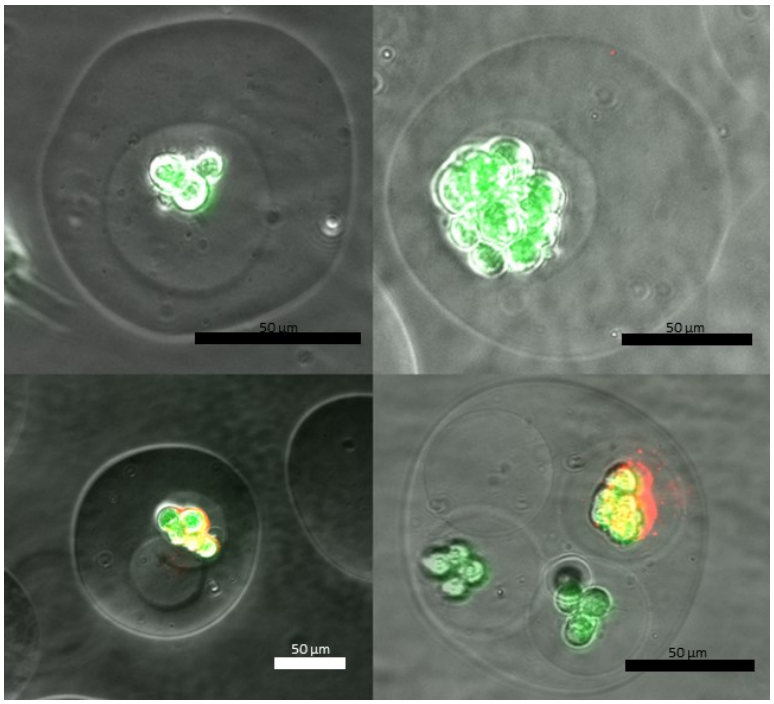

Figure 60: Encapsulated cells after 48 hours. From top left to bottom right: Typical cells in a cocoon with potential spreading underneath the bottom right of the cells, Large mass of cocoons taking up most of the hollow potentially due to proliferation, Cells exhibiting both live and dead stain, Large cocoon with multiple hollows that show a range of cell behavior .

While this is just an introductory look into cell behaviour and the effects hollow cocoons will have there are some early conclusions. It is clear that the double encapsulation process has little impact on viability of cells as initially there were no Ethd-1 stained cells in any of the cocoons. Even with non-functionalized agarose the viability in cells remains high across the 48 hours, with one likely case of apoptosis and a small fraction of the viewed cocoons showing the Ethd-1 fluorescence in the hollows observed. There appears to be signs of attempts of the cells to adhere to the walls of the cocoons. Should attachment sites be somehow added to the agarose, it seems likely that the cells would in fact begin to spread on the inner surface of the cocoons in line with current expectations. Additionally, while the true amount of egress is unknown, there are demonstrated cases where cells are unwilling or unable to breach thin hydrogel walls. All together, this shows that the hollow cocoon method of encapsulating cells holds merit moving forwards, though with much to build on and improve.

3.4.3 Hollow Cocoon Cell Occupancy Analysis

While showing the successful generation of hollow cocoons and the viability of encapsulated cells are important factors in the eventual use of these cocoons in therapeutics, another factor of importance is the ability to produce a cell product that meets the dosing requirements for *in vivo* testing,

The therapeutic efficacy of cells encapsulated in the hollow cocoons is currently unavailable without *in vivo* testing, so the number of cells a dose of these hollow cocoons requires to show a beneficial effect is still unknown. However, the protocols of more established *in vivo* experiments can act as a initial guide to see if the hollow cocoon production process would be able to meet those standards. The amount of cells required and the size of the dose that can be administered will vary depending on the organism, the organs, and the type of disease or injury that is to be treated. For the intramyocardial injection of therapeutic cells into a mouse for heart infarctions, a typical number of cells that is injected to show therapeutic benefit is 100,000 cells. The general maximum volume that can be injected in this method is a total volume of 50 µL. [106], [110]

By using the occupancy of cells estimated from the Poisson distribution (Equation 12) to calculate values similar to those found in Tables 4 and 5, it is possible to determine the number of hollow cocoons necessary to inject 100,000 cells based on the occupancy of cells in the cores, and the subsequent occupancy of cores in the hollow cocoons. Once the number of cocoons is known, the volume of hydrogel that these cocoons make up can be derived. The injection will need to be partially fluid to suspend the cocoons, so the final volume of hydrogel needs to be somewhere less than 50 µL.

The parameters used in this thesis to show the ability to encapsulate cells in hollow cocoons were an initial cell concentration of 8.5 million cells/mL to produce 50 µm diameter gelatin cores containing cells, and a gelatin core concentration of 850,000 cocoons/mL to produce 130 µm hollow cocoons containing those gelatin cores. From Tables 4 and 5, the calculated occupancies of these were 42% of cores containing at least one cell, and 62% for the hollow cocoons to contain at least one core. Due to the spread of occurring events in a Poisson process, an occupied core

can have more than a single cell. Of the 43% gelatin core occupancy, 32% have one cell, 9% have 2 and 2% have 3 cells. For the hollow cocoons the spread ranges even higher, with 37% having one core, 18% having two cores, 6% having 3 while 1.5% can have as many as 4 cores. When accounting for the range of core occupancy, and the range of cells that can be in those cores, it is possible to calculate the average number of hollow cocoons that will contain any given number of cells. For the process in this thesis, 185,000 hollow cocoons would contain 100,000 cells on average, coming to a total hydrogel volume of 212 µL. The additional solution required to suspend these hydrogel cocoons further increases the required injection bolus. This is clearly not meeting the required volume of less than 50 µL at these parameters.

In order to reach 100,000 cells in a total volume of cocoons smaller than the maximum 50 µL dose, the size of the cores and cocoons, and the sample concentration of cells and cores can be easily changed. Table 9 shows the results of Poisson based analysis of different groupings of concentrations and cocoon sizes to demonstrate how the process could be adapted once the encapsulation process becomes more stable. It shows the number of cocoons needed to have a dose of 100,000 cells, and the total volume of those cocoons, without a carrier fluid. The initial cell concentration was increased by a factor of 2 and 3 to show the influence of a higher cell occupancy, both from more cores containing cells and more cells in a core at a time. The concentration of gelatin cores was also shown at twice the concentration used in this thesis for a similar effect on the occupancy of hollow cocoons. Table 9 also highlights the influence of using smaller 90 µm cocoons. This reduced overall cocoon size was chosen as it is currently the lower limit for the device. This smaller diameter also results in less “wasted” volume of hydrogel compared to the currently “thick” agarose shell. Finally a smaller core size of 30 µm with the 3x cell concentration is also highlighted to show the effects of a smaller core. This also provided the chance to show the potential to downsize the hollow cocoons further to a 60 µm outer shell at these higher concentrations.

Table 9: Poisson Based Cocoon and Volume of Cocoons Required for 100,000 Cells with Varying Size and Concentrations

Core Size (µm)	*Core Concentration (#/mL)*	*Cell Concentration (#/mL)*	*60 µm Hollow Cocoons*		*90 µm Hollow Cocoons*		*130 µm Hollow Cocoons*	
			#	V (µL)	#	V (µL)	#	V (µL)
50	850,000	8,500,000			554,000	212	185,000	212
		17,000,000			279,000	106	93,000	106
		25,500,000			184,000	71	62,000	71
50	1,700,000	8,500,000			277,000	106	93,000	106
		17,000,000			140,000	53	46,000	53
		25,500,000			92,000	35	31,000	35
30	4,250,000	25,500,000	290,000	32	86,000	32	28,000	32

From these calculations a few things are clear. When examining the final volume of the cocoons needed to produce a dose, at a given concentration of cells and cores the 60, 90 and 130 µm cocoons will require the same volume of hydrogel, though they will require differing numbers of cocoons to produce that volume. Meanwhile the volume required shows a linear relation to the concentration of cells making up the final hollow cocoons.

As the encapsulation is a random process, the major important factor in the final volume of a "dose" is going to be the concentration of cells. By changing the size of the final hollow cocoon, one can change the number of cocoons to produce a dose, but not the volume of hydrogel needed to have 100,000 cells, as that is dictated by the frequency that cells enter the channel. This holds true for the encapsulation of cores as well, as doubling the cores on average doubles the number of cells in the sample as well.

Based on this, at the current encapsulation parameters even if the process demonstrated in this thesis was meeting the expected occupancy levels it would not meet the requirements for a in vivo testing dose. Fortunately, by increasing the final concentration of cells roughly 4-fold,

Poisson estimates show the produced sample reaching the bare minimum of 50 µL, though this does not leave any additional volume for the carrier fluid. Going even further, a 6-fold increase in the final cell concentration will potentially reach a viable hydrogel volume of 35 µL.

Whether these higher concentrations will function in the microfluidic channel without disrupting flow will require future investigation. At 25.5 million cells/mL, roughly 10% of the sample volume is cells, up from the current 3.5% for 8.5 million/mL. The doubled 1.7 million/mL gelatin core concentration also takes roughly 11% of the sample volume. The potential that these higher concentrations will clog the device or to disrupt the flow column in the nozzle due to too many cells or cores entering at the same time is high, but hopefully between changing the concentrations of the two steps a functioning level can be found.

That all said, the intended function of these hollow cocoons is to promote cell retention, viability and proliferation. Should they function as intended, it is possible that a smaller dose of cells than 100,000 would be required to meet the same therapeutic impact as with single layered cocoons. Should that be the case this would reduce the required volume of hydrogel as less cocoons would be needed to provide the required number of cells.

One final note about this analysis is that it relies on the assumption that empty cocoons will be injected along with the occupied cocoons. Should a reasonable method of separating these cocoons become available, empty hydrogel cocoons can be excluded shrinking the required hydrogel volume.

4 Conclusions

Four main project milestones were met in this research project. First the existing method of forming agarose emulsions were tested and adapted to both F-127 poloxamer and gelatin hydrogel, with gelatin hydrogel successfully meeting the goal targets. Secondly, the process of forming these emulsions was explored and better optimized to form more monodisperse droplets at higher throughputs. Thirdly, a new microfluidic channel design was created and enhanced to mix gelatin cocoons and liquid agarose inlet flows on chip, to produce hollow hydrogel cocoons. Finally, cells encapsulated in hollow hydrogel cocoons were observed over 48 hours using fluorescent Live/Dead staining to show the short term viability and persistence of encapsulated cells, and to begin documenting behaviours such as proliferation and adherence.

To form the inner cores of the hollow cocoon, 10% gelatin was found to be the best option. When paired with 1.5% Span 80 surfactant, pressures 121 kPa for the continuous phase and 100 kPa in the dispersed phase produced 50 µm droplets at a throughput of at minimum 300 droplets/s with 1.5% monodispersity. When encapsulating cells, cell viability was 98% with a standard deviation of 1%, and an occupancy rate of 51% with a standard deviation of 3%. When actively monitoring cocoons size, the average measured cocoon size during the entire run was 49 µm with a standard deviation of 1 µm, showing tight control over the size of the produced cocoons.

To encapsulate the gelatin cocoons in agarose, a new style of microfluidic flow-focusing channel was designed. Mixing two inlet flows on chip was successfully done using a Y-Junction and mixing serpentine before the nozzle. When encapsulating gelatin cocoons, hollow cocoons could be produced in sizes between 110-180 µm, with monodispersities of about 1.5% Due to shear in the serpentine, the highest flow rates caused larger cocoons to break into droplets, but at a continuous phase pressure of 100 kPa 140 µm cocoons could be produced at a throughput of 150-200 cocoons/second. This is an improvement over the similar in concept and size “double emulsions” explored previously which had throughputs typically less than 100 cocoons/s. Due to periodic disruptions in the flow out of the nozzle and egress of cocoons, the occupancy of the generated cocoons was lower than the theoretical value of 70%, reaching only 30-40%

occupancy. These disruptions became even worse when encapsulating cocoons with encapsulated cells, as the cocoons were “sticky” in the inlet leading to periodic swells of cocoon numbers.

Immediately after encapsulation, there were no signs of loss in viability of encapsulated cells. Even after 48 hours while there were some signs of potential cell death, the majority of cells remained viable. In terms of cell egress, cells were frequently found remaining in cocoons even with walls consisting of less than 5 µm separating them from the petri dish designed to promote cell adhesion, indicating that while egress may be occurring there is still some tendency for cells to remain in the cocoons. Without constant monitoring of cells, or being able to statistically prove an increase in the population of cells, proliferation is currently not confirmed. That said there were instances of cocoons containing too many cells to be just from encapsulation, making proliferation in the hollow cocoons a plausible process that is occurring.

Current results highlight a path towards the successful encapsulation of cells within hollow microcapsules. But further exploration is necessary to transition towards in vitro and *in vivo* validation of potential therapeutic efficacy. During moments of proper flow, hollow cocoons can be made at higher throughputs and monodispersity, with clear areas of further improvement that can be achieved. For cells encapsulated in these cocoons, initial results appear to support the hypothesis that these cocoons will limit cell egress while promoting viability and proliferation. In order to fully verify this and prepare these hollow cocoons for future tests, additional work will need to be done in both the preparation and analysis of the cocoons.

5 Future Work

Due to Covid-related disruptions in laboratory access during the course of this thesis and from new outcomes and directions that came to light during experimentation, there are a great deal of future alterations and improvements that can be made to the devices and process for encapsulation of cells in hollow cocoons.

During the investigations in how HLB value affects the generation of gelatin emulsions, it was found that the lower HLB 4.3 value was more stable in every combination. As faster throughputs equate to quicker experiment duration and less time for cells being out of the incubator, further improvements are always beneficial. Span 65 is a surfactant with an HLB of 2.1. When paired with Tween 65 this could make surfactant mixes of lower than HLB 4.3, which may make even higher pressure ranges possible.

One of the current issues affecting the occupancy of the hollow cocoons is the egress of the gelatin cores. Due to the size of the core in relation to the larger shell, it is often that the core will be too close to the edge, and will pop out of the shell during sample purification leading to a loose gelatin core. Some current research has shown that delaying the gelation of cocoons with serpentines can induce centering of a particle in a hydrogel micro-droplet. Microfluidic designs incorporating these centering features into the hollow cocoon flow-focusing geometry have already been produced, and test examining their efficacy will soon be undertaken.

Currently the encapsulation of cocoons using the hollow cocoon producing flow-focusing device is beset with frequent disruptions in the flow. This is a vital issue that needs to be addressed if cocoon production is to ever produce fully monodisperse cocoons across an entire encapsulation run. Investigation in the cause of these disruptions should be undertaken, if they are not resolved during the next iteration of devices being designed based on the results of these results.

One element of the devices that needs to be redesigned is the cooling serpentine. With the current design, at higher flow rates shear in the bends of the serpentine rip apart cocoons. Newly

designed turns will have to be modelled then designed in order to use highest flowrates to improve throughput.

Once the occupancy of the hollow cocoons has improved, more thorough analysis of the behavior of cells will need to be undertaken. To begin with, this includes the statistical analysis of changing viability, proliferation and egress to compare against previous data taken on cells encapsulated in solid agarose. However there are also other aspects that would be beneficial. Right now, that the structure of the generated cocoons is hollow is an assumption. Confocal microscopy Z-Stacks to show the 3D shape of the cocoons would offer additional insight into the hollow cocoon structure. Additionally, timelapse microscopy of the hollow cocoons would likely be able to show if cells are egressing or proliferating in the cocoons by direct observation rather than statistical changes in egress.

Experiments with therapeutic cells is a future milestone for the project. Previous work encapsulating cells shows that therapeutic cells show lower viability and higher egress from solid agarose cocoons when compared to 3T3 cells. As the desired outcome of this project is the eventual inclusion into cellular therapies, showing the benefits with therapeutic cell lines is a vital step. To meet this goal, exploration needs to occur to show the upper limits of cell and core concentrations to reduce the amount of sample needed to provide a therapeutic dose of cells.

Finally, there is modification to the agarose shell material itself. Currently agarose is chosen due to its thermal stability and biocompatibility, which is at the cost of it being a non-adherable surface for cells. By incorporating ECM materials into the hydrogel matrix, or by modifying it with moieties that cells can interact with the cells would ideally be able to spread on the inner wall for a more beneficial environment and reduction of anoikis related cell death, and may also provide opportunities for controlled degradation of the cocoons *in vivo*.

Bibliography

[1] R. Lanza and A. Atala, *Handbook of Stem Cells*, 2nd ed. San Diego: Elsevier, 2013.

[2] D. R. Davis and D. J. Stewart, "Autologous cell therapy for cardiac repair," *Expert Opin. Biol. Ther.*, vol. 11, no. 4, pp. 489–508, 2011, doi: 10.1517/14712598.2011.556615.

[3] P. De Vos, H. A. Lazarjani, D. Poncelet, and M. M. Faas, "Polymers in cell encapsulation from an enveloped cell perspective," *Adv. Drug Deliv. Rev.*, vol. 67–68, pp. 15–34, 2014, doi: 10.1016/j.addr.2013.11.005.

[4] L. Gasperini, J. F. Mano, and R. L. Reis, "Natural polymers for the microencapsulation of cells," *J. R. Soc. Interface*, vol. 11, no. 100, 2014, doi: 10.1098/rsif.2014.0817.

[5] A. Subramanian, U. M. Krishnan, and S. Sethuraman, "Development of biomaterial scaffold for nerve tissue engineering: Biomaterial mediated neural regeneration.," *J. Biomed. Sci.*, vol. 16, p. 108, 2009, doi: 10.1186/1423-0127-16-108.

[6] Y. Ichihara *et al.*, "Self-assembling peptide hydrogel enables instant epicardial coating of the heart with mesenchymal stromal cells for the treatment of heart failure," *Biomaterials*, vol. 154, pp. 12–23, 2018, doi: 10.1016/j.biomaterials.2017.10.050.

[7] J. Müller-Ehmsen *et al.*, "Effective engraftment but poor mid-term persistence of mononuclear and mesenchymal bone marrow cells in acute and chronic rat myocardial infarction," *J. Mol. Cell. Cardiol.*, vol. 41, no. 5, pp. 876–884, 2006, doi: 10.1016/j.yjmcc.2006.07.023.

[8] E. Mathieu *et al.*, "Intramyocardial Delivery of Mesenchymal Stem Cell-Seeded Hydrogel Preserves Cardiac Function and Attenuates Ventricular Remodeling after Myocardial Infarction," *PLoS One*, vol. 7, no. 12, 2012, doi: 10.1371/journal.pone.0051991.

[9] P. Kanda *et al.*, "Deterministic Encapsulation of Human Cardiac Stem Cells in Variable Composition Nanoporous Gel Cocoons to Enhance Therapeutic Repair of Injured Myocardium," *ACS Nano*, vol. 12, no. 5, pp. 4338–4350, 2018, doi: 10.1021/acsnano.7b08881.

[10] C. J. Young, L. A. Poole-Warren, and P. J. Martens, "Combining submerged electrospray and UV photopolymerization for production of synthetic hydrogel microspheres for cell encapsulation," *Biotechnol. Bioeng.*, vol. 109, no. 6, pp. 1561–1570, 2012, doi: 10.1002/bit.24430.

[11] P. Zhu and L. Wang, "Passive and active droplet generation with microfluidics: a review," *Lab Chip*, vol. 17, no. 1, pp. 34–75, 2017, doi: 10.1039/C6LC01018K.

[12] L. Desbois *et al.*, "A microfluidic device for on-chip agarose microbead generation with ultralow reagent consumption," *Biomicrofluidics*, vol. 6, no. 4, pp. 1–10, 2012, doi: 10.1063/1.4758460.

[13] S. Köster *et al.*, "Drop-based microfluidic devices for encapsulation of single cells," *Lab Chip*, vol. 8, no. 7, pp. 1110–1115, 2008, doi: 10.1039/b802941e.

[14] A. Benavente-Babace, K. Haase, D. J. Stewart, and M. Godin, "Strategies for controlling egress of therapeutic cells from hydrogel microcapsules," *J. Tissue Eng. Regen. Med.*, vol. 13, no. 4, pp. 612–624, 2019, doi: 10.1002/term.2818.

[15] R. Panchal, "Tracking Egress of Doubly Encapsulated Cells," University of Ottawa, 2019.

[16] M. W. Lai, D. Rubin, and E. Krempl, *Introduction to continuum mechanics*, 4th ed. Burlington:

Elsevier In, 2010.

[17] R. W. Johnson, *Handbook of Fluid Dynamics*, 2nd ed. Boca Raton: CRC Press, 2016.

[18] S. Colin, *Microfluidics*, 1st ed. Hoboken: John Wiley & Sons, Inc, 2010.

[19] C. Kleinstrueuer, *Microfluidics and Nanofluidics*, 1st ed. Hoboken: John Wiley & Sons, Inc, 2014.

[20] R. B. Bird, W. E. Stewart, and E. N. Lightfoot, *Transport Phemonena*, 2nd ed. New York: John Wiley & Sons, Inc, 2002.

[21] T. M. Squires and S. R. Quake, "Microfluidics: : Fluid physics at the nanoliter scale.," *Rev. Mod. Phys.*, vol. 77, no. 3, pp. 977–1026, 2005.

[22] F. Delplace, "Laminar flow of Newtonian liquids in ducts of rectangular cross-section a model for both physics and mathematics," *Open Access J. Math. Theor. Phys.*, vol. 1, no. 5, pp. 198–201, 2018, doi: 10.15406/oajmtp.2018.01.00034.

[23] J. Dambrine, B. Géraud, and J. B. Salmon, "Interdiffusion of liquids of different viscosities in a microchannel," *New J. Phys.*, vol. 11, 2009, doi: 10.1088/1367-2630/11/7/075015.

[24] A. Hatch, E. Garcia, and P. Yager, "Diffusion-based analysis of molecular interactions in microfluidic devices," *Proc. IEEE*, vol. 92, no. 1, pp. 126–139, 2004, doi: 10.1109/JPROC.2003.820547.

[25] M. P. Boruah, A. Sarker, P. R. Randive, S. Pati, and S. Chakraborty, "Wettability-mediated dynamics of two-phase flow in microfluidic T-junction," *Phys. Fluids*, vol. 30, no. 12, 2018, doi: 10.1063/1.5054898.

[26] Y. Song, D. Cheng, and L. Zhao, *Microfluidics Fundamentals, Devices and Applications*. Weinheim: Wiley-VCH, 2018.

[27] A. S. Utada, A. Fernandez-Nieves, H. A. Stone, and D. A. Weitz, "Dripping to jetting transitions in coflowing liquid streams," *Phys. Rev. Lett.*, vol. 99, no. 9, pp. 1–4, 2007, doi: 10.1103/PhysRevLett.99.094502.

[28] P.-G. de Gennes, F. Brochard-Wyart, and D. Quéré, *Capillarity and Wetting Phenomena*. New York: Springer Science+Business Media, 2004.

[29] T. P. Lagus and J. F. Edd, "A review of the theory, methods and recent applications of high-throughput single-cell droplet microfluidics," *J. Phys. D. Appl. Phys.*, vol. 46, no. 11, 2013, doi: 10.1088/0022-3727/46/11/114005.

[30] F. Y. Ushikubo and R. L. Cunha, "Stability mechanisms of liquid water-in-oil emulsions," *Food Hydrocoll.*, vol. 34, pp. 145–153, 2014, doi: 10.1016/j.foodhyd.2012.11.016.

[31] D. Wei, F. Taotao, Z. Chunying, and M. Youguang, "Breakup Dynamics for High-Viscosity Droplet Formation in a Flow-Focusing Device: Symmetrical and Asymmetrical Ruptures," *AIChE J.*, vol. 62, no. 1, pp. 325–337, 2016, doi: 10.1002/aic.15043.

[32] A. M. Gañán-Calvo and P. Riesco-Chueca, "Jetting-dripping transition of a liquid jet in a lower viscosity co-flowing immiscible liquid: The minimum flow rate in flow focusing," *J. Fluid Mech.*, vol. 553, no. May 2014, pp. 75–84, 2006, doi: 10.1017/S0022112006009013.

[33] D. M. Petsev, *Emulsion: Structure Stability and Interactions*, 1st ed. London: Elsevier Ltd, 2004.

[34] D. Mobius, R. Miller, and V. B. Fainerman, *Surfactants: Chemistry, Interfacial Properties, Applications*, 1st ed. Amsterdam: Elsevier Science, 2001.

[35] V. Norn, *Emulsifiers in Food Technology: Second Edition*, vol. 9780470670. 2015.

[36] Xi Yuan Hua and M. J. Rosen, "Dynamic surface tension of aqueous surfactant solutions. I. Basic paremeters," *J. Colloid Interface Sci.*, vol. 124, no. 2, pp. 652–659, 1988, doi: 10.1016/0021-9797(88)90203-2.

[37] M. G. A. Kassem, A. M. M. Ahmed, H. H. Abdel-Rahman, and A. H. E. Moustafa, "Use of Span 80 and Tween 80 for blending gasoline and alcohol in spark ignition engines," *Energy Reports*, vol. 5, pp. 221–230, 2019, doi: 10.1016/j.egyr.2019.01.009.

[38] J. M. Williams, "High Internal Phase Water-in-Oil Emulsions: Influence of Surfactants and Cosurfactants on Emulsion Stability and Foam Quality," *Langmuir*, vol. 7, no. 7, pp. 1370–1377, 1991, doi: 10.1021/la00055a014.

[39] A. M. Hocking and N. S. Gibran, "Mesenchymal stem cells: Paracrine signaling and differentiation during cutaneous wound repair," *Exp. Cell Res.*, vol. 316, no. 14, pp. 2213–2219, 2010, doi: 10.1016/j.yexcr.2010.05.009.

[40] R. Lanza, R. Langer, and J. Vacanti, *Principals of Tissue Engineering*, 4th ed. San Diego: Elsevier Inc., 2014.

[41] L. Chen, E. E. Tredget, P. Y. G. Wu, Y. Wu, and Y. Wu, "Paracrine factors of mesenchymal stem cells recruit macrophages and endothelial lineage cells and enhance wound healing," *PLoS One*, vol. 3, no. 4, 2008, doi: 10.1371/journal.pone.0001886.

[42] P. Lu, L. L. Jones, and M. H. Tuszynski, "Axon regeneration through scars and into sites of chronic spinal cord injury," *Exp. Neurol.*, vol. 203, no. 1, pp. 8–21, 2007, doi: 10.1016/j.expneurol.2006.07.030.

[43] M. Gnecchi *et al.*, "Paracrine action accounts for marked protection of ischemic heart by Akt-modified mesenchymal stem cells," *Nat. Med.*, vol. 11, no. 4, 2005, doi: 10.1096/fj.04-2702fje.

[44] M. Pfeffer and E. Braunwald, "Ventricular Remodeling After Myocardial Infarction," *Circulation*, vol. 81, no. 4, pp. 1161–1172, 1990, doi: 10.1161/01.CIR.81.4.1161.

[45] M. Laflamme and C. Murray, "Heart Regeneration," *Nature*, vol. 473, no. 7347, pp. 326–335, 2011, doi: 10.1038/jid.2014.371.

[46] D. Hou *et al.*, "Radiolabeled cell distribution after intramyocardial, intracoronary, and interstitial retrograde coronary venous delivery: Implications for current clinical trials," *Circulation*, vol. 112, no. 9 SUPPL., pp. 150–156, 2005, doi: 10.1161/CIRCULATIONAHA.104.526749.

[47] K. Ban *et al.*, "Cell Therapy with Embryonic Stem Encapsulated in Injectable Nanomatrix Gel Enhances Cell Engraftment and," *ACS Nano*, vol. 8, no. 10, pp. 10815–10825, 2014.

[48] B. D. RATNER, A. S. Hoffman, F. J. Schoen, and J. E. Lemons, *Biomaterials Science: An Introduction to Materials in Medicine*. San Diego: Academic Press, 1996.

[49] Y. Zhang, D. Khan, J. Delling, and E. Tobiasch, "Mechanisms underlying the osteo- and adipo-differentiation of human mesenchymal stem cells," *Sci. World J.*, vol. 2012, 2012, doi: 10.1100/2012/793823.

[50] K. A. Kilian, B. Bugarija, B. T. Lahn, and M. Mrksich, “Geometric cues for directing the differentiation of mesenchymal stem cells,” *Proc. Natl. Acad. Sci. U. S. A.*, vol. 107, no. 11, pp. 4872–4877, 2010, doi: 10.1073/pnas.0903269107.

[51] A. Tiwari, B. Garipcan, and U. Lokman, *Advanced Surfaces for Stem Cell Research*. Linkoping: Scrivener Publishing, 2017.

[52] G. Karoubi, M. L. Ormiston, D. J. Stewart, and D. W. Courtman, “Single-cell hydrogel encapsulation for enhanced survival of human marrow stromal cells,” *Biomaterials*, vol. 30, no. 29, pp. 5445–5455, 2009, doi: 10.1016/j.biomaterials.2009.06.035.

[53] M. Hashemi and F. Kalalinia, “Application of encapsulation technology in stem cell therapy,” *Life Sci.*, vol. 143, pp. 139–146, 2015, doi: 10.1016/j.lfs.2015.11.007.

[54] G. D. Nicodemus and S. J. Bryant, “Cell encapsulation in biodegradable hydrogels for tissue engineering applications,” *Tissue Eng. - Part B Rev.*, vol. 14, no. 2, pp. 149–165, 2008, doi: 10.1089/ten.teb.2007.0332.

[55] I. Perea-Gil, C. Prat-Vidal, and A. Bayes-Genis, “In vivo experience with natural scaffolds for myocardial infarction: The times they are a-changin’,” *Stem Cell Res. Ther.*, vol. 6, no. 1, pp. 1–25, 2015, doi: 10.1186/s13287-015-0237-4.

[56] N. C. Panda *et al.*, “Improved conduction and increased cell retention in healed MI using mesenchymal stem cells suspended in alginate hydrogel,” *J. Interv. Card. Electrophysiol.*, vol. 41, no. 2, pp. 117–127, 2014, doi: 10.1007/s10840-014-9940-9.

[57] P. De Vos, A. Andersson, S. K. Tam, M. M. Faas, and J. P. Hallé, “Advances and barriers in mammalian cell encapsulation for treatment of diabetes,” *Immunol. Endocr. Metab. Agents Med. Chem.*, vol. 6, no. 2, pp. 139–153, 2006.

[58] A. Scarano, F. Carinci, and A. Piattelli, “Lip augmentation with a new filler (agarose gel): a 3-year follow-up study,” *Oral Surgery, Oral Med. Oral Pathol. Oral Radiol. Endodontology*, vol. 108, no. 2, pp. e11–e15, 2009, doi: 10.1016/j.tripleo.2009.04.025.

[59] W. C. Mak *et al.*, “Controlled delivery of human cells by temperature responsive microcapsules,” *J. Funct. Biomater.*, vol. 6, no. 2, pp. 439–453, 2015, doi: 10.3390/jfb6020439.

[60] N. M. Catafard, “HIGH-THROUGHPUT CELL ENCAPSULATION IN MONODISPERSE AGAROSE MICROCAPSULES USING A MICROFLUIDIC DEVICE,” University of Ottawa, 2014.

[61] K. te Nijenhuis, *Thermoreversible Networks: Viscoelastic Properties and Structure of Gels*, 1st ed. New York: Springer-Verlag Berlin Heidelberg, 1997.

[62] Sigma-Aldrich, “A-2576.” https://api.sigmaaldrich.com/deepweb/assets/sigmaaldrich/quality/spec/prod/238/540/A2576-BULK_____SIAL_____.pdf.

[63] K. Dhingra, “Manipulation and Sorting of Cell-Laden Hydrogel Microcapsules Within Microfluidic Environment,” 2019.

[64] Sigma-Aldrich, “A-5030.” https://www.sigmaaldrich.com/Graphics/COfAInfo/SigmaSAPQM/SPEC/A5/A5030/A5030-BULK_____SIAL_____.pdf_SIAL_____.pdf.

[65] P. Alexandridis and T. Alan Hatton, “Poly(ethylene oxide)poly(propylene oxide)poly(ethylene oxide) block copolymer surfactants in aqueous solutions and at interfaces: thermodynamics, structure, dynamics, and modeling,” *Colloids Surfaces A Physicochem. Eng. Asp.*, vol. 96, no. 1–2, pp. 1–46, 1995, doi: 10.1016/0927-7757(94)03028-X.

[66] D. Bardin, T. D. Martz, P. S. Sheeran, R. Shih, P. A. Dayton, and A. P. Lee, “High-speed, clinical-scale microfluidic generation of stable phase-change droplets for gas embolotherapy,” *Lab Chip*, vol. 11, no. 23, pp. 3990–3998, 2011, doi: 10.1039/c1lc20615j.

[67] D. R. Devi, P. Sandhya, and B. N. V. Hari, “Poloxamer: A novel functional molecule for drug delivery and gene therapy,” *J. Pharm. Sci. Res.*, vol. 5, no. 8, pp. 159–165, 2013.

[68] H. Geng, H. Song, J. Qi, and D. Cui, “Sustained release of VEGF from PLGA-nanoparticles mbedded thermo-sensitive hydrogel in full-thickness porcine bladder acellular matrix,” *Nanoscale Res. Lett.*, vol. 6, no. 1, p. 312, 2011, doi: 10.1186/1556-276X-6-312.

[69] S. F. Khattak, S. R. Bhatia, and S. C. Roberts, “Pluronic F127 as a cell encapsulation material: Utilization of membrane-stabilizing agents,” *Tissue Eng.*, vol. 11, no. 5–6, pp. 974–983, 2005, doi: 10.1089/ten.2005.11.974.

[70] I. M. A. Diniz *et al.*, “Pluronic F-127 hydrogel as a promising scaffold for encapsulation of dental-derived mesenchymal stem cells,” *J. Mater. Sci. Mater. Med.*, vol. 26, no. 3, pp. 1–10, 2015, doi: 10.1007/s10856-015-5493-4.

[71] K. R. Stevens, N. J. Einerson, J. A. Burmania, and W. J. Kao, “In vivo biocompatibility of gelatin-based hydrogels and interpenetrating networks,” *J. Biomater. Sci. Polym. Ed.*, vol. 13, no. 12, pp. 1353–1366, 2002, doi: 10.1163/15685620260449741.

[72] L. J. Yang, W. Z. Lin, T. J. Yao, and Y. C. Tai, “Photo-patternable gelatin as protection layers in low-temperature surface micromachinings,” *Sensors Actuators, A Phys.*, vol. 103, no. 1–2, pp. 284–290, 2003, doi: 10.1016/S0924-4247(02)00338-2.

[73] X. Li, S. Makino, and K. Gekko, “Effects of Polyols and Sugars on the Sol-Gel Transition of Gelatin,” *Biosci. Biotechnol. Biochem.*, vol. 56, no. 8, pp. 1279–1284, 1992, doi: 10.1271/bbb.56.1279.

[74] Sigma-Aldrich, “G2500.” https://www.sigmaaldrich.com/Graphics/COfAInfo/SigmaSAPQM/SPEC/G2/G2500/G2500-BULK_____SIGMA____.pdf.

[75] Z. Jiang, B. Xia, R. McBride, and J. Oakey, “A microfluidic-based cell encapsulation platform to achieve high long-term cell viability in photopolymerized PEGNB hydrogel microspheres,” *J Mater Chem B Mater Biol Med*, vol. 5, no. 1, pp. 173–180, 2017, doi: 10.1016/j.physbeh.2017.03.040.

[76] D. J. Collins, A. Neild, A. deMello, A. Q. Liu, and Y. Ai, “The Poisson distribution and beyond: Methods for microfluidic droplet production and single cell encapsulation,” *Lab Chip*, vol. 15, no. 17, pp. 3439–3459, 2015, doi: 10.1039/c5lc00614g.

[77] P. Blaesild and J. Granfeldt, *Statistics with Applications in Biology and Geology*, 1st ed. New York: Chapman and Hall/CRC, 2002.

[78] A. S. Mao *et al.*, “Deterministic encapsulation of single cells in thin tunable microgels for niche modelling and therapeutic delivery,” *Nat. Mater.*, vol. 16, no. 2, pp. 236–243, 2017, doi: 10.1038/nmat4781.

[79] A. E. Mayfield *et al.*, "The effect of encapsulation of cardiac stem cells within matrix-enriched hydrogel capsules on cell survival, post-ischemic cell retention and cardiac function," *Biomaterials*, vol. 35, no. 1, pp. 133–142, 2014, doi: 10.1016/j.biomaterials.2013.09.085.

[80] T. Kamperman, S. Henke, C. W. Visser, M. Karperien, and J. Leijten, "Centering Single Cells in Microgels via Delayed Crosslinking Supports Long-Term 3D Culture by Preventing Cell Escape," *Small*, vol. 13, no. 22, pp. 1–10, 2017, doi: 10.1002/smll.201603711.

[81] W. Wang, M. J. Zhang, and L. Y. Chu, "Microfluidic approach for encapsulation via double emulsions," *Curr. Opin. Pharmacol.*, vol. 18, pp. 35–41, 2014, doi: 10.1016/j.coph.2014.08.003.

[82] A. S. Utada, L. Chu, D. R. Link, C. Holtze, and D. A. Weitz, "Dripping , Jetting , Drops , and Wetting : The Magic of Microfluidics," *MRSBulletin*, vol. 32, no. September 2007, pp. 702–708, 2007.

[83] S. Sakai, I. Hashimoto, S. Tanaka, B. Salmons, and K. Kawakami, "Small agarose microcapsules with cell-enclosing hollow core for cell therapy: Transplantation of ifosfamide-activating cells to the mice with preestablished subcutaneous tumor," *Cell Transplant.*, vol. 18, no. 8, pp. 933–939, 2009, doi: 10.3727/096368909X471143.

[84] S. Sakai *et al.*, "Cell-enclosing gelatin-based microcapsule production for tissue engineering using a microfluidic flow-focusing system," *Biomicrofluidics*, vol. 5, no. 1, pp. 1–7, 2011, doi: 10.1063/1.3516657.

[85] K. Zhu, Y. Yu, Y. Cheng, C. Tian, G. Zhao, and Y. Zhao, "All-Aqueous-Phase Microfluidics for Cell Encapsulation," *ACS Appl. Mater. Interfaces*, vol. 11, no. 5, pp. 4826–4832, 2019, doi: 10.1021/acsami.8b19234.

[86] S. Sakai, I. Hashimoto, and K. Kawakami, "Production of Cell-Enclosing Hollow-Core Agarose Microcapsules Via Jetting in Water-Immiscible Liquid Paraffin and Formation of Embryoid Body-Like Spherical Tissues From Mouse ES Cells Enclosed Within These Microcapsules," *Biotechnol. Bioeng.*, vol. 99, no. 1, 2007, doi: 10.1002/bit.

[87] T. Watanabe, I. Motohiro, and T. Ono, "Microfluidic Formation of Hydrogel Microcapsules with a Single Aqueous Core by Spontaneous Cross-Linking in Aqueous Two-Phase System Droplets," *Langmuir*, vol. 35, no. 6, pp. 2358–2367, 2019, doi: 10.1021/acs.langmuir.8b04169.

[88] R. Zaouk, B. Park, and M. Madou, "Fabrication of Polydimethylsiloxane Microfluidics Using SU-8 Molds," in *Microfluidic Techniques Reviews and Protocols*, 1st ed., S. Minteer, Ed. Totowa: Humana Press Inc., 2006, pp. 17–23.

[89] M. Ionescu *et al.*, "Enhanced biocompatibility of PDMS (polydimethylsiloxane) polymer films by ion irradiation," *Nucl. Instruments Methods Phys. Res. Sect. B Beam Interact. with Mater. Atoms*, vol. 273, pp. 161–163, 2012, doi: 10.1016/j.nimb.2011.07.065.

[90] The Dow Chemical Company, "SYLGARD™ 184," 2017. https://www.ellsworth.com/products/by-market/consumer-products/encapsulants/silicone/dow-sylgard-184-silicone-encapsulant-clear-0.5-kg-kit/.

[91] J. C. Mcdonald, D. C. Duffy, J. R. Anderson, and D. T. Chiu, "Review General Fabrication of microfluidic systems in poly (dimethylsiloxane)," *Electrophoresis*, vol. 21, no. 1, pp. 27–40, 2000, [Online]. Available: http://www.ncbi.nlm.nih.gov/pubmed/10634468.

[92] D. C. Duffy, J. C. McDonald, O. J. A. Schueller, and G. M. Whitesides, "Rapid prototyping of

microfluidic systems in poly(dimethylsiloxane)," *Anal. Chem.*, vol. 70, no. 23, pp. 4974–4984, 1998, doi: 10.1021/ac980656z.

[93] R.-H. Chen and C.-M. Cheng, "Study of Spin coating properties of SU-8 thick-layer photoresist," *Adv. Resist Technol. Process. XVIII*, vol. 4345, p. 494, 2001, doi: 10.1117/12.436881.

[94] Microchem, "SU-8 2000," 2010. microchem.com/pdf/SU-82000DataSheet2000_5thru2015Ver4.pdf.

[95] and S. G. S. Bhattacharya, A. Datta, J. M. Berg, "Studies on Surface Wettability of Poly (Dimethyl) Siloxane (PDMS) and Glass Under Oxygen-Plasma," *J.MicroElecMechSys*, vol. 14, no. 3, pp. 590–597, 2005, doi: 10.1109/JMEMS.2005.844746.

[96] S. I. T. Tridecafluoro- and T. Trichlorosilane, "(tridecafluoro-1,1,2,2-tetrahydrooctyl)trichlorosilane," 2019. https://s3.amazonaws.com/gelest/sds/SIT8174.0_GHS+EU_English.pdf.

[97] Sigma-Aldrich, "Optiprep." https://api.sigmaaldrich.com/deepweb/assets/sigmaaldrich/quality/spec/826/613/D1556-BULK_____SIGMA____.pdf (accessed Dec. 10, 2020).

[98] H. Sato and K. Ueberreiter, "Surface tension of aqueous gelatin solutions, 1. Concentration dependence," *Die Makromol. Chemie*, vol. 180, no. 3, pp. 829–835, 1979, doi: 10.1002/macp.1979.021800330.

[99] A. F. Davidson, C. Glasscock, D. R. McClanahan, J. D. Benson, and A. Z. Higgins, "Toxicity Minimized Cryoprotectant Addition and Removal Procedures for Adherent Endothelial Cells," *PLoS One*, vol. 10, no. 11, pp. 1–22, 2015, doi: 10.1371/journal.pone.0142828.

[100] National Instruments, "USB-6212." https://www.ni.com/pdf/manuals/375196d.pdf.

[101] Sigma-Aldrich, "M5904." https://www.sigmaaldrich.com/Graphics/COfAInfo/SigmaSAPQM/SPEC/M5/M5904/M5904-BULK_____SIGMA____.pdf.

[102] G. D. Noudeh, P. Khazaeli, S. Mirzaei, F. Sharififar, and S. Nasrollahosaiani, "Determination of the toxicity effect of sorbitan esters surfactants group on biological membrane," *Journal of Biological Sciences*, vol. 9, no. 5. pp. 423–430, 2009, doi: 10.3923/jbs.2009.423.430.

[103] CFF, "NIH 3T3 Cell Culture." https://www.cff.org/Research/Researcher-Resources/Tools-and-Resources/CFFT-Biorepository/NIH-3T3-Culture-Protocol.pdf (accessed Jun. 08, 2020).

[104] L. V. K. *for mammalian Cells*, "LIVE/DEAD Viability/Cytotoxicity Kit for mammalian cells," 2005. https://www.thermofisher.com/document-connect/document-connect.html?url=https%3A%2F%2Fassets.thermofisher.com%2FTFS-Assets%2FLSG%2Fmanuals%2Fmp03224.pdf&title=TElWRSYjNDc7REVBRCBWaWFiaWxpdHkmIzQ3O0N5dG90b3hpY2l0eSBLaXQ=.

[105] E. Biosciences, "Using a Counting Chamber," [Online]. Available: http://www.ruf.rice.edu/~bioslabs/methods/microscopy/cellcounting.html.

[106] P. Kanda *et al.*, "Deterministic paracrine repair of injured myocardium using microfluidic-based cocooning of heart explant-derived cells," *Biomaterials*, vol. 247, 2020, doi:

10.1016/j.biomaterials.2020.120010.

[107] A. P. Debon, R. C. R. Wootton, and K. S. Elvira, “Droplet confinement and leakage: Causes, underlying effects, and amelioration strategies,” *Biomicrofluidics*, vol. 9, no. 2, pp. 1–16, 2015, doi: 10.1063/1.4917343.

[108] J. Winter and D. Shifler, “The material properties of gelatin gels,” 1975.

[109] V. Sibillo, G. Pasquariello, M. Simeone, V. Cristini, and S. Guido, “Drop deformation in microconfined shear flow,” *Phys. Rev. Lett.*, vol. 97, no. 5, 2006, doi: 10.1103/PhysRevLett.97.054502.

[110] T. Poggioli, P. Sarathchandra, N. Rosenthal, and M. P. Santini, “Intramyocardial cell delivery: Observations in murine hearts,” *J. Vis. Exp.*, no. 83, pp. 1–9, 2014, doi: 10.3791/51064.